FERMILAB-PUB-14-230-T

Charmed and light pseudoscalar meson decay constants from four-flavor lattice QCD with physical light quarks

A. Bazavov*

Physics Department, Brookhaven National Laboratory, Upton, NY, USA

C. Bernard† and J. Komijani‡

Department of Physics, Washington University, St. Louis, MO, USA

C.M. Bouchard

Department of Physics, The Ohio State University, Columbus, OH, USA

C. DeTar

Department of Physics and Astronomy,
University of Utah, Salt Lake City, UT, USA

D. Du and J. Laiho

Department of Physics, Syracuse University, Syracuse, NY, USA

A.X. El-Khadra

Physics Department, University of Illinois, Urbana, IL, USA

J. Foley and L. Levkova

Physics Department, University of Utah, Salt Lake City, UT, USA

E.D. Freeland

Liberal Arts Department, School of the Art Institute of Chicago, Chicago, IL, USA

E. Gámiz

CAFPE and Departamento de Fisica Teórica y del Cosmos,
Universidad de Granada, Granada, Spain

Steven Gottlieb

Department of Physics, Indiana University, Bloomington, IN, USA

Operated by Fermi Research Alliance, LLC under Contract No. De-AC02-07CH11359 with the United States Department of Energy.

U.M. Heller

American Physical Society, Ridge, NY, USA

J. Kim[§] and D. Toussaint[¶]

Physics Department, University of Arizona, Tucson, AZ, USA

A.S. Kronfeld, P.B. Mackenzie, J.N. Simone, R.S. Van de Water, and R. Zhou

Fermi National Accelerator Laboratory, Batavia, IL, USA

E.T. Neil

Department of Physics, University of Colorado, Boulder, CO, USA and

RIKEN-BNL Research Center, Brookhaven National Laboratory, Upton, NY, USA

R. Sugar

Department of Physics, University of California, Santa Barbara, CA, USA

[Fermilab Lattice and MILC Collaborations]

(Dated: July 15, 2014)

Abstract

We compute the leptonic decay constants f_{D^+}, f_{D_s}, and f_{K^+}, and the quark-mass ratios m_c/m_s and m_s/m_l in unquenched lattice QCD using the experimentally determined value of f_{π^+} for normalization. We use the MILC Highly Improved Staggered Quark (HISQ) ensembles with four dynamical quark flavors — up, down, strange, and charm — and with both physical and unphysical values of the light sea-quark masses. The use of physical pions removes the need for a chiral extrapolation, thereby eliminating a significant source of uncertainty in previous calculations. Four different lattice spacings ranging from $a \approx 0.06$ fm to 0.15 fm are included in the analysis to control the extrapolation to the continuum limit. Our primary results are $f_{D^+} = 212.6(0.4)(^{+1.0}_{-1.2})$ MeV, $f_{D_s} = 249.0(0.3)(^{+1.1}_{-1.5})$ MeV, and $f_{D_s}/f_{D^+} = 1.1712(10)(^{+29}_{-32})$, where the errors are statistical and total systematic, respectively. The errors on our results for the charm decay constants and their ratio are approximately two to four times smaller than those of the most precise previous lattice calculations. We also obtain $f_{K^+}/f_{\pi^+} = 1.1956(10)(^{+26}_{-18})$, updating our previous result, and determine the quark-mass ratios $m_s/m_l = 27.35(5)(^{+10}_{-7})$ and $m_c/m_s = 11.747(19)(^{+59}_{-43})$. When combined with experimental measurements of the decay rates, our results lead to precise determinations of the CKM matrix elements $|V_{us}| = 0.22487(51)(29)(20)(5)$, $|V_{cd}| = 0.217(1)(5)(1)$ and $|V_{cs}| = 1.010(5)(18)(6)$, where the errors are from this calculation of the decay constants, the uncertainty in the experimental decay rates, structure-dependent electromagnetic corrections, and, in the case of $|V_{us}|$, the uncertainty in $|V_{ud}|$, respectively.

PACS numbers: 12.38.Gc,14.20.Dh

*Present address: Department of Physics and Astronomy, University of Iowa, Iowa City, IA, USA

†cb@lump.wustl.edu

‡jkomijani@physics.wustl.edu

§Present address: Department of Physics and Astronomy, Seoul National University, Seoul, Korea

¶doug@physics.arizona.edu

I. INTRODUCTION AND MOTIVATION

The leptonic decays of pseudoscalar mesons enable precise determinations of Cabibbo-Kobayashi-Maskawa (CKM) quark-mixing matrix elements within the Standard Model. In particular, experimental rates for the decays $D^+ \to \mu^+\nu$, $D_s \to \mu^+\nu$ and $D_s \to \tau^+\nu$, when combined with lattice calculations of the charm-meson decay constants f_{D^+} and f_{D_s}, allow one to obtain $|V_{cd}|$ and $|V_{cs}|$. Indeed, this approach results in the most precise current determination of $|V_{cd}|$. Similarly, the light-meson decay-constant ratio f_{K^+}/f_{π^+} can be used to extract $|V_{us}|/|V_{ud}|$ from the experimental ratio of kaon and pion leptonic decay widths [1, 2]. Here we calculate the charm decay constants for the first time using physical values for the light sea-quark mass. We obtain f_{D^+} and f_{D_s} to about 0.5% precision and their ratio f_{D_s}/f_{D^+} to about 0.3% precision; we also update our earlier calculation of f_{K^+}/f_{π^+} [3] to almost 0.2% precision. This is the most precise lattice calculation of the charm decay constants to date, and improves upon previous results by a factor of two to four. We also compute the quark-mass ratios m_c/m_s and m_s/m_l, which are fundamental parameters of the Standard Model.

We use the lattice ensembles generated by the MILC collaboration with four flavors ($n_f = 2+1+1$) of dynamical quarks using the highly improved staggered quark (HISQ) action, and a one-loop tadpole improved Symanzik improved gauge action [4–7]. The generation algorithm uses the fourth-root procedure to remove the unwanted taste degrees of freedom [8–20]. Our data set includes ensembles with four values of the lattice spacing ranging from approximately 0.15 fm to 0.06 fm, enabling good control over the continuum extrapolation. The data set includes both ensembles with the light (up-down), strange, and charm sea-masses close to their physical values ("physical-mass ensembles") and ensembles where either the light sea-mass is heavier than in nature, or the strange sea-mass is lighter than in nature, or both.

The physical-mass ensembles enable us to perform first a straightforward analysis that does not require chiral fits. This analysis, which we refer to as the "physical-mass analysis" below, gives our results for f_{K^+}/f_{π^+}, as well as ratios of physical quark masses. The quark-mass ratios are then used as input to a more sophisticated analysis of the charm decay constants that includes the ensembles with unphysical sea-quark masses. In this second analysis, referred to as the "chiral analysis," we analyze our complete data set within

the framework of staggered chiral perturbation theory (SχPT) for all-staggered heavy-light mesons [21, 23, 24]. The inclusion of the unphysical-mass ensembles gives us tighter control on discretization effects because SχPT connects the quark-mass and lattice-spacing dependence of the data, reducing the statistical errors on the decay constants significantly, and allowing us to make more refined adjustments for mistuning of masses. We therefore take our final central values for f_{D^+}, f_{D_s}, and f_{D_s}/f_{D^+} from the chiral analysis. The physical-mass analysis provides a cross check of the chiral analysis and is used in our final estimate of systematic uncertainties.

An earlier result for f_{K^+}/f_{π^+} was presented in Ref. [3]. Here we update this analysis with slightly more statistics and improved estimates for the systematic errors. Preliminary results for the charm decay constants and quark masses were presented in Ref. [25].

This paper is organized as follows. Section II gives details about the lattice ensembles used in our calculation and the method for extracting the decay constants from two-point correlation functions. As discussed in Sec. III, the first stage in our analysis is to fit the two-point correlators to determine the meson masses and decay amplitudes for each pair of valence-quark masses. Section IV presents the main body of our analysis, which proceeds in two stages. In the first stage, described in Sec. IV A, we use the physical-mass ensembles to compute quark-mass ratios and f_{K^+}/f_{π^+}, as well as some additional intermediate quantities required for the later chiral analysis of the D-meson decay constants. In the first part of the physical-mass analysis, Sec. IV A 1, we fit the valence-quark mass dependence of the masses and amplitudes, and evaluate the decay amplitudes at the resulting tuned valence masses. Next, in Sec. IV A 2, we adjust the quark-mass ratios and decay amplitudes to account for the slight sea-quark mass mistuning and extrapolate these results to the continuum. In the last part of the physical-mass analysis, Sec. IV A 3, we consider systematic errors from finite-volume and electromagnetic effects. In the second analysis stage described in Sec. IV B, we use heavy-light staggered chiral perturbation theory to combine the unphysical light- and strange-quark mass ensembles with the nearly-physical quark mass ensembles to obtain the charm-meson decay constants. We first present the chiral perturbation theory for all-staggered heavy-light mesons in Sec. IV B 1. We then discuss the required mass-independent scale setting in Sec. IV B 2, where we take care to correct for effects on the scale and quark-mass estimates of mistunings of the sea-quark masses. We present the chiral-continuum fits

in Sec. IV B 3, and discuss the systematic errors from the continuum extrapolation, as well as from other sources, in Sec. IV B 4. We present our final results for the decay constants and quark-mass ratios with error budgets in Sec. V, in which we also compare our results to other unquenched lattice calculations. Finally, we discuss the impact of our results on CKM phenomenology in Sec. VI. Appendix A gives details about the inclusion of nonleading heavy-quark effects in our chiral formulas.

II. LATTICE SIMULATION PARAMETERS AND METHODS

Table I summarizes the lattice ensembles used in this calculation. Discussion of the parameters relevant to the lattice generation, such as integration step sizes and acceptance rates, choice of the RHMC or RHMD algorithm, and autocorrelations of various quantities can be found in Ref. [7]. In particular, we find that the effects of using the RHMD algorithm rather than the RHMC algorithm in some of our ensembles are negligible. The dependence of error estimates for the decay constants in this work on the jackknife block size is consistent with the more general results on autocorrelations in Ref. [7]. Reference [7] also shows the molecular dynamics time evolution of the topological charge for many of these ensembles and histograms of the topological charge. We have since also verified that on the $a \approx 0.06$ fm physical quark mass ensemble the autocorrelation time for the topological charge is much shorter than the topological charge autocorrelation time on the $a \approx 0.06$ fm $m'_l = m'_s/5$ ensemble shown in Fig. 2 of Ref. [7]. The dependence on the light-quark mass can be understood by thinking of the decorrelation process as a random walk in the topological charge.

Our extraction of the pseudoscalar decay constants with staggered quarks follows that used for asqtad quarks [2, 26] and for f_{K^+} with the HISQ action [3, 27]. The decay constant f_{PS} is given by the matrix element of $\bar{\psi}\gamma_5\psi$ between the vacuum and the pseudoscalar meson. For staggered fermions, using the pion taste corresponding to the axial symmetry broken only by quark masses, this becomes the operator

$$\mathcal{O}_P(\vec{x},t) = \bar{\chi}^a(\vec{x},t)(-1)^{x+y+z+t}\chi^a(\vec{x},t) \quad , \tag{1}$$

where a is a color index. The desired matrix element can be obtained from the amplitude

TABLE I: Ensembles used in this calculation. The first column is the gauge coupling $\beta = 10/g^2$, and the next three columns are the sea-quark masses in lattice units. The primes on the masses indicate that they are the values used in the runs, and in general differ from the physical values either by choice, or because of tuning errors. The lattice spacings in this table are obtained separately on each ensemble using f_{π^+} as the length standard, following the procedure described in Sec. IV A 1. (In Sec. IV B we use a mass-independent lattice spacing, described there.) The lattice spacings here differ slightly from those in Ref. [7] since we use f_{π^+} as the length scale, while those in Ref. [7] were determined using F_{p4s} (discussed at the beginning of Sec. IV A). Values of the strange quark mass chosen to be unphysical are marked with a dagger (†); while the asterisk (*) marks an ensemble that we expect to extend in the future.

β	am'_l	am'_s	am'_c	$(L/a)^3 \times (T/a)$	N_{lats}	a (fm)	L (fm)	$M_\pi L$	M_π (MeV)
5.80	0.013	0.065	0.838	$16^3 \times 48$	1020	0.14985(38)	2.38	3.8	314
5.80	0.0064	0.064	0.828	$24^3 \times 48$	1000	0.15303(19)	3.67	4.0	214
5.80	0.00235	0.0647	0.831	$32^3 \times 48$	1000	0.15089(17)	4.83	3.2	130
6.00	0.0102	0.0509	0.635	$24^3 \times 64$	1040	0.12520(22)	3.00	4.5	299
6.00	0.00507	0.0507	0.628	$24^3 \times 64$	1020	0.12085(28)	2.89	3.2	221
6.00	0.00507	0.0507	0.628	$32^3 \times 64$	1000	0.12307(16)	3.93	4.3	216
6.00	0.00507	0.0507	0.628	$40^3 \times 64$	1028	0.12388(10)	4.95	5.4	214
6.00	0.01275	0.01275†	0.640	$24^3 \times 64$	1020	0.11848(26)	2.84	5.0	349
6.00	0.00507	0.0304†	0.628	$32^3 \times 64$	1020	0.12014(16)	3.84	4.3	219
6.00	0.00507	0.022815†	0.628	$32^3 \times 64$	1020	0.11853(16)	3.79	4.2	221
6.00	0.00507	0.012675†	0.628	$32^3 \times 64$	1020	0.11562(14)	3.70	4.2	226
6.00	0.00507	0.00507†	0.628	$32^3 \times 64$	1020	0.11311(19)	3.62	4.2	230
6.00	0.0088725	0.022815†	0.628	$32^3 \times 64$	1020	0.12083(17)	3.87	5.6	286
6.00	0.00184	0.0507	0.628	$48^3 \times 64$	999	0.12121(10)	5.82	3.9	133
6.30	0.0074	0.037	0.440	$32^3 \times 96$	1011	0.09242(21)	2.95	4.5	301
6.30	0.00363	0.0363	0.430	$48^3 \times 96$	1000	0.09030(13)	4.33	4.7	215
6.30	0.0012	0.0363	0.432	$64^3 \times 96$	1031	0.08779(08)	5.62	3.7	130
6.72	0.0048	0.024	0.286	$48^3 \times 144$	1016	0.06132(22)	2.94	4.5	304
6.72	0.0024	0.024	0.286	$64^3 \times 144$	1166	0.05937(10)	3.79	4.3	224
6.72	0.0008	0.022	0.260	$96^3 \times 192$	583*	0.05676(06)	5.44	3.7	135

of a correlator using this operator at the source and sink,

$$P_{PP}(t) = \frac{1}{V_s}\sum_{\vec{y}}\langle \mathcal{O}_P(\vec{y},0)\mathcal{O}_P(\vec{0},t)\rangle = C_{PP}e^{-Mt} + \text{excited state contributions} \quad , \qquad (2)$$

where V_s is the spatial volume, M is the pseudoscalar meson mass and the sum over $\vec{y}$ isolates the zero spatial momentum states. Then the decay constant is given by [28, 29]

$$f_{PS} = (m_A + m_B)\sqrt{\frac{V_s}{4}}\sqrt{\frac{C_{PP}}{M^3}} \quad , \qquad (3)$$

where m_A and m_B are valence quark masses and M is the pseudoscalar meson mass.

In our computations, we use a "random-wall" source for the quark propagators, where a randomly oriented unit vector in color space is placed on each spatial site at the source time. Then quark and antiquark propagators originating on different lattice sites are zero when averaged over the sources. We use three such source vectors for each source time slice.

We also compute pion correlators using a "Coulomb-wall" source, where the gauge field is fixed to the lattice Coulomb gauge, and then a uniform color vector source is used at each spatial site. In practice these vectors are the "red", "green," and "blue" color axes. The Coulomb-wall source correlators are somewhat less contaminated by excited states than the random wall source correlators, so by simultaneously fitting the correlators with common masses we are able to determine the masses better, and hence get a better determined amplitude for the random-wall source correlator.

Four source time slices are used on each lattice, with the exception of the 0.06 fm physical quark-mass ensemble where, because these lattices are longer in the Euclidean time direction, six source time slices are used. The location of the source time slices on successive lattices is advanced by an amount close to one half of the spacing between sources, but incommensurate with the lattice time size, so that the source location cycles among all possible values.

In each lattice ensemble, two-point correlators are computed for a range of valence-quark masses. The complete set of valence-quark masses is given in Table II. The lightest valence mass used is one-tenth the strange quark mass for the coarser ensembles with heavier sea-quark masses, 1/20 the strange quark mass for the $a \approx 0.06$ fm ensembles with heavier than physical sea-quark mass, and the physical light-quark mass for the ensembles with physical sea-quark mass. The valence masses chosen then cover the range from this lightest mass up to the estimated strange-quark mass. We then choose additional masses at the estimated charm-quark mass (the same as the charm-quark mass in the sea), as well as nine-tenths

TABLE II: Valence-quark masses used in this project. Correlators with random wall and Coulomb-wall sources are computed for each possible pair of valence-quark masses. Light valence masses $m_{\rm v}$ are given in units of the (ensemble value of the) sea strange quark mass m'_s. Note that for the four ensembles with near-physical sea-quark mass, the lightest valence mass is the same as the light sea mass. The two heavy valence masses are in units of the charm sea-quark mass m'_c. For the ensembles with unphysical strange quark mass (included in "all" at $\beta = 6.0$), the valence masses are given in units of the approximate physical strange quark mass, 0.0507.

β	sea quark masses			light valence masses	charm valence masses
	am'_l	am'_s	am'_c	$m_{\rm v}/m'_s$	$m_{\rm v}/m'_c$
5.80	0.013	0.065	0.838	0.1,0.15,0.2,0.3,0.4,0.6,0.8,1.0	0.9,1.0
5.80	0.0064	0.064	0.828	0.1,0.15,0.2,0.3,0.4,0.6,0.8,1.0	0.9,1.0
5.80	0.00235	0.0647	0.831	0.036,0.07,0.1,0.15,0.2,0.3,0.4,0.6,0.8,1.0	0.9,1.0
6.00	0.0102	0.0509	0.635	0.1,0.15,0.2,0.3,0.4,0.6,0.8,1.0	0.9,1.0
6.00	0.00507	all	0.628	0.1,0.15,0.2,0.3,0.4,0.6,0.8,1.0	0.9,1.0
6.00	0.00184	0.0507	0.628	0.036,0.073,0.1,0.15,0.2,0.3,0.4,0.6,0.8,1.0	0.9,1.0
6.30	0.0074	0.037	0.440	0.1,0.15,0.2,0.3,0.4,0.6,0.8,1.0	0.9,1.0
6.30	0.00363	0.0363	0.430	0.1,0.15,0.2,0.3,0.4,0.6,0.8,1.0	0.9,1.0
6.30	0.0012	0.0363	0.432	0.033,0.066,0.1,0.15,0.2,0.3,0.4,0.6,0.8,1.0	0.9,1.0
6.72	0.0048	0.024	0.286	0.05,0.1,0.15,0.2,0.3,0.4,0.6,0.8,1.0	0.9,1.0
6.72	0.0024	0.024	0.286	0.05,0.1,0.15,0.2,0.3,0.4,0.6,0.8,1.0	0.9,1.0
6.72	0.0008	0.022	0.260	0.036,0.068,0.1,0.15,0.2,0.3,0.4,0.6,0.8,1.0	0.9,1.0

of that value, so that we can make adjustments for mistuning of the charm-quark mass. For these last two quarks, the coefficient of the three-link term in the fermion action (the "Naik term") is adjusted to improve the quark's dispersion relation [30]. Specifically, the expansion resulting from combining Eqs. (24) and (26) of Ref. [30] is used; the improvement has been checked in HISQ simulations [6, 30].

III. TWO-POINT CORRELATOR FITS

To find the pseudoscalar masses and decay amplitudes, the random-wall and Coulomb-wall correlators are fitted to common masses but independent amplitudes. With staggered quarks the Goldstone-taste pseudoscalar correlators with unequal quark masses contain contributions from opposite-parity states, which show up as exponentials multiplied by an alternating sign, $(-1)^t$. For valence-quark masses up to and including the strange quark mass these contributions are small, and good fits can be obtained while neglecting them. In fact, in our previous analyses with the asqtad quark action, these states were not included in the two-point fits. However, with these data sets, slightly better fits are obtained when an opposite-parity state is included in the light-light fits, and so we include such a state in the unequal quark mass correlators.

The light-charm correlators (where "light" here includes masses up to the physical strange quark mass m_s) are more difficult to fit than the light-light correlators for several reasons. First, because the difference in the valence-quark mass is large, the amplitude of the opposite-parity states is not small. Second, the mass splitting between the ground state and the lowest excited single particle state is smaller. For the light-light correlators, the approximate chiral symmetry makes the ground state mass smaller than typical hadronic scales, which has the side effect of making the mass gap to the excited single particle states large, and these excited states can be suppressed by simply taking a large enough minimum distance. For the charm-light correlators we include an excited state in the fit function. (In principle, multiparticle states also appear in these correlators. For example, the lowest excited state in the pion correlator would be a three-pion state. Empirically these states do not enter with large amplitudes, and the important excited states correspond more closely to single particle states.)

To make the fits converge reliably, it is necessary to loosely constrain the masses of the opposite-parity and excited states by Gaussian priors. The central value of the gap between the ground state and opposite parity states is taken to be 400 MeV, motivated by the 450 MeV gap between the D mass and the 0^+ light-charm mass, and the 350 MeV gap between the D_s mass and a poorly established 0^+ strange-charm meson [31]. The central value for the gap between the ground state and excited state masses is taken to be 700 MeV, motivated by the 660 MeV gap between the η_c and the corresponding 2S state. In most cases the

widths of the priors for the opposite-parity and excited state gaps are taken to be 200 MeV and 140 MeV respectively, although in some cases these need to be adjusted to get all of the jackknife fits to converge.

Another factor that makes the light-charm correlators more difficult to fit is the faster growth of the statistical error. The time dependence of the variance of a correlator is expected to depend on time as $e^{-E_2 t}$, where E_2 is the energy of the lowest lying state created by $\mathcal{O}\mathcal{O}^\dagger$, where $\mathcal{O}$ is the source operator for the correlator itself, with the proviso that quark and antiquark lines all go from source to sink, rather than coming back to the source [32]. For the pion correlator, the state created by $\mathcal{O}\mathcal{O}^\dagger$ is just the two pion state, leading to the expectation that the fractional statistical error on the pion correlator is roughly independent of distance. However, for the light-charm correlator, the quarks and antiquarks created by $\mathcal{O}\mathcal{O}^\dagger$ can pair up to form an η_c and a pion. Then, the reduction of the pion's mass from chiral symmetry makes this state much lighter than $2M_D$, so the fractional error of the propagator grows rapidly with distance. This makes it essential to use smaller minimum distances in the fit range for the light-charm correlators, which of course makes the problem of excited states discussed in the previous paragraph even more serious.

Table III shows our expectations for the states controlling the growth of statistical errors for the various pseudoscalar correlators. Figure 1 shows the fractional errors for the random-wall correlators for the 0.09 fm physical quark-mass ensemble, with comparison to the slopes expected from Table III. With the exception of the charm-charm correlator, the behavior of the statistical error agrees with our theoretical expectations.

Figures 2 and 3 show the masses in the 2+1 state fits for the light-charm correlators in the $a \approx 0.09$ fm physical quark-mass ensemble as a function of the minimum distance included in the fit, where the light-quark mass is the physical $(m_u + m_d)/2$ (Fig. 2) and m_s (Fig. 3). Fit ranges are chosen from graphs like this for all the ensembles, and analogous graphs for the light-light and charm-charm correlators. We show this ensemble because it, together with the $a \approx 0.06$ fm physical mass ensemble, is the most important to the final results. In these graphs the error bars on the right show the central values and widths of the priors used for the opposite-parity and excited masses. At short distances, these masses are more accurately determined by the data, while at larger D_{min} the input prior controls the mass. The linear sizes of the symbols in these figures are proportional to the p value of the fit, with the size of the symbols in the legend corresponding to 50%. In the two-point

TABLE III: States expected to control the statistical errors on the correlators, for the pseudoscalars with physical valence-quark masses. The second column shows the state expected to control the growth of the statistical error on the correlator, the third column the mass gap between half the mass of the error state and the particle mass, and the fourth column the length scale for the growth of the fractional statistical error. Here $\bar{s}s$ is the unphysical flavor nonsinglet state, with mass 680 MeV.

State	Error	Energy gap (MeV)	Growth length (fm)
π	2π	0	∞
K	$\pi + \bar{s}s$	90	2.26
η_c	$2\eta_c$	0	∞
D_s	$\eta_c + \bar{s}s$	140	1.42
D	$\eta_c + \pi$	310	0.64

correlator fits used to choose the fit types and ranges, as in Figs. 2 and 3, autocorrelations among the lattices are minimized by first blocking the data in blocks of four lattices, or 20 to 24 molecular dynamics time units. However, statistical errors on results in later sections are obtained from the jackknife procedures described in Secs. IV A and IV B. In these analyses the two-point fits are repeated in each jackknife resampling. From these and similar graphs for other ensembles and different numbers of excited states, keeping the minimum distance in physical units reasonably constant, the minimum distances and fit forms in Table IV are chosen. The need for using a smaller minimum distance and including an excited state in the heavy-light fits is consistent with our expectations from Table III and Fig. 1. Because the statistical errors increase with distance from the source, the fits are much less sensitive to the choice of maximum distance. In most cases the maximum distance is taken to be one less than the midpoint of the lattice. However, in the $a \approx 0.09$ and 0.06 fm ensembles, the light-charm and charm-charm fits used a smaller maximum distance because having fewer points in the fit gave a better conditioned covariance matrix. These maximum distances are also included in Table IV.

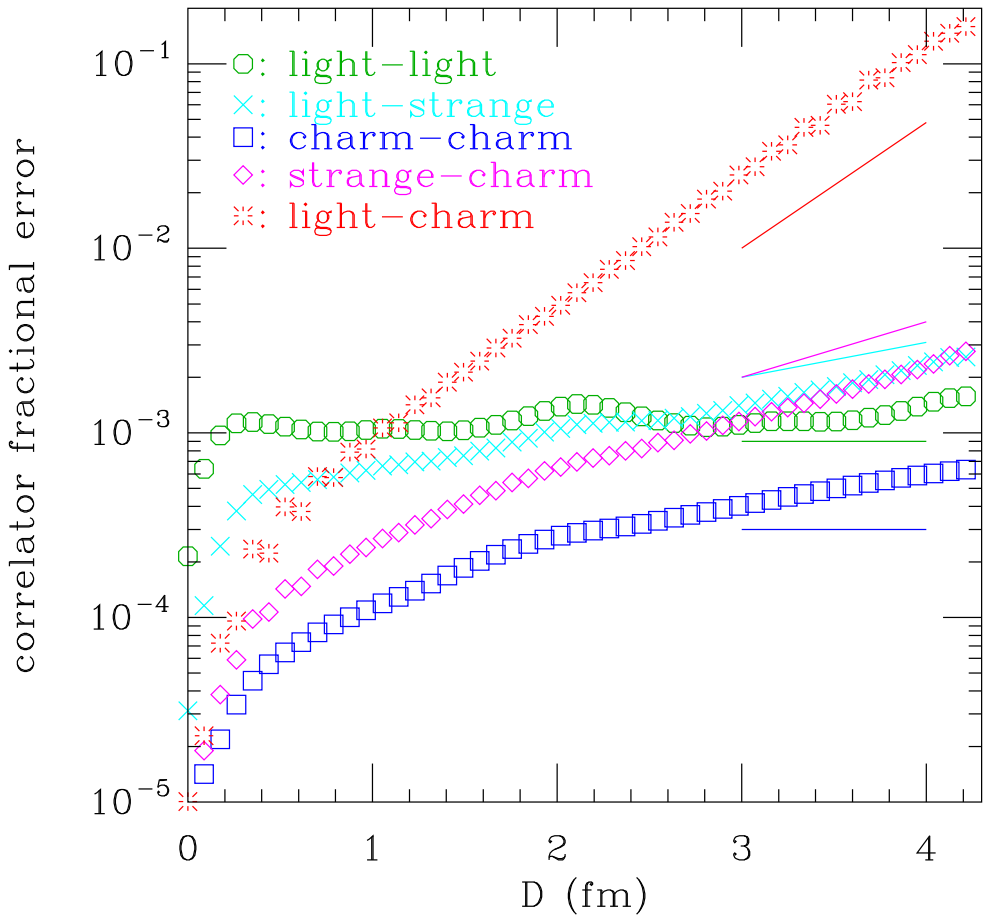

FIG. 1: Fractional errors for pseudoscalar correlators as a function of distance from the 0.09 fm physical quark-mass ensemble. The line segments show the slope expected from the states in Table III, which give a good approximation to the observed growth of the errors with the exception of the charm-charm correlator.

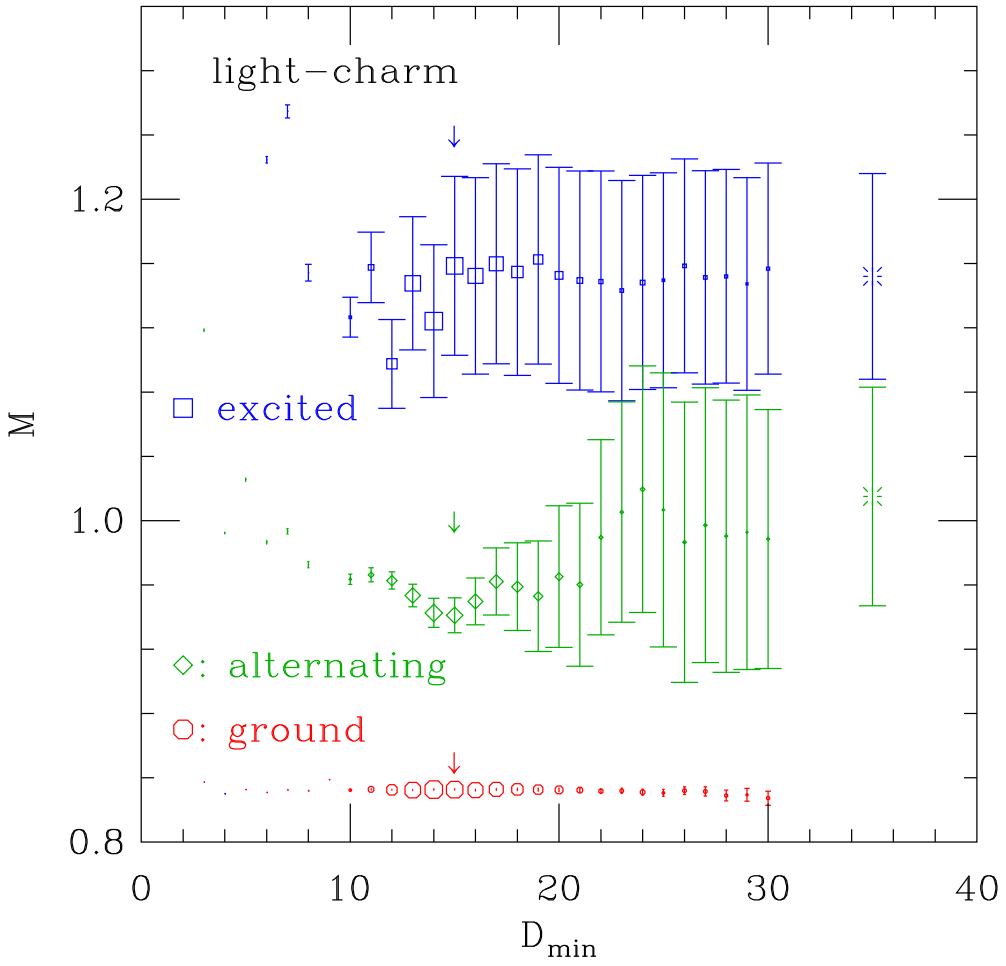

FIG. 2: Fits for the light-charm pseudoscalar correlator (mass M) in the ensemble with $a \approx 0.09$ fm and physical sea-quark masses. We plot the ground state, alternating state (opposite parity) and excited state masses as a function of minimum distance included in the fit. The size of the symbols is proportional to the p value of the fit, with the size of the symbols in the legend corresponding to 0.5. The two bursts on the right show the priors and their errors for the alternating and excited masses. The vertical arrows at $D_{min} = 15$ indicate the fit that is chosen. Further discussion is in the text.

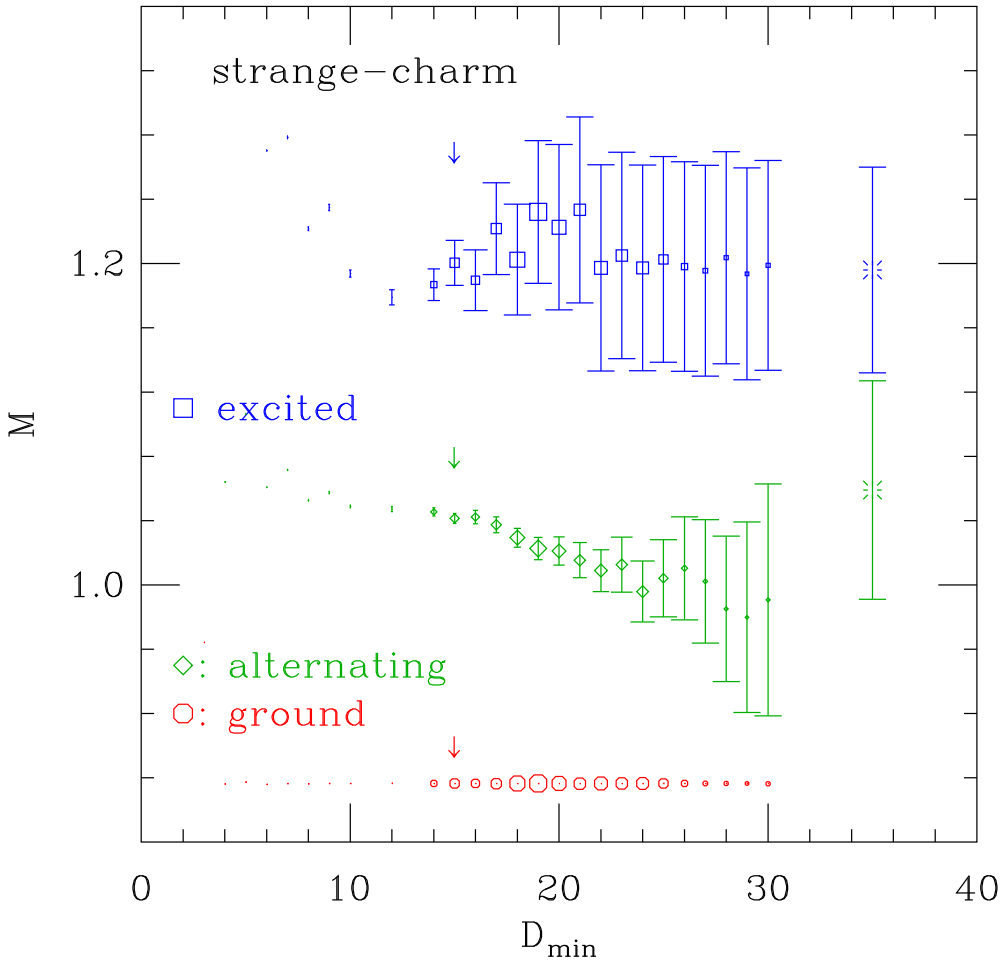

FIG. 3: Fits for the strange-charm correlator in the ensemble with $a \approx 0.09$ fm and physical sea-quark masses. The format and symbols are the same as in Fig. 2.

TABLE IV: Fit forms and minimum distance included for the two-point correlator fits. Here the fit form is the number of negative parity (*i.e.*, pseudoscalar) states "plus" the number of positive parity states. When the valence quarks have equal masses, the opposite-parity states are not included. In this work the charm-charm fits are needed only for computing the mass of the η_c meson, used as a check on the quality of our charm physics.

	light-light			light-charm			charm-charm		
	form	D_{min}	D_{max}	form	D_{min}	D_{max}	form	D_{min}	D_{max}
$a \approx 0.15$ fm	1+1	16	23	2+1	8	23	2+0	9	23
$a \approx 0.12$ fm	1+1	20	31	2+1	10	31	2+0	12	23
$a \approx 0.09$ fm	1+1	30	47	2+1	15	37	2+0	18	35
$a \approx 0.06$ fm	1+1	40	71	2+1	20	51	2+0	21	50

IV. DETERMINATION OF DECAY CONSTANTS AND QUARK-MASS RATIOS

This section describes the details of the analyses that produce our results for light-light and heavy-light decay constants and the ratios of quark masses. We perform two versions of the analysis. The first, the "physical-mass analysis" described in Sec. IV A, is a straightforward procedure that essentially uses only the physical-quark mass ensembles. On these ensembles, a chiral extrapolation is not needed: only interpolations are required in order to find the physical quark-mass point. The physical-mass analysis produces our results for quark-mass ratios and f_{K^+}/f_{π^+}, as well as some additional intermediate quantities required for the chiral analysis of the D meson decay constants, described in Sec. IV B. The second analysis of charm decay constants, described in Sec. IV B, uses chiral perturbation theory to perform a combined fit to all of our physical-mass and unphysical-mass data, and to thereby significantly reduce the statistical uncertainties of the results. We take the more precise values of f_{D^+}, f_{D_s}, and their ratio from the chiral analysis as our final results, and use those from the simpler physical-mass analysis only as a consistency check, and to aid in the estimation of systematic errors.

In the physical-mass analysis of Sec. IV A, we first determine the lattice spacing and quark masses separately for each ensemble, using, in essence, the five experimental values of f_{π^+}, M_{π^0}, M_{K^0}, M_{K^+} and M_{D_s}, as explained in Sec. IV A 1. In order to adjust for mistuning of the sea-quark masses, we perform a parallel scale-setting and quark-mass determination on the unphysical-mass ensembles; there, however, an extrapolation in the valence-quark mass is generally required. We extrapolate the quark-mass ratios to the continuum, after small sea-quark mistuning adjustments, in Sec. IV A 2. We follow the same procedure on the physical-mass ensembles to also obtain values for decay constants. In particular, we update our result for f_{K^+}/f_{π^+} from Ref. [3]. Although the results for charm decay constants from the physical-mass analysis are not taken as our final values, they are used as additional inputs in the estimation of systematic errors from the continuum extrapolation. Finally, the physical-mass analysis allows us to make straightforward estimates of systematic errors coming from finite-volume and electromagnetic (EM) effects on the decay constants and quark-mass ratios, as described in Sec. IV A 3.

The values of the physical quark-mass ratios m_c/m_s, m_s/m_l, and (to a lesser extent, in order to take into account isospin-violating effects) m_u/m_d obtained in Sec. IV A are used

in the subsequent chiral analysis in Sec. IV B. Further, in the physical-mass analysis, we determine the useful quantity F_{p4s} [7], which is the light-light pseudoscalar decay constant F evaluated at a fiducial point with both valence masses equal to $m_{p4s} \equiv 0.4m_s$ and physical sea-quark masses. The meson mass at the same fiducial point, M_{p4s}, as well as the ratio $R_{p4s} \equiv F_{p4s}/M_{p4s}$, are similarly determined. The unphysical decay constant F_{p4s} provides an extremely precise and convenient quantity to set the relative scale in the chiral analysis (see Sec. IV B 2), while we use R_{p4s} to tune the strange sea-quark mass.

The chiral analysis of the decay constants of charm mesons is described in detail in Sec. IV B. With chiral perturbation theory, one can take advantage of all our data by including both the physical-mass and unphysical-mass ensembles in a unified procedure. In particular, the statistical error in Φ_{D^+} is slightly more than a factor of two smaller with the chiral analysis than in the physical-mass analysis of Sec. IV A. In addition, the use of the relevant form of staggered chiral perturbation theory for this case, heavy-meson, rooted, all-staggered chiral perturbation theory (HMrASχPT) [24], allows us to relate the quark-mass and lattice-spacing dependence of the data, and thereby use the unphysical-mass ensembles to tighten the control of the continuum extrapolation. Our final central values for the charm decay constants given in the conclusions are taken from the chiral analysis. We increase some of the systematic uncertainties, however, to take into account differences with the results of the physical-mass analysis.

A. Simple analysis from physical quark-mass ensembles

Here we determine the quark-mass ratios and decay constants employing primarily the physical quark-mass ensembles. First, in Sec. IV A 1, we determine the lattice spacing, quark masses, and decay constants separately for each ensemble. Next, in Sec. IV A 2, we adjust the quark masses and decay constants for slight sea-quark mass mistuning, and extrapolate to the continuum. Finally, we estimate the systematic uncertainties in the quark-mass ratios and decay constants in Sec. IV A 3. We present results and error budgets for these quantities obtained from the physical mass analysis in Table VI.

1. *Valence-quark mass interpolation*

In this stage of the analysis we determine tuned quark masses and the lattice spacing (using f_{π^+} to fix the scale) for each ensemble, and then find the decay constants by interpolation or extrapolation in valence-quark mass to these corrected quark masses. There are a number of possible choices for the procedure used, and we include the differences among a few sets of choices in our systematic error estimate. It is important to remember that there is inherent ambiguity in defining a lattice spacing for ensembles with unphysical sea-quark masses, but all sensible choices should have the same limit at zero lattice spacing and physical sea-quark masses. For example, in the ensemble-by-ensemble fitting procedure described in this section, we take the value of f_{π^+} on each ensemble to be 130.41 MeV, independent of sea-quark masses, while for the chiral perturbation theory analysis we take the lattice spacing to be independent of the sea-quark masses.

Figure 4 illustrates some of the features of our procedure, and referring to it may help clarify the following description. Since the decay amplitude F depends on valence-quark mass, and we wish to use $f_{\pi^+} = 130.41$ MeV to set the lattice scale, we must determine the lattice spacing and tuned light-quark mass simultaneously. To do so, we find the light valence-quark mass where the mass and amplitude of the pseudoscalar meson with degenerate valence quarks have the physical ratio of $M_\pi^2/f_{\pi^+}^2$. (Actually we adjust this ratio for finite size effects, using the pion mass and decay constant in a 5.5 fm box. This correction is discussed in Sec. IV A 3.) This light-quark mass is the average of the up and down quark masses, $m_l = (m_u + m_d)/2$. Here we use the mass of the π^0, since it is less affected by electromagnetic corrections than the π^+. Since the π^+ contains one up and one down quark, the error in f_{π^+} from using degenerate light valence quarks is negligible. This tuning is illustrated in the upper left panel of Fig. 4, which shows this ratio as a function of light valence mass for the 0.09 fm physical quark-mass ensemble, one of the two ensembles that are most important in our analysis. The octagons in this panel are the ratio at the valence-quark masses where we calculated correlators, with error bars that are too small to be visible. The horizontal red line is the desired value of this ratio, and the green vertical line shows the light-quark mass where the ratio has its desired value. With the tuned light-quark mass determined, we use the decay amplitude at this mass, f_{π^+}, to fix the lattice spacing.

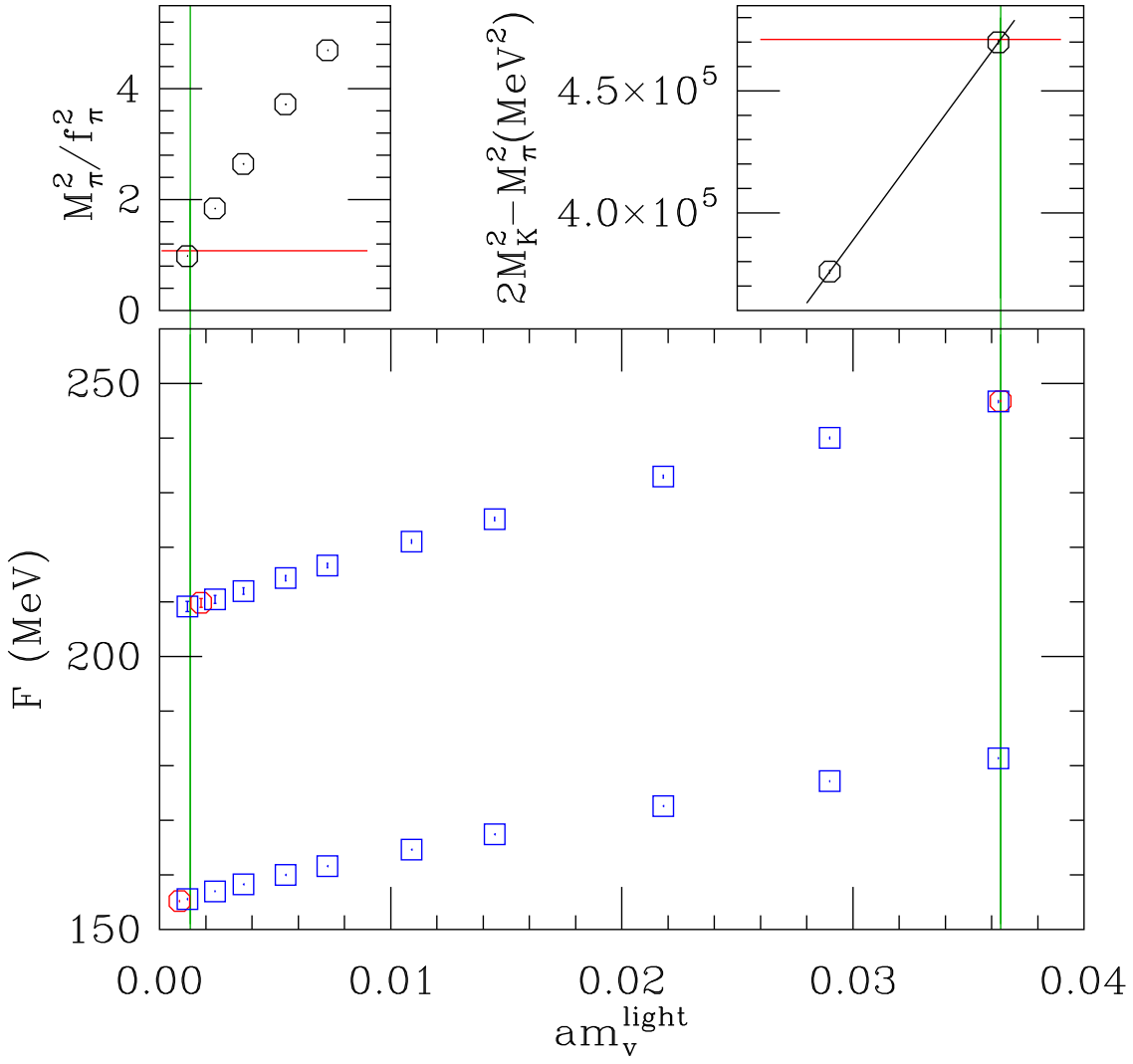

FIG. 4: Illustration of the "f_π" tuning for the $a \approx 0.09$ fm physical quark mass ensemble. F is the decay constant of a generic pseudoscalar meson. The procedure illustrated is described in the text.

In performing the interpolation or extrapolation of M_π^2/f_π^2 we use points with degenerate light valence-quark mass $m_{\rm v}$ and employ a continuum, partially quenched, SU(2) χPT form [22, 23],

$$\begin{aligned}\frac{M_\pi^2}{f_\pi^2} &= \frac{B2m_{\rm v}}{f^2}\left\{1+\frac{1}{16\pi^2 f^2}\left[B(4m_{\rm v}-2m_l')\log(2Bm_{\rm v}/\Lambda_\chi^2)\right.\right.\\ &\qquad\left.\left.+4B(m_{\rm v}+m_l')\log(B(m_{\rm v}+m_l')/\Lambda_\chi^2)\right]+Cm_{\rm v}\right\}\\ f_\pi &= f\left\{1-\frac{2B(m_{\rm v}+m_l')}{16\pi^2 f^2}\log(B(m_{\rm v}+m_l')/\Lambda_\chi^2)+Cm_{\rm v}+Dm_{\rm v}^2\right\}\ , \end{aligned} \tag{4}$$

where m_l' is the light sea-quark mass and Λ_χ is the chiral scale. In applying Eq. (4), we fix the low energy constants B and f in the coefficients of the logarithms to values determined from lowest order χPT using the smallest valence-quark mass. We then fix the coefficients of $m_{\rm v}$ and $m_{\rm v}^2$ in M_π^2/f_π^2 using the smallest two valence-quark masses available, and we fix the analytic coefficients in f_π using the three smallest valence-quark masses. In the physical quark-mass ensembles, such as the one shown in Fig. 4, this is only a small correction to the quark mass. On the other hand, in most of the ensembles with $m_l'/m_s' = 0.1$ or 0.2, the lightest valence-quark mass is $0.05m_s'$ or $0.1m_s'$, and a significant extrapolation is made. However, these unphysical-mass ensembles are used only in the analysis of this section to correct the results of the physical-mass ensembles for small mistunings of the sea masses in the physical-mass ensembles.

We then fix the tuned strange quark mass to the mass that gives the correct $2M_K^2 - M_\pi^2$. This is illustrated in the upper right panel of Fig. 4. In all of our ensembles, we use valence "strange" quark masses at the expected strange quark mass and at 0.8 times this mass. The two data points shown in the figure have these strange masses and the lightest available light-quark valence mass. A linear interpolation or extrapolation is performed through these two points. Again, the horizontal red line shows the desired value of this mass difference, and the vertical green line the resulting value of m_s. In this stage of the tuning the kaon mass is corrected for finite volume effects, electromagnetic effects and isospin breaking effects, where again we defer the details to the discussion of systematic errors in Sec. IV A 3.

Next we determine the up-down quark mass difference, and hence the up and down quark

masses. We use the difference in K^0 and K^+ masses,

$$m_d - m_u = \frac{M^2_{K^0_{\rm adj}} - M^2_{K^+_{\rm adj}}}{\frac{\partial M^2_K}{\partial m_l}} \quad . \tag{5}$$

Here the kaon masses are adjusted for finite volume and electromagnetic effects, and again we defer the details to Sec. IV A 3. We note that the electromagnetic corrections are a small effect on the strange quark mass tuning, but are absolutely crucial in the determination of $m_d - m_u$. To estimate the derivative $\partial M^2_K/\partial m_l$, we use the masses of kaons containing a valence quark near the strange quark mass and a second valence quark that is one of the two lightest valence quarks we have.

Then the tuned charm quark mass is determined from the experimental value of M_{D_s}. We use M_{D_s} rather than M_D because it has much smaller statistical errors. In all of our ensembles we have correlators with valence-quark masses at the expected charm quark mass and at 0.9 times this mass. Using linear interpolations in m_s of the D_s meson mass at these two "charm" masses to the strange quark mass found earlier, and a linear interpolation in m_c between these, we find a tuned charm quark mass.

Now that we have found the lattice spacing and tuned quark masses, we can find decay constants and masses of other mesons by interpolating or extrapolating to these quark masses. The bottom panel of Fig. 4 illustrates this process. The lower set of points in this graph are the decay constants at each light valence mass, interpolated using the two "strange" valence masses to the tuned strange quark mass. Then f_{K^+} is found by extrapolating these points to the tuned m_u, illustrated by the red octagon at the lower left. Similarly, the upper set of data points is the decay constant at each light-quark mass, linearly interpolated or extrapolated using the two "charm" valence masses to the tuned m_c. This graph is then interpolated or extrapolated to the tuned m_d to find f_{D^+}, shown in the red octagon at the upper left, or to the tuned m_s to find f_{D_s}, shown by the red octagon at the upper right.

As checks on our procedure, we also similarly interpolate or extrapolate in the meson masses to find M_{D^0}, M_{D^+} and M_{η_c}.

2. Sea-quark mass adjustment and continuum extrapolation

In this stage we combine the results from the individual ensembles and fit to a function of the lattice spacing to find the continuum limit. We use the ensembles with unphysical

TABLE V: Tuned lattice spacings (using f_{π^+} to set the scale) and quark masses for the physical quark-mass ensembles. The quark mass entries show the light, strange and charm quark masses in units of the lattice spacing. The column labeled am' gives the run values of the sea quark masses.

a_{approx}(fm)	a_{tuned}(fm)	am'	am_{tuned}
0.15	0.15089(17)	0.00235/0.0647/0.831	0.002426(8)/0.06730(16)/0.8447(15)
0.12	0.12121(10)	0.00184/0.0507/0.628	0.001907(5)/0.05252(10)/0.6382(8)
0.09	0.08779(8)	0.0012/0.0363/0.432	0.001326(4)/0.03636(9)/0.4313(6)
0.06	0.05676(6)	0.0008/0.0220/0.260	0.000799(3)/0.02186(6)/0.2579(4)

sea-quark masses to make small adjustments for the fact that the sea-quark masses in the physical quark-mass ensembles were fixed after short tuning runs, and inevitably turned out to be slightly mistuned when the full runs are done. The amount of mistuning is shown in Table V, which gives the sea-quark masses and the tuned quark masses for the physical quark-mass ensembles.

Fitting to the lattice spacing dependence is straightforward, because the results from each ensemble are statistically independent. We have performed continuum extrapolations for the ratios of quark masses, m_u/m_d, m_s/m_l, and m_c/m_s, which come automatically from the fitting for each ensemble described in Sec. IV A 1. Figures 5, 6, and 7 show the results for each ensemble, together with fits to the lattice spacing dependence. In these plots the abscissa is $a^2\alpha_S$, where α_S is an effective coupling constant determined from taste violations in the pion masses. The relative value of α_S at a given coupling β, compared to its value at a fixed, fiducial coupling β_0, is given by

$$\frac{\alpha_S(\beta)}{\alpha_S(\beta_0)} = \sqrt{\frac{(a^2\bar{\Delta})_\beta \; a^2(\beta_0)}{(a^2\bar{\Delta})_{\beta_0} \; a^2(\beta)}} \,, \tag{6}$$

where $(a^2\bar{\Delta})_\beta$ is the mean squared taste splitting at coupling β, and $a(\beta)$ is the lattice spacing given below in Table VIII. Equation (6) assumes that $a^2\bar{\Delta}$ is proportional to $\alpha_S^2 a^2$, its leading behavior. We use $\beta_0 = 5.8$ in these plots, and scale α_S to agree with the coupling α_V at $\beta_0 = 5.8$, which in turn may be determined from the plaquette [33] as explained after Eq. (9) of Ref. [7].

In these figures the fit used to determine the central value is shown in black. This is a quadratic polynomial fit through the four physical quark-mass points. In this fit, small

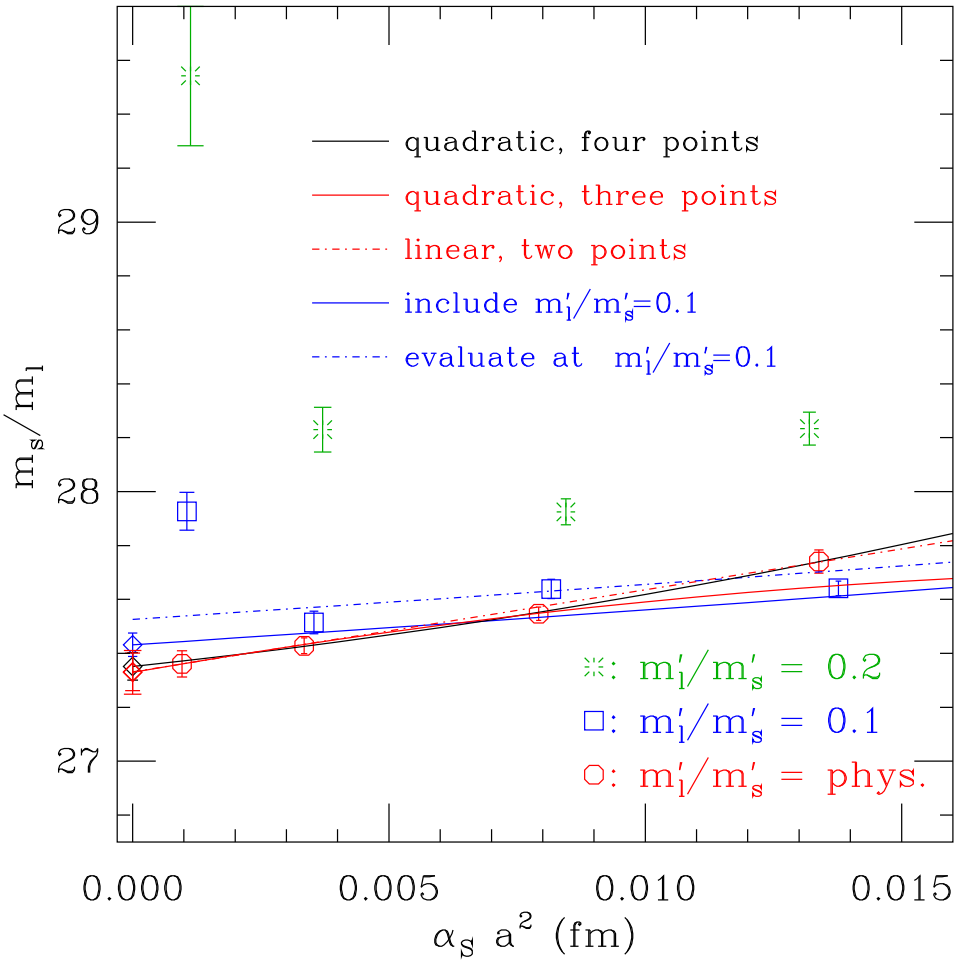

FIG. 5: The tuned ratio of strange quark mass to light-quark mass, m_s/m_l, on each ensemble, for the physical quark-mass ensembles (red octagons), for $m'_l/m'_s = 0.1$ (blue squares) and for $m'_l/m'_s = 0.2$ (green bursts). The fits shown in this and subsequent figures are described in the text. The diamonds at the left indicate the continuum extrapolations of the various fits.

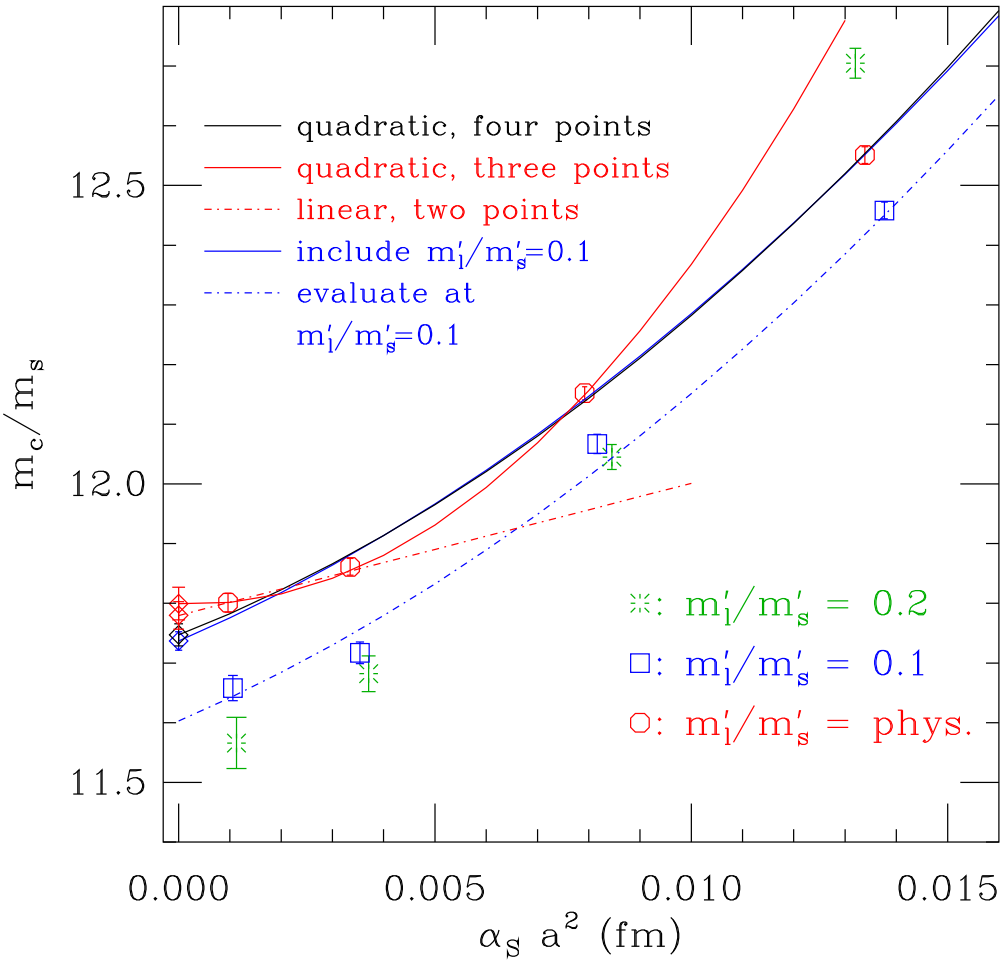

FIG. 6: The tuned ratio of charm quark mass to strange quark mass, m_c/m_s, on each ensemble. The notation and choice of fits is the same as in Fig. 5.

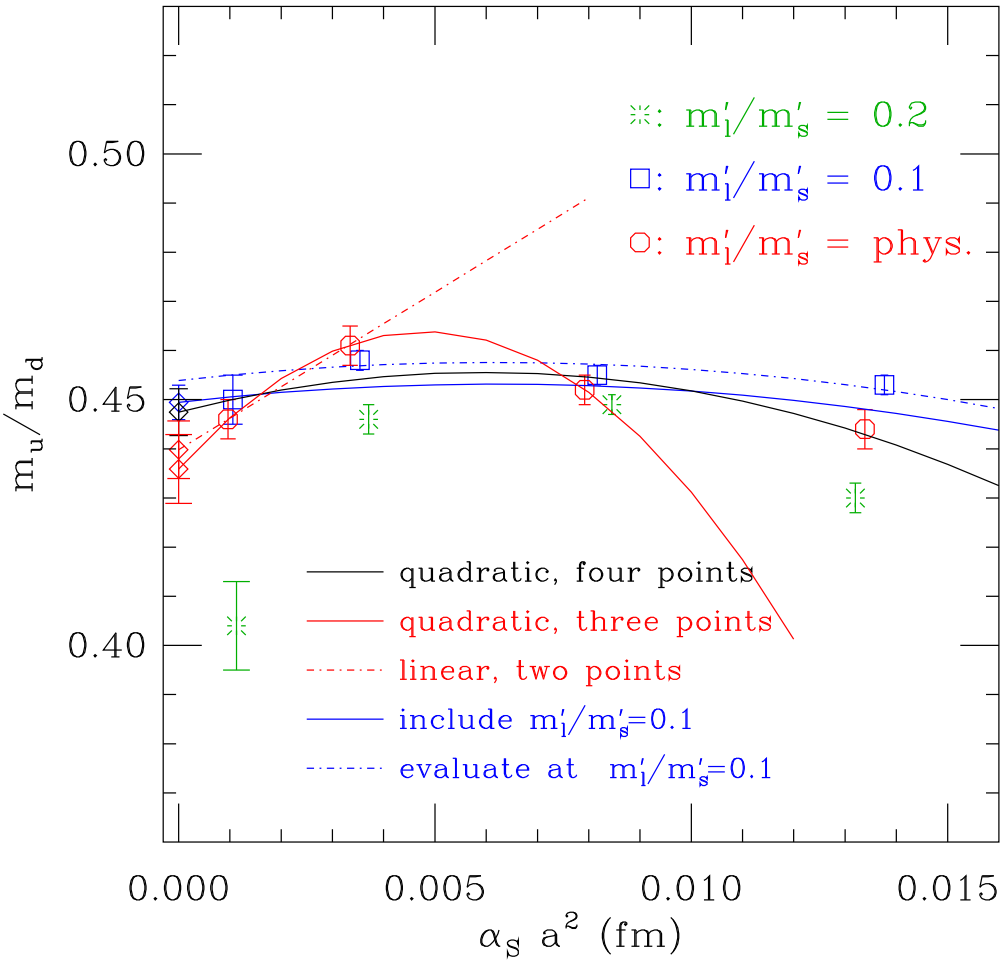

FIG. 7: The ratio of up quark mass to down quark mass, m_u/m_d, on each ensemble. The notation and choice of fits is the same as in Fig. 5.

adjustments have been made to compensate for sea-quark mass mistuning. To make these adjustments, the derivative of each quantity with respect to sea-quark mass is found from a fit including both the physical quark-mass ensembles and the $0.1m'_s$ ensembles, and this derivative is used to adjust each point in the fit. The resulting adjustments are too small to be visible in Figs. 5, 6, and 7. Other fits shown in these figures are used in estimating the systematic error resulting from our choice of fitting forms. The blue lines in each figure show the fit including the $0.1m'_s$ points, where the fit is quadratic in a^2 and linear in m'_l/m'_s. Here the solid line is the fit evaluated at the physical sea-quark mass, and the dashed line is the fit evaluated at $m'_l = 0.1m'_s$. The red lines are extrapolations using only the finer lattice spacings, while the curved solid line is a quadratic through the 0.06, 0.09 and 0.12 fm ensembles, and the dashed straight line a line through the finest two points. The diamonds at $\alpha_S a^2 = 0$ indicate the continuum extrapolations of the various fits. It is clear from the curvature in Figs. 5, 6, and 7 that a quadratic term is needed. However, it makes only a negligible difference whether this quadratic term is taken to be $(\alpha_S a^2)^2$, as is done here for convenience, or simply $(a^2)^2$. Other continuum extrapolations not shown here use $\alpha_V a^2$, where α_V is the strong coupling constant computed from the plaquette, or simply a^2 as the abscissa.

The four extrapolations in Figs. 5, 6, and 7, together with quadratic fits to the physical mass points using $\alpha_V a^2$ or a^2 as the abscissa, make a set of six continuum extrapolations for these and other quantities. The six versions are used to estimate the systematic errors of the quark mass ratios and light-meson decay constants, and to inform the systematic error analysis of Sec. IV B 4.

In Fig. 5 and, to a lesser extent in Figs. 6 and 7, the points at small lattice spacing with unphysical light sea quark masses deviate strongly from the physical sea quark mass points. This is mostly a partial quenching effect that shows up for valence quark masses small compared to the light sea quark mass. In particular, the squared pseudoscalar meson mass is increased by a partially quenched chiral log, which means that a smaller tuned light valence quark mass is needed to give the desired M^2/F^2. This has the direct effect of increasing m_s/m_l, with smaller effects on all other quantities. This is mostly seen at the smallest lattice spacing because at larger lattice spacings taste violations smear out the chiral logs. Note that this partial quenching effect has negligible effect on our results for m_s/m_l and m_c/m_s, which depend almost exclusively on the data from the physical-mass

ensembles.

We perform similar continuum extrapolations for the ratios of decay constants F_{p4s}/f_{π^+}, f_{K^+}/f_{π^+}, f_{D^+}/f_{π^+}, f_{D_s}/f_{π^+}, and f_{D_s}/f_{D^+}, and for M_{p4s} and $R_{p4s} = F_{p4s}/M_{p4s}$. Figure 8 shows the individual ensemble value and the same set of continuum extrapolations for the ratio f_{K^+}/f_{π^+}. As an example of a quantity involving a charm quark, Fig. 9 shows values and continuum extrapolations for the ratio f_{D_s}/f_{π^+}. The resulting continuum values for M_{p4s}, F_{p4s}/f_{π^+} and R_{p4s} are used in the later analysis in Sec. IV B, and the extrapolated value for f_{K^+}/f_{π^+} is our result for this quantity. The values for the charm-meson decay constants provide consistency checks on the analysis in Sec. IV B, and the spread in continuum values among the different extrapolations is included in our estimates of the systematic uncertainty from the continuum extrapolation. Finally, as a check, we extrapolate the mass of the η_c meson. These continuum extrapolations and their statistical errors are shown in Table VI.

Statistical errors on these quark mass ratios and decay constants are estimated with a jackknife method, where for each ensemble we perform the entire fitting procedure eliminating one configuration at a time. Autocorrelations are handled by estimating the final error from the variance of the jackknife resamples, after first blocking the jackknife results in blocks of 20 (eliminated) lattices, which corresponds to 100 molecular dynamics time units for the $a \approx 0.15$ and 0.12 fm ensembles and 120 time units for the $a \approx 0.09$ and 0.06 fm ensembles.

3. Finite volume and electromagnetic uncertainties

Our treatment of finite volume effects on the pion and kaon masses and decay constants is the same as described in Ref. [3], and we refer the reader to the discussion there. To summarize very briefly, we adjust these masses and decay constants to their values in a 5.5 fm box, the size of our physical quark mass lattices, and use these adjusted values in the tuning procedure described above. After the tuning and continuum extrapolation, at which point we have determined f_{K^+} in a 5.5 fm box, the adjustment is removed to get our result for f_{K^+} in infinite volume. As an estimate of the remaining finite size uncertainty we use the difference between results using staggered chiral perturbation theory and continuum chiral perturbation theory (NNLO for M_π and f_{π^+}, NLO for M_K and f_{K^+}) [3]. This difference, along with other systematic effects, is tabulated in Table VI. Finite size effects on the

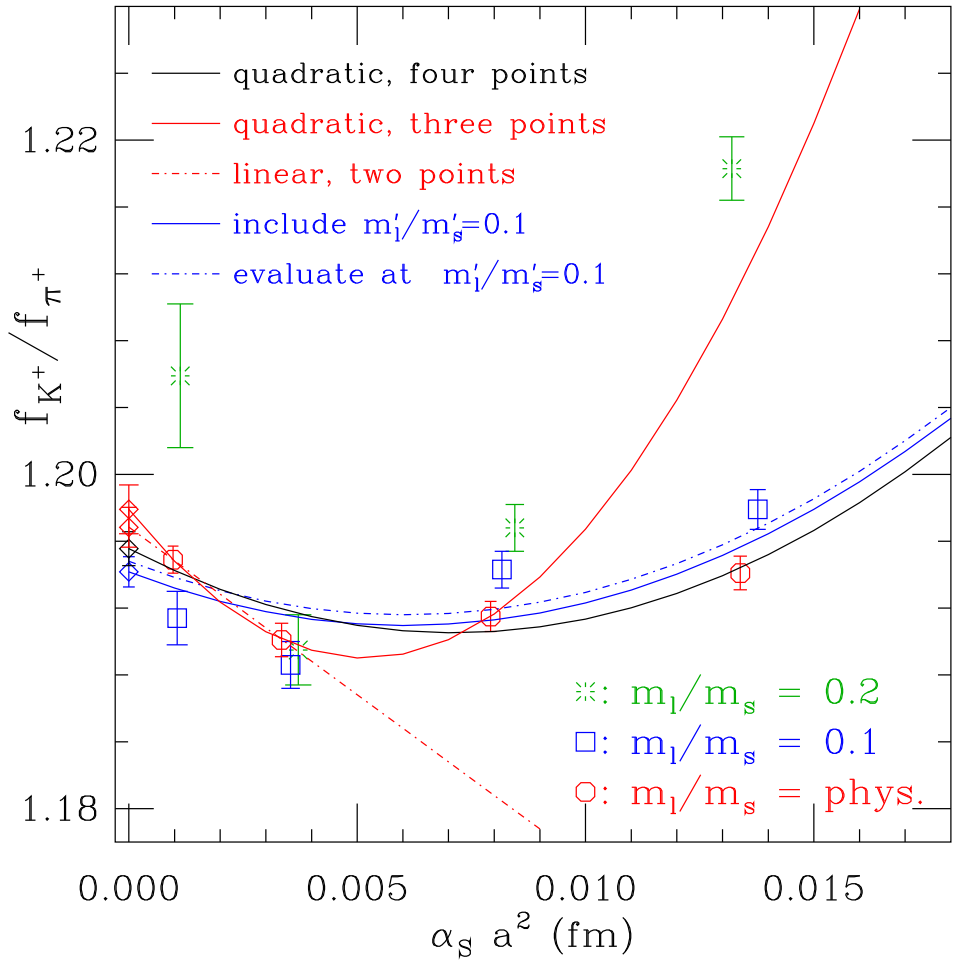

FIG. 8: The ratio f_{K^+}/f_{π^+} on each ensemble, The notation and choice of fits is the same as in Fig. 5.

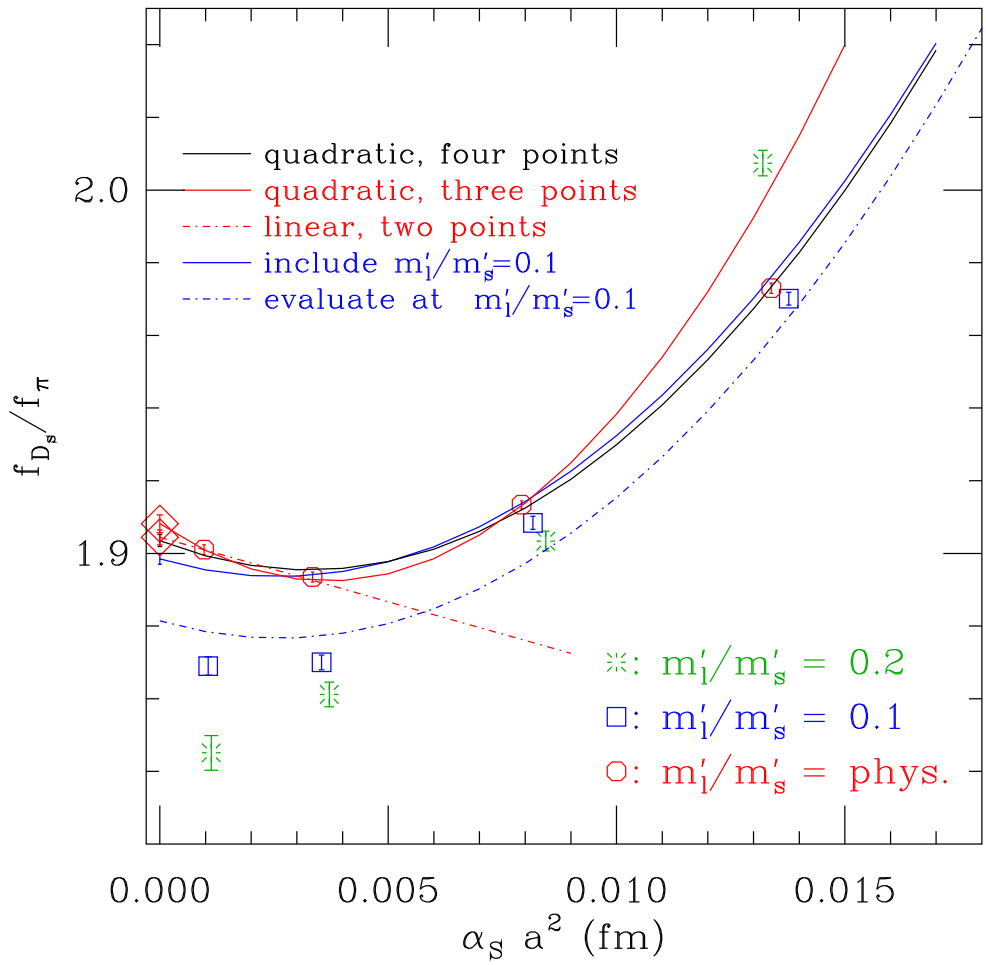

FIG. 9: The ratio f_{D_s}/f_{π^+} on each ensemble. The notation and choice of fits is the same as in Fig. 5.

TABLE VI: Values for various physical quantities evaluated at zero lattice spacing, as well as statistical and systematic errors, obtained from the simple physical-mass ensemble analysis. Here $\Phi_{D^+} \equiv f_{D^+}\sqrt{M_{D^+}}$ etc. We also include the p value of the central fit of this analysis. For the systematic errors, we tabulate the amount by which the central values change. Finite size errors are the difference between results using staggered chiral perturbation theory and continuum chiral perturbation theory (NNLO for M_π and f_{π^+}, NLO for M_K and f_{K^+}) [3]. "EM1" is the effect of varying ϵ by 0.021, or one standard deviation. "EM2" is the effect of subtracting 450 MeV^2 from M_K^2. "EM3" is the effect of lowering the D_s meson mass by 1 MeV. "Cont. extrap." is the full amount of variation among the alternative continuum extrapolation fits. "Priors" is the effect of using narrower priors for the mass gaps in the 0.09 and 0.06 fm physical quark mass correlator fits. More details on these systematic effects are in the text.

Quantity	Central value	stat.	p val.	Finite size	EM1	EM2	EM3	Cont. extrap.	Priors
M_{η_c}	2982.33	0.35	0.18	0.29	0.11	0.35	−1.81	$^{+1.41}_{-0.88}$	0.01
f_{K^+}/f_{π^+}	1.1956	0.0010	0.025	−0.0010	−0.0003	−0.0004	0.0000	$^{+0.0023}_{-0.0014}$	0.0002
F_{p4s}	153.90	0.09	0.10	−0.15	−0.02	−0.05	0.00	$^{+0.14}_{-0.23}$	0.00
M_{p4s}	433.24	0.17	0.11	−0.02	−0.12	−0.41	0.00	$^{+0.01}_{-0.33}$	−0.01
R_{p4s}	0.35527	0.00024	0.035	−0.00030	0.00007	0.00023	0.00000	$^{+0.00052}_{-0.00015}$	0.00001
m_u/m_d	0.4482	0.0048	0.025	0.0001	−0.0156	0.0000	0.0000	$^{+0.0021}_{-0.0115}$	0.0000
m_s/m_l	27.352	0.051	0.72	−0.039	−0.015	−0.053	0.000	$^{+0.080}_{-0.020}$	−0.001
m_c/m_s	11.747	0.019	0.010	−0.006	0.009	0.025	−0.010	$^{+0.052}_{-0.032}$	0.001
f_{D_s}/f_{D^+}	1.1736	0.0036	0.97	0.0003	−0.0003	−0.0003	0.0000	$^{+0.0004}_{-0.0015}$	−0.0002
f_{D^+}/f_{π^+}	1.6232	0.0057	0.59	−0.0016	0.0003	0.0000	−0.0001	$^{+0.0097}_{-0.0034}$	0.0006
f_{D_s}/f_{π^+}	1.9035	0.0017	0.010	−0.0015	−0.0001	−0.0004	−0.0001	$^{+0.0089}_{-0.0050}$	−0.0001
Φ_{D^+}	9161.5	33.7	0.61	−9.3	1.6	0.6	−3.1	$^{+16.1}_{-44.9}$	3.0
Φ_{D_s}	11012.9	9.7	0.007	−8.9	−0.7	−2.6	−3.4	$^{+51.6}_{-28.8}$	−0.1

charm-meson masses and decay constants are, as expected, quite small. Figure 10 shows the charm-meson masses and decay constants on the three ensembles differing only in spatial size, showing no detectable finite size effects.

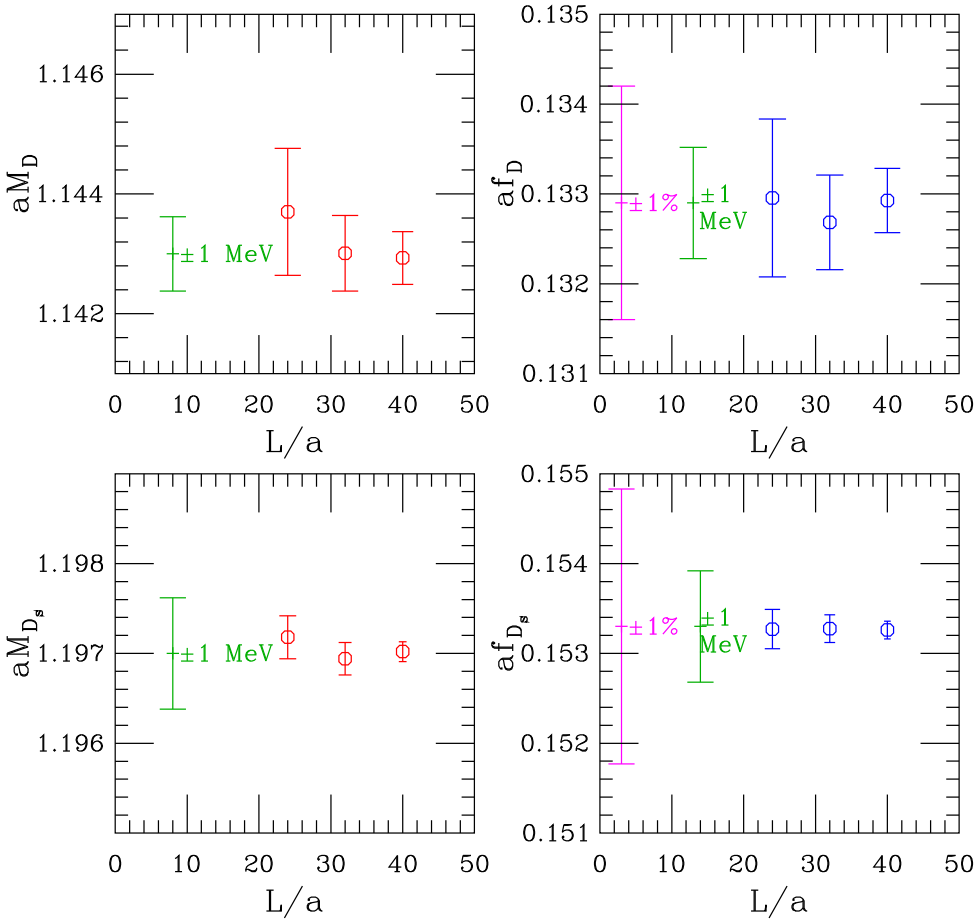

FIG. 10: Spatial size effects on M_D, M_{D_s}, f_D and f_{D_s}. To show the magnitude of the effects, green error bars show an arbitrary value ±1 MeV, and magenta error bars ±1%.

Our treatment of EM effects also follows Ref. [3], which in turn follows Ref. [2]. The current analysis uses updated inputs for the electromagnetic effects, so we repeat some of the discussion. Because our sea quarks are isospin symmetric, we adjust the experimental inputs to what they would be in a world without electromagnetism or sea-quark isospin violation before matching the simulation data to experiment to find the strange quark mass m_s and the average light-quark mass $\hat{m} = (m_u + m_d)/2$. Specifically, we do not adjust the neutral pion mass because the leading-order isospin correction to $M_{\pi^0}^2$ is $\propto (m_u - m_d)^2/\Lambda_\chi^2$ in χPT and therefore small, and the electromagnetic corrections vanish in the chiral limit for neutral mesons and are thus also small. For the kaon, we consider the isospin-averaged mass $M_{\hat{K}}^2 = (M_{K^+}^2 + M_{K^0}^2)_{\rm QCD}/2$, where the subscript "QCD" indicates that the leading EM effects in the masses are removed from the experimental masses [31]. To remove these effects we use results from our ongoing lattice QED+QCD simulations with asqtad sea quarks [34, 35] for the parameter ϵ that characterizes violations of Dashen's theorem:

$$(M_{K^\pm}^2 - M_{K^0}^2)^\gamma = (1+\epsilon)(M_{\pi^\pm}^2 - M_{\pi^0}^2)^\gamma \ , \tag{7}$$

where the superscript γ denotes the EM contribution to the splittings. In Refs. [34, 35], we found $\epsilon = 0.65(7)(14)(10)$, but this result did not yet adjust for finite volume effects on the photon field. A recent preliminary result [36] including finite volume effects is $\epsilon = 0.84(21)$, and we use that here.

We estimate the uncertainty due to EM effects by varying the values of the EM-subtracted meson masses used in the quark-mass tuning; this affects m_u the most. We vary the parameter ϵ by its error. We also consider possible EM effects on the neutral kaon mass itself, which are less well understood than the EM effects on the K^+–K^0 splitting that are described by ϵ. In Ref. [35], the EM contribution to the squared K^0 mass was estimated to be about 900 MeV^2. However, this estimate did not take into account the effects of EM quark mass renormalization, which should be subtracted from the result. A rough calculation of the renormalization effect (using one-loop perturbation theory) suggests it is of order of half the size of the contribution. We thus include as a systematic error the effect of shifting the squared K^0 mass by 450 MeV^2. We do not consider direct EM effects on the weak matrix elements f_{π^+}, f_{K^+}, f_{D^+} and f_{D_s}, which are by definition pure QCD quantities [31]. Such direct EM effects, however, are relevant in the extraction of CKM elements by comparison with experimental rates, as described in Sec. VI.

The shifts in various quantities resulting from these electromagnetic uncertainties are also tabulated in Table VI. The two effects labeled "EM1" and "EM2" are combined in quadrature to give our quoted EM systematic errors for m_s/m_l and f_{K^+}/f_{π^+}. The "EM3" column in Table VI shows the effect of lowering the input D_s meson mass by 1 MeV, an order-of-magnitude estimate for the electromagnetic effect on this mass, which affects the tuning of the charm-quark mass. This effect has not been directly determined in QCD+QED simulations. Although this affects Φ_D and Φ_{D_s} through the factor of $M_D^{1/2}$ or $M_{D_s}^{1/2}$ in these quantities, it has only a small effect on the decay constants. It leads to a significant uncertainty on m_c/m_s, and we include it in our systematic error estimate for this quantity.

B. Chiral perturbation theory analysis of f_D and f_{D_s} including unphysical quark-mass ensembles

In this section, we present the combined chiral extrapolation/interpolation and continuum extrapolations used to obtain the physical values of the D^+ and D_s meson decay constants. We first discuss chiral perturbation theory for all-staggered heavy-light mesons in Sec. IV B 1, giving the formulas used for the chiral fits and describing our method for incorporating discretization effects into the extrapolation. An explanation of our method for setting the lattice scale follows in Sec. IV B 2. Chiral perturbation theory assumes a mass-independent scale-setting procedure. In practice, we use F_{p4s} to set the scale and F_{p4s}/M_{p4s} to tune the strange sea-quark mass. We take these values from the physical quark-mass analysis in Sec. IV A. This means that the absolute scale comes ultimately from f_{π^+}, which is used to set the scale in Sec. IV A.

The chiral fits themselves are presented in Sec. IV B 3, while systematic errors in the chiral analysis are described in Sec. IV B 4. Chiral/continuum extrapolation errors are found by considering a large number (18) of alternative chiral fits, as well as six versions of the continuum extrapolation of the inputs, resulting in 108 possibilities. We also estimate finite volume and EM errors within the chiral analysis by propagating the errors in the corresponding inputs through the chiral fits. Equations (28)–(30) show our results for the charm decay constants from the self-contained chiral analysis with complete systematic error budgets.

1. *Chiral perturbation theory for f_{D^+} and f_{D_s}*

The quark-mass and lattice-spacing dependence of the decay constant has been derived at one loop in heavy-meson, rooted, all-staggered chiral perturbation theory (HMrASχPT) in Ref. [24]. At fixed heavy-quark mass m_Q, one may argue following Ref. [37] that inclusion of hyperfine splittings (*e.g.*, $M_D^* - M_D$) and flavor splittings (*e.g.*, $M_{D_s} - M_D$), but no other $1/m_Q$ effects, constitutes a systematic approximation at NLO in HMrASχPT. The argument is based on the power counting introduced by Boyd and Grinstein [38]. With v denoting the light valence quark, Y the v$\bar{\text{v}}$ valence meson, and $\Phi_{D_\text{v}} \equiv f_{D_\text{v}}\sqrt{M_{D_\text{v}}}$, Ref. [24] obtains for the pseudoscalar-taste heavy-light meson:

$$
\begin{aligned}
\Phi_{D_\text{v}} \;=\; \Phi_0\Bigg\{ 1 + \frac{1}{16\pi^2 f^2}\frac{1}{2}\Bigg(& -\frac{1}{16}\sum_{\mathcal{S},\Xi}\ell(M^2_{\mathcal{S}\text{v},\Xi}) - \frac{1}{3}\sum_{j\in\mathcal{M}_I^{(3,\text{v})}}\frac{\partial}{\partial M^2_{Y,I}}\Big[R_j^{[3,3]}(\mathcal{M}_I^{(3,\text{v})};\mu_I^{(3)})\ell(M_j^2)\Big] \\
& - \Big(a^2\delta'_V \sum_{j\in\mathcal{M}_V^{(4,\text{v})}}\frac{\partial}{\partial M^2_{Y,V}}\Big[R_j^{[4,3]}(\mathcal{M}_V^{(4,\text{v})};\mu_V^{(3)})\ell(M_j^2)\Big] + [V\to A]\Big) \\
& - 3g_\pi^2\frac{1}{16}\sum_{\mathcal{S},\Xi} J(M_{\mathcal{S}\text{v},\Xi},\Delta^* + \delta_{\mathcal{S}\text{v}}) - g_\pi^2\sum_{j\in\mathcal{M}_I^{(3,\text{v})}}\frac{\partial}{\partial M^2_{Y,I}}\Big[R_j^{[3,3]}(\mathcal{M}_I^{(3,\text{v})};\mu_I^{(3)})J(M_j,\Delta^*)\Big] \\
& - 3g_\pi^2\Big(a^2\delta'_V\sum_{j\in\mathcal{M}_V^{(4,\text{v})}}\frac{\partial}{\partial M^2_{Y,V}}\Big[R_j^{[4,3]}(\mathcal{M}_V^{(4,\text{v})};\mu_V^{(3)})J(M_j,\Delta^*)\Big] + [V\to A]\Big)\Bigg) \\
& + L_\text{s}(x_u + x_d + x_s) + L_\text{v}x_\text{v} + L_a\frac{x_{\bar{\Delta}}}{2}\Bigg\}\,,
\end{aligned}
\tag{8}
$$

where Φ_0, L_s, L_v, and L_a are low-energy constants (LECs); the indices $\mathcal{S}$ and Ξ run over sea-quark flavors and meson tastes, respectively; Δ^* is the lowest-order hyperfine splitting; $\delta_{\mathcal{S}\text{v}}$ is the flavor splitting between a heavy-light meson with light quark of flavor $\mathcal{S}$ and one of flavor v; and g_π is the D-D^*-π coupling. In infinite volume, the chiral logarithm functions ℓ and J are defined by [23, 37]

$$
\ell(m^2) \;=\; m^2\ln\frac{m^2}{\Lambda_\chi^2} \qquad \text{[infinite volume]}, \tag{9}
$$

$$
J(M,\Delta) \;=\; (M^2 - 2\Delta^2)\log(M^2/\Lambda^2) + 2\Delta^2 - 4\Delta^2 F(M/\Delta) \qquad \text{[infinite volume]}, \tag{10}
$$

with [39]

$$
F(1/x) \equiv \begin{cases} -\frac{\sqrt{1-x^2}}{x}\left[\frac{\pi}{2} - \tan^{-1}\frac{x}{\sqrt{1-x^2}}\right], & \text{if } |x|\le 1, \\ \frac{\sqrt{x^2-1}}{x}\ln(x+\sqrt{x^2-1}), & \text{if } |x|\ge 1. \end{cases} \tag{11}
$$

The residue functions $R_j^{[n,k]}$ are given by

$$R_j^{[n,k]}\left(\{m\};\{\mu\}\right) \equiv \frac{\prod_{i=1}^{k}(\mu_i^2 - m_j^2)}{\prod_{r\neq j}^{n}(m_r^2 - m_j^2)} \ . \tag{12}$$

The sets of masses in the residues are

$$\mu^{(3)} = \{m_U^2, m_D^2, m_S^2\} \ , \tag{13}$$

$$\mathcal{M}^{(3,\mathrm{v})} = \{m_Y^2, m_{\pi^0}^2, m_\eta^2\} \ , \tag{14}$$

$$\mathcal{M}^{(4,\mathrm{v})} = \{m_Y^2, m_{\pi^0}^2, m_\eta^2, m_{\eta'}^2\} \ . \tag{15}$$

Here taste labels (*e.g.*, I or V for the masses) are implicit. We define dimensionless quark masses and a measure of the taste splitting by

$$x_{u,d,s,\mathrm{v}} \equiv \frac{4B}{16\pi^2 f_\pi^2} m_{u,d,s,\mathrm{v}} \ , \text{ and } \qquad x_{\bar{\Delta}} \equiv \frac{2}{16\pi^2 f_\pi^2} a^2\bar{\Delta} \ , \tag{16}$$

where B is the LEC that gives the Goldstone pion mass $M_\pi^2 = B(m_u + m_d)$, and $a^2\bar{\Delta}$ is the mean-squared pion taste splitting. The x_i are natural variables of HMrASχPT; the LECs L_s, L_v, and L_a are therefore expected to be $\mathcal{O}(1)$. All ensembles in the current analysis have degenerate light sea quarks: $x_u = x_d \equiv x_l$. The taste splittings have been determined to $\sim$ 1–10% precision [7] and are used as input to Eq. (8), as are the taste-breaking hairpin parameters δ'_A and δ'_V, whose ranges are taken from chiral fits to light pseudoscalar mesons [40].

To include the finite-volume effects for a spatial volume L^3 in Eq. (8), we replace [37]

$$\ell(m^2) \ \to \ \ell(m^2) + m^2\delta_1(mL) \qquad \text{[finite volume]}, \tag{17}$$

$$J(m,\Delta) \ \to \ J(m,\Delta) + \delta J(m,\Delta,L) \qquad \text{[finite volume]}, \tag{18}$$

where

$$\delta J(m,\Delta,L) = \frac{m^2}{3}\delta_1(mL) - 16\pi^2\left[\frac{2\Delta}{3}J_{FV}(m,\Delta,L) + \frac{\Delta^2 - m^2}{3}K_{FV}(m,\Delta,L)\right] \ , \tag{19}$$

with

$$K_{FV}(m,\Delta,L) \equiv \frac{\partial}{\partial\Delta}J_{FV}(m,\Delta,L), \tag{20}$$

and with $\delta_1(mL)$ and $J_{FV}(m,\Delta,L)$ defined in Refs. [41, 42].

Because we have data with $\sim$1% to less than 0.1% statistical errors and 314 to 366 data points (depending on whether $a \approx 0.15$ fm is included), NLO HMrASχPT is not adequate

to describe fully the quark-mass dependence, in particular for masses near m_s. We therefore include all NNLO and NNNLO mass-dependent analytic terms. There are four independent functions of $x_{\rm v}$, x_l and x_s at NNLO and seven at NNNLO, for a total of eleven additional fit parameters. It is not necessary to keep all the seven terms appearing at NNNLO to get a good fit, nevertheless we include all of them to make it a systematic approximation at the level of analytic terms.

While Eq. (8) is a systematic NLO approximation for the decay constant at fixed m_Q, we have data on each ensemble with two different values of the valence charm mass: m'_c and $0.9m'_c$, where m'_c is the value of the charm sea mass of the ensembles, and is itself not precisely equal to the physical charm mass m_c because of tuning errors, which are in some cases as large as this difference (*i.e.*, 10% of m'_c). Since such changes in the value of the charm mass lead to corrections to decay constants that are comparable in size to those from the pion masses at NLO, Eq. (8) needs to be modified in order to fit the data. We therefore allow the LEC Φ_0 to depend on m_Q as suggested by HQET. For acceptable fits to the highly correlated data at valence charm masses m'_c and $0.9m'_c$, we need to introduce both $1/m_Q$ and $1/m_Q^2$ terms. (For more details see Appendix A.) Furthermore, Φ_0 has generic lattice-spacing dependence that must be included to obtain good fits. With HISQ quarks, the leading generic discretization errors are $\mathcal{O}(\alpha_S a^2)$. But because the high degree of improvement in the HISQ action drastically reduces the coefficient of these leading errors, formally higher $\mathcal{O}(a^4)$ errors are also apparent, as can be seen from the curvature in Figs. 5 – 9. In Eq. (8), we thus replace

$$\Phi_0 \to \Phi_0 \left(1 + k_1 \frac{\Lambda_{\rm HQET}}{m_Q} + k_2 \frac{\Lambda_{\rm HQET}^2}{m_Q^2}\right) \left(1 + c_1 \alpha_S (a\Lambda)^2 + c_2 (a\Lambda)^4\right) , \tag{21}$$

where the k_i are new physical LECs, c_i are additional fit parameters, $\Lambda_{\rm HQET}$ is a physical scale for HQET effects, and Λ is the scale of discretization effects.

In cases where the valence and sea values of the charm quark mass differ, m_Q in Eq. (21) is taken equal to the valence mass. This is based on the expectation from decoupling [43] that effects due to variations in the charm sea mass on low-energy physical quantities are small. Note that HQET tells us that heavy-light decay constants come from the physics of the light-quark at scale $\Lambda_{\rm QCD}$, despite the presence of the heavy valence quark. Thus we do not introduce extra terms corresponding to the charm sea mass here. As discussed in Sec. IV B 4, however, such terms are included in alternative fits used to estimate systematic

errors.

Generic dependence on a is also allowed for the physical LECs $L_{\rm s}$, $L_{\rm v}$, k_1 and k_2. However, because these parameters first appear at NLO in the chiral or HQET expansions, it is sufficient to include at most the leading a-dependence, for example:

$$L_{\rm v} \to L_{\rm v} + L_{{\rm v}\delta}\ \alpha_S(a\Lambda)^2 \tag{22}$$

Thus we add 4 fit parameters related to generic discretization effects: $L_{{\rm v}\delta}$, $L_{{\rm s}\delta}$, $k_{1\delta}$, and $k_{2\delta}$. There are also 3 parameters related to taste-violation effects: L_a, δ'_A and δ'_V. These parameters are taken proportional to the measured average taste splitting $a^2\bar{\Delta}$, which depends on a approximately as $\alpha_S^2 a^2$ [7]. In addition, we find that m_Q-dependent discretization errors must be considered if data at the coarsest lattice spacing ($a \approx 0.15$ fm) is included in the fits. This is not surprising because $am_c^{\rm phys} \approx 0.84$ at this lattice spacing, which by the power counting estimates of Ref. [4] suggests $\sim 5\%$ discretization errors (although this may be reduced by dimensionless factors). We therefore add $c_3\alpha_S(am_Q)^2 + c_4(am_Q)^4$ to the analytic terms in Eq. (8), where m_Q is taken to denote the valence charm mass. If the $a \approx 0.15$ fm data is omitted, good fits may be obtained with c_3 and c_4 set to zero. As discussed below, one can also add similar terms for the charm sea mass.

For the LEC g_π, a reasonable range is $g_\pi = 0.53(8)$, which comes from recent lattice calculations [44, 45]. When this central value and range are included as Bayesian priors, fits to our full data set tend to pull g_π low, several sigma below 0.53. Hence, we simply fix $g_\pi = 0.45$, 1-sigma below its nominal value, in our central fit. This problem is ameliorated for alternative fits, used to estimate the systematic errors, that drop the data at $a \approx 0.15$ fm or that use the experimental value of f_{K^+}, rather than that of f_{π^+}, for f in Eq. (8). Other alternatives considered in the systematic error estimates are to allow g_π to be a free parameter, or to keep it fixed at its nominal value.

2. Setting the Relative Lattice Scale

Relative scale setting in the combined chiral analysis is done using F_{p4s}. The value of F_{p4s} in physical units, which is only needed at the end of this analysis, has been obtained by comparison with f_{π^+} in Sec. IV A, as are the other needed inputs: $R_{p4s} \equiv F_{p4s}/M_{p4s}$ and the quark-mass ratios m_c/m_s, m_s/m_l and m_u/m_d. All those quantities are listed in Table VI.

We use F_{p4s} in the chiral analysis, rather than f_{π^+} itself, for several reasons. First of all, F_{p4s} gives highly-precise relative lattice spacings between ensembles. Precision scale setting is required in order to get good chiral fits to our large partially-quenched data set (366 points) with large correlations of the points within each ensemble. Second, F_{p4s} can be accurately adjusted for mistunings in the sea-quark masses using unphysical-mass ensembles for which the physical valence-quark mass values needed to find f_{π^+} can only be reached by extrapolation. Finally, and perhaps most importantly, there are no logarithms of light pseudoscalar masses ($\sim m_\pi$) in the SχPT expression for the decay constant [23] evaluated at the relevant quark masses for F_{p4s}. The lightest meson that enters is a valence-sea meson for quark masses $0.4m_s$ and m_l, which has mass $\sim$325 MeV (for the Goldstone taste). This means that F_{p4s} should be well approximated by its Taylor series in a^2, and we do not need to modify Eq. (8) to take into account chiral logarithms that enter through the scale-setting procedure. We have checked this assumption by performing a more complicated three-step analysis: (1) The degenerate light-light decay-constant data for all ensembles are fit to the NLO SχPT form of Ref. [23]. (2) From the fit, we determine F_{p4s} as a function of a^2. (3) The data for $\Phi_{D_v}/F_{p4s}^{3/2}$ are fit to Eq. (8) divided by the 3/2 power of $F_{p4s}(a^2)$. The results of this procedure differ from the results reported in Table IX below by less than half of the statistical errors, and the systematic errors are essentially the same in both approaches.

We use a mass-independent scale-setting scheme. We first determine aF_{p4s} and am_{p4s} on the physical-mass ensembles; then, by definition, all ensembles at the same β as a given physical-mass ensemble have a lattice spacing a and value of am_{p4s} equal to those of the physical-mass ensemble. Since we do not know the correct strange-quark mass until after the lattice spacing is fixed, aF_{p4s} and am_{p4s} must be determined self-consistently. We find am_{p4s} and aF_{p4s} on a given physical-mass ensemble by adjusting am_v until $aF/(aM)$ has the expected physical ratio R_{p4s}.

To determine aF_{p4s} and am_{p4s} accurately, data must be adjusted for mistunings in the sea-quark masses. The sea-quark masses of the physical-mass ensembles are tuned relatively well (especially at 0.09 and 0.06 fm), and adjustments are small. Nevertheless, the adjustments may change the final results of f_{D^+} and f_{D_s} by more than the size of the statistical errors.

To make these adjustments, we first find an approximate value of am_{p4s} on each physical-mass ensemble by passing a parabola through $(M/F)^2$ as a function of m_v, for the three values of m_v closest to m_{p4s}. The sea-quark masses are kept fixed (initially, to their values

in the run) in this process. We use $(M/F)^2$ here rather than F/M, since we expect M^2 to be approximately linear in $\mathrm{m_v}$, and F^2 to be approximately constant. The value of am_{v} where the ratio takes its expected value $1/R_{p4s}^2$ is the tentative value of am_{p4s}, and the corresponding value of aF is the tentative value of aF_{p4s}. The procedure also gives tentative values of the physical sea-quark masses in lattice units: $am_s \cong 2.5\, am_{p4s}$, $am_l \cong 2.5\, am_{p4s}/(m_s/m_l)$, and $am_c \cong 2.5\, am_{p4s}(m_c/m_s)$. We then adjust the data for aF and aM to the values they would have at the tentative new sea-quark masses, and iterate the whole process until it converges.

The adjustment of the data requires a determination of the following derivatives

$$\frac{\partial F^2}{\partial m'_l},\ \frac{\partial F^2}{\partial m'_s},\ \frac{\partial F^2}{\partial m'_c},\ \frac{\partial M^2}{\partial m'_l},\ \frac{\partial M^2}{\partial m'_s},\ \frac{\partial M^2}{\partial m'_c},\ \frac{\partial^2 M^2}{\partial m'_l \partial m_{\mathrm{v}}},\ \frac{\partial^2 M^2}{\partial m'_s \partial m_{\mathrm{v}}},\ \frac{\partial^2 M^2}{\partial m'_c \partial m_{\mathrm{v}}}, \tag{23}$$

where the derivatives should be evaluated at $m_{\mathrm{v}} = m_{p4s}$, and with m'_l, m'_s and m'_c at their physical values. All quantities here are in "$p4s$ units", which are (semi-) physical units in which aF and aM have been divided by (the tentative value of) aF_{p4s}, and quark masses in lattice units have been divided by (the tentative value of) am_{p4s} (and therefore do not require renormalization). The mixed partial derivatives with m_{v} are needed because we must adjust the data at different values of m_{v} in order to iterate the process. Because M^2 is approximately linear in m_{v}, the effect of the mixed partials in Eq. (23) is non-negligible, while mixed partials of F^2 may be neglected. Since the effects of mistunings are already not much larger than our statistical errors, we expect that we may neglect discretization errors and any mistuning effects in the derivatives themselves. This means that we may use, at all lattice spacings, the values determined for the derivatives in Eq. (23) at any one lattice spacing. This expectation is confirmed by alternative determinations of the derivatives, which give results in agreement with the method we now describe.

Many of the derivatives may be calculated using the twelve ensembles that we have at $a \approx 0.12$ fm. Figure 11 shows the light and strange sea masses of these ensembles. Most of the ensembles have the same charm sea masses, which allows us to determine the derivatives with respect to m'_l and m'_s accurately. We first convert the lattice data to $p4s$ units using (tentative values of) am_{p4s} and aF_{p4s}. Ensembles in which the light sea mass is tuned close to $0.1m'_s$, shown inside the dashed blue ellipse in Fig. 11, are then used to determine $\partial F^2/\partial m'_s$, $\partial M^2/\partial m'_s$ and $\partial^2 M^2/\partial m'_s \partial m_{\mathrm{v}}$. The three derivatives with respect to m'_s are found by fitting a quadratic function to the corresponding quantities of these ensembles, as

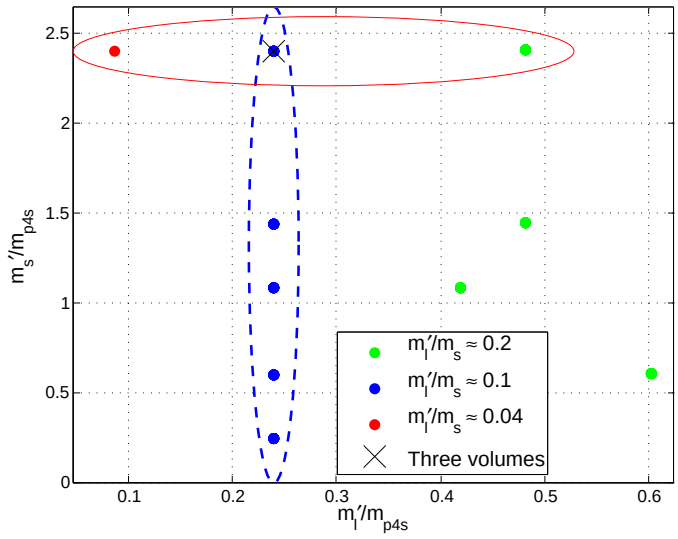

FIG. 11: Values of m'_s and m'_l of the ensembles at $\beta = 6.0$. At one value of m'_s and m'_l, indicated by the black cross, we have three ensembles with different volumes; the intermediate volume ensemble, which is equal in volume to all the other ensembles shown here, is used in our calculation of the derivatives. Five ensembles inside the blue ellipse are used to calculate $\partial F^2/\partial m'_s$, $\partial M^2/\partial m'_s$, and $\partial^2 M^2/\partial m'_s \partial m_{\rm v}$. These five ensembles have the same charm sea masses. Three ensembles inside the red ellipse are used to calculate $\partial F^2/\partial m'_l$, $\partial M^2/\partial m'_l$, and $\partial^2 M^2/\partial m'_l \partial m_{\rm v}$. One of these ensembles has a slightly different charm sea mass, which is adjusted before calculating the derivatives.

shown in Fig. 12.

To calculate $\partial F^2/\partial m'_l$, $\partial M^2/\partial m'_l$ and $\partial^2 M^2/\partial m'_l \partial m_{\rm v}$, we use the three ensembles with strange sea mass close to its physical value, the ensembles inside the red ellipse in Fig. 11. We fit straight lines to the corresponding data, as shown in Fig. 13. Note that there are small differences in the charm and strange sea masses of these ensembles, but they are taken into account by a small adjustment using the derivatives with respect to m'_s and m'_c.

The derivatives with respect to m'_c cannot be calculated directly, because we do not have a group of ensembles with different charm sea masses but equal light and strange sea masses. So we have to determine the charm-mass derivatives indirectly, by investigating ensembles with different charm sea masses after adjusting for their differences in strange and light sea masses. This procedure can be carried out using the three ensembles available at $\approx$0.06 fm. Since m'_s and m'_c vary by about 10% on these three ensembles, the lever arm is large enough to calculate the derivatives with respect to m'_c. We first use the derivatives with respect to m'_s obtained at $\approx$0.12 fm to adjust the data at $\approx$0.06 fm for mistuning of the strange sea

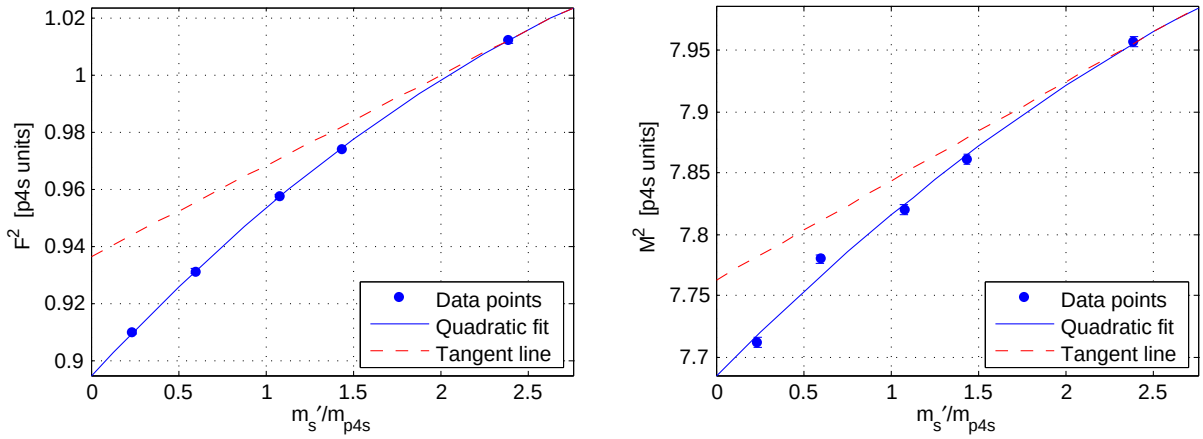

FIG. 12: Data from the $a \approx 0.12$ fm, $m'_l/m_s \approx 0.1$ ensembles, which are shown inside the blue ellipse in Fig. 11. F_{p4s} and M_{p4s} are the light-light pseudoscalar decay constant and mass for $m_{\rm v} = m_{p4s}$; quantities are expressed in $p4s$ units, as described in the text. The needed derivatives are given by the slope of the tangent line at m'_s/m_{p4s}=2.5

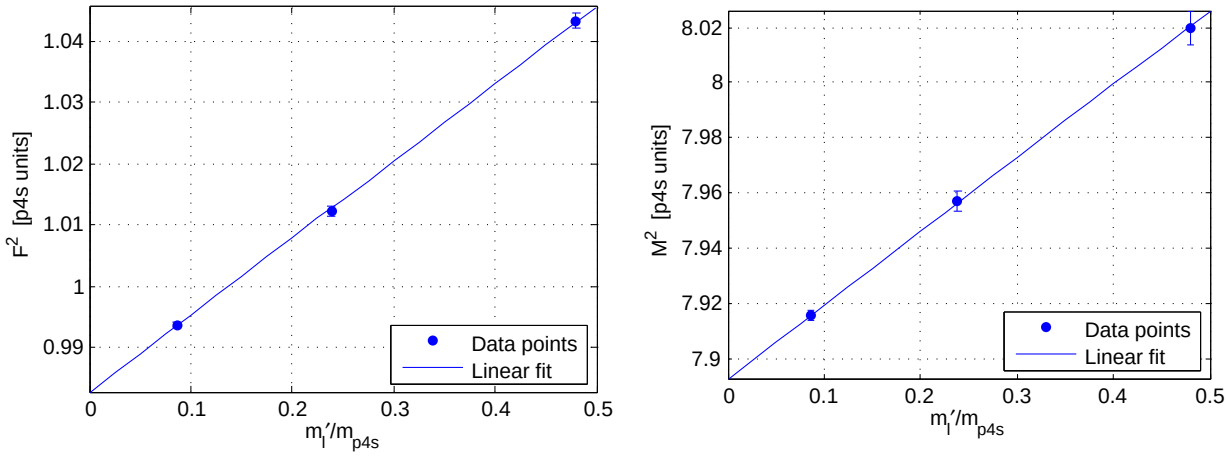

FIG. 13: Data from three ensembles with strange sea masses tuned close to m_s, the ensembles inside the red ellipse in Fig. 11.

masses, so only m'_l and m'_c dependence remains. Then we calculate the m'_c derivatives by passing a function linear in both m'_l and m'_c through the three data points for each quantity. The m'_c derivatives thus found feed back into the small adjustments needed at $a \approx 0.12$ fm in order to calculate m'_l derivatives, as discussed in the preceding paragraph. Our estimates of all the needed derivatives are tabulated in Table VII.

It is noteworthy that we can analytically determine the first order derivatives with respect to m'_c by integrating out the charm quark for processes that occur at energies well below its mass. By decoupling [43], the effect of a heavy (enough) sea quark on low-energy quantities occurs only through the change it produces in the effective value of $\Lambda_{\rm QCD}$ in the low-energy (three-flavor) theory [46]. (For a pedagogical discussion see Sec. 1.5 of Ref. [47].) Thus,

TABLE VII: The values of derivatives needed for adjusting the data for mistunings. All the derivatives are in $p4s$ units, and are evaluated at the valence mass $m_{\rm v} = m_{p4s}$ and at physical values of sea masses m_l, m_s, and m_c. Derivatives are found using 0.12 fm and 0.06 fm ensembles, as described in the text.

$\frac{\partial F^2}{\partial m'_l}$	0.1255(32)	$\frac{\partial M^2}{\partial m'_l}$	0.266(15)	$\frac{\partial^2 M^2}{\partial m'_l \partial m_{\rm v}}$	0.182(55)
$\frac{\partial F^2}{\partial m'_s}$	0.0318(17)	$\frac{\partial M^2}{\partial m'_s}$	0.0810(85)	$\frac{\partial^2 M^2}{\partial m'_s \partial m_{\rm v}}$	0.060(30)
$\frac{\partial F^2}{\partial m'_c}$	0.00554(85)	$\frac{\partial M^2}{\partial m'_c}$	0.0209(41)	$\frac{\partial^2 M^2}{\partial m'_c \partial m_{\rm v}}$	0.023(13)

assuming m'_c is heavy enough, we may calculate the m'_c derivatives of any quantity that is proportional to $\Lambda_{\rm QCD}$, where the proportionality constant is some pure number, independent of the light quark masses. Examples of such quantities are the LEC B in Eq. (16) and the light-light decay constant in the chiral limit, f. At leading order in weak-coupling perturbation theory, one then obtains (see Eq.(1.114) in Ref. [47]),

$$\frac{\partial B}{\partial m'_c} = \frac{2}{27}\frac{B}{m'_c}\,, \qquad \frac{\partial f}{\partial m'_c} = \frac{2}{27}\frac{f}{m'_c}\,. \tag{24}$$

At the nonzero values of $m_{\rm v}$, m'_l, and m'_s at which we need to evaluate the derivatives in Eq. (23), there are corrections to these expressions. However, chiral perturbation theory suggests that such corrections are relatively small. At the relevant light masses, we therefore expect

$$\frac{\partial F^2}{\partial m'_c} = 2F\frac{\partial F}{\partial m'_c} \approx \frac{4}{27}\frac{F^2}{m'_c} = 0.00504 \quad [p4s \text{ units}], \tag{25}$$

$$\frac{\partial M^2}{\partial m'_c} \approx 2m_{p4s}\frac{\partial B}{\partial m'_c} \approx \frac{2}{27}\frac{M^2}{m'_c} = 0.01998 \quad [p4s \text{ units}], \tag{26}$$

which agree with our numerical results within 10%; see Table VII. Indeed, the fact that the agreement is this close is probably due to chance, especially for the derivative of the decay constant: Our argument has neglected the difference between f and F_{p4s}, but that difference is $\sim$40%.

Having the required derivatives, we now iteratively adjust for mistunings. We first compute am_{p4s} and aF_{p4s}, then adjust the data, and repeat the entire process two more times. The values of am_{p4s} and aF_{p4s} have then converged to well within their statistical errors. The results for the lattice spacing a and am_s are listed in Table VIII. The error estimates of these quantities will be discussed below. Our investigation shows that the errors in the

TABLE VIII: Lattice spacing a and am_s, as a function β, in the $p4s$ mass-independent scale-setting scheme.

$\beta = 5.8$	$a = 0.15305(17)_{\rm stat}(^{+46}_{-23})_{a^2\,\rm extrap}(29)_{\rm FV}(4)_{\rm EM}$ fm
	$am_s = 0.06863(16)_{\rm stat}(^{+43}_{-24})_{a^2\,\rm extrap}(26)_{\rm FV}(7)_{\rm EM}$ [Lattice Units]
$\beta = 6.0$	$a = 0.12232(14)_{\rm stat}(^{+36}_{-19})_{a^2\,\rm extrap}(23)_{\rm FV}(3)_{\rm EM}$ fm
	$am_s = 0.05304(13)_{\rm stat}(^{+33}_{-18})_{a^2\,\rm extrap}(20)_{\rm FV}(6)_{\rm EM}$ [Lattice Units]
$\beta = 6.3$	$a = 0.08791(10)_{\rm stat}(^{+26}_{-13})_{a^2\,\rm extrap}(17)_{\rm FV}(2)_{\rm EM}$ fm
	$am_s = 0.03631(9)_{\rm stat}(^{+23}_{-13})_{a^2\,\rm extrap}(14)_{\rm FV}(4)_{\rm EM}$ [Lattice Units]
$\beta = 6.72$	$a = 0.05672(7)_{\rm stat}(^{+17}_{-9})_{a^2\,\rm extrap}(11)_{\rm FV}(1)_{\rm EM}$ fm
	$am_s = 0.02182(5)_{\rm stat}(^{+14}_{-8})_{a^2\,\rm extrap}(8)_{\rm FV}(2)_{\rm EM}$ [Lattice Units]

derivatives change a and am_s by less than their statistical errors, so those errors are not included in the analysis.

Comparing Table VIII with Table V, which uses f_{π^+} to set the scale, we see significant differences at the coarser lattice spacings, but not at the finest spacing. This is as expected for two different schemes, which should only agree exactly in the continuum limit.

3. *Chiral-continuum fits to D system*

So far, we have introduced eight fit parameters related to discretization effects (c_1, c_2, c_3, c_4, $L_{\rm v\delta}$, $L_{\rm s\delta}$, $k_{1\delta}$, and $k_{2\delta}$) and three parameters related to taste-violation effects (L_a, $\delta'_{\rm A}$, and $\delta'_{\rm V}$). The latter parameters appear at NLO in SχPT and must be kept since our expansion is supposed to be completely systematic through NLO. This is not the case for the former parameters; several of them (c_2, c_3, c_4, $L_{\rm v\delta}$, $L_{\rm s\delta}$, and $k_{2\delta}$) are formally NNLO and may be dropped. We indeed get acceptable fits when some of these parameters are dropped, especially if the $a \approx 0.15$ fm data is omitted. In order to see the effects of these parameters, we present the results of two fits, with different sets of parameters, to data at the three finer lattice spacings, and we study the extrapolation of the chiral fit back to the coarsest lattice spacing ($a \approx 0.15$ fm, $\beta = 5.8$).

Figure 14 shows a fit to partially quenched data at the three finer lattice spacings. (The $a \approx 0.15$ fm data is omitted.) Among the introduced fit parameters related to discretization effects, only c_1 in Eq. (21) and $k_{1\delta}$ in Eq. (22) are taken as free parameters in this fit,

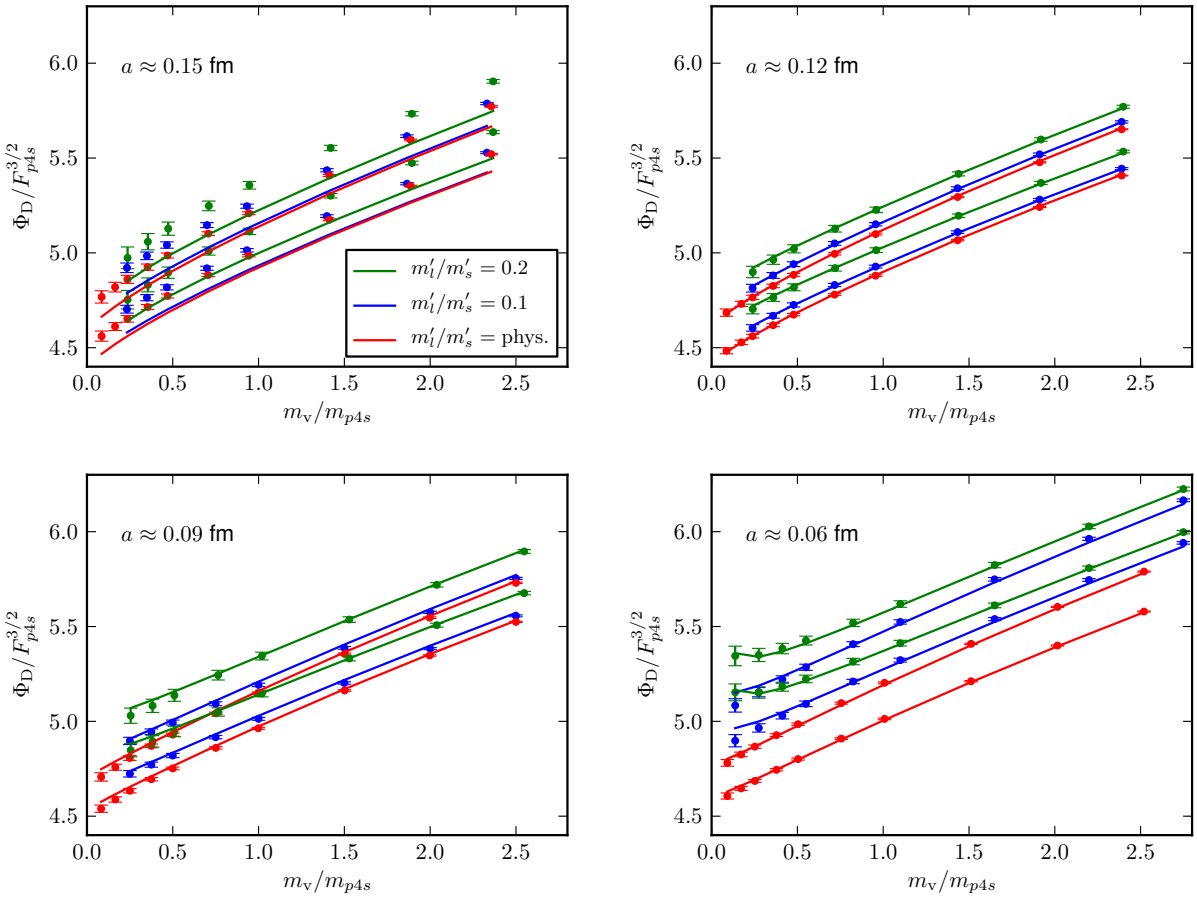

FIG. 14: Simultaneous chiral fit to Φ_D as a function of m_v, the valence-quark mass (in units of m_{p4s}), at the three finer lattice spacings. The $a \approx 0.15$ fm ($\beta = 5.8$) data is not included in the fit, although the data and the extrapolation of the chiral fit to it are shown at the left in the top row. At the right of the top row we show the $a \approx 0.12$ fm ($\beta = 6.0$) data, and in the bottom row are $a \approx 0.09$ fm ($\beta = 6.3$, left) and $a \approx 0.06$ fm ($\beta = 6.72$, right). The colors denote different light sea-quark masses, as indicated. For each color there are two lines, one for heavy valence-quark mass $\approx m_c'$ (higher line), and one for $\approx 0.9 m_c'$. In this fit, g_π is fixed to 0.53. The fit has $\chi^2/\text{dof} = 339/293$, giving $p = 0.033$.

and the others are set to zero. This fit gives $p = 0.033$, and as illustrated in Fig. 14, the extrapolation of the fit to the coarsest lattice spacing does not follow the corresponding data points. We note that this fit and all other chiral fits in this paper include additional data (not shown) from ensembles at $a \approx 0.12$ fm ($\beta = 6.0$) either with m_s' lighter than physical, or with volumes $24^3 \times 64$ and $40^3 \times 64$, which were generated to check finite volume effects. (See Table I.) Moreover, it is important to realize that the biggest source of variation in the

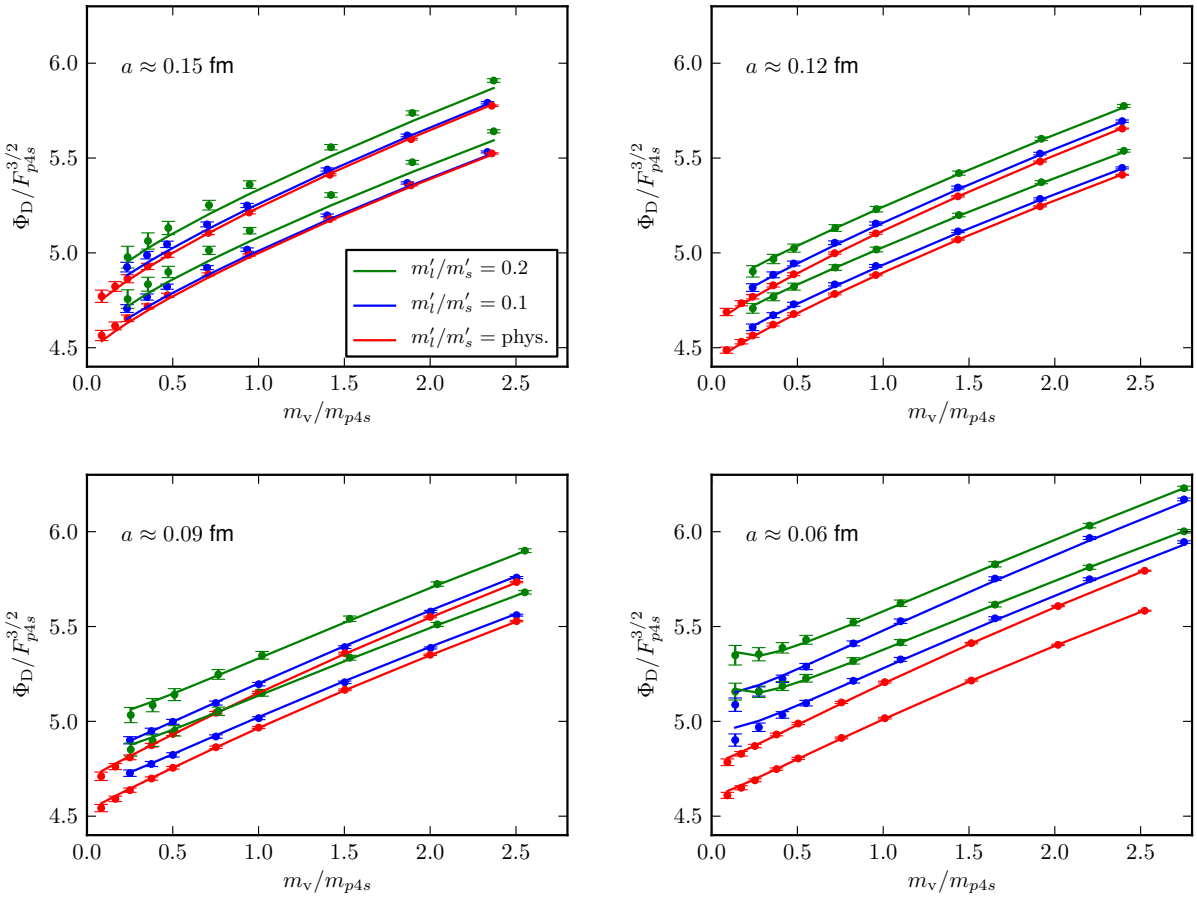

FIG. 15: Simultaneous chiral fit to Φ_D as a function of m_v at the three finer lattice spacings. Similar to the fit in Fig. 14, but with three extra fit parameters: c_2, c_3, and c_4. This fit has $\chi^2/\text{dof} = 239/290$, giving $p = 0.986$.

data in the four plots shown in Fig. 14 is not discretization errors, but mistunings of the strange and, most importantly, charm-quark masses.

Adding $c_3\alpha_S(am_Q)^2 + c_4(am_Q)^4$ to the analytic terms in Eq. (8), as well as including c_2 in Eq. (21), we get a new fit to the partially quenched data at the three finer lattice spacings. By including these three extra parameters, an excellent fit is achieved, as shown in Fig. 15, and extrapolation of the fit to the coarsest lattice spacing gives lines that pass relatively well through the corresponding data points. This comparison makes clear that higher-order discretization errors are important for the HISQ data, in which the leading-order discretization effects are suppressed.

We have a total of 18 acceptable ($p > 0.1$) versions of the continuum/chiral fits. Five of the fits drop the $a \approx 0.15$ fm ensembles; the rest keep those ensembles. The chiral coupling

f is generally set to f_{π^+}, except for two fits with the coupling constant set to f_{K^+}. The LEC g_π is usually fixed to either its nominal value or to $1\,\sigma$ below its nominal value, however it is allowed to be a free parameter in four of the fits. The LEC B in Eq. (16) is generally determined for each lattice spacing separately by fitting all data for the squared meson mass M^2 vs. the sum of the valence masses to a straight line. (At $a \approx 0.12$ fm only the ensembles with strange sea masses close to its physical mass are included in the fit.) However, in two versions of the chiral fits, B is determined from just the data on the physical-mass ensembles at each lattice spacing.

Another difference among the fits is how we determine the strong coupling α_S in discretization terms such as those with coefficients c_1 and c_3. Since the coefficients are free parameters, all that we actually need in the fits is the relative value of α_S at a given coupling β compared to its value at a fixed, fiducial coupling β_0. In most of the fits, we have used measured light-light pseudoscalar taste splittings to fix this relative value, as in Eq. (6). An alternative, which is used in two of our fits, is to use for α_S the coupling α_V, determined from the plaquette [33]. The scale for α_V is taken to be $q^* = 2.0/a$. Note that the NLO perturbative corrections to α_V have not been calculated for the HISQ action, so we use the result for the asqtad action. Since the n_f dependence of the NLO result is small, we expect the difference to have negligible effects on the results of the fit. This expectation can be tested by, for example, flipping the sign of the n_f term in the asqtad result, which is likely a much bigger change than would actually come from changing from asqtad to HISQ. When we do this, we find that the results change by amounts comparable to or smaller than the statistical errors, and significantly smaller than the total systematic errors. Similar, but usually smaller, changes result from replacing $q^* = 2.0/a$ with $q^* = 1.5/a$, which is another reasonable choice, as discussed in Ref. [7].

We have introduced eight fit parameters related to discretization effects (c_1, c_2, c_3, c_4, $L_{\mathrm{v}\delta}$, $L_{\mathrm{s}\delta}$, $k_{1\delta}$, and $k_{2\delta}$), but it is not necessary to keep all of them to get an acceptable fit. Dropping some of these parameters, we have different continuum/chiral fits with the number of parameters ranging from 23 to 28. We may also choose to constrain, with priors, the LECs in higher-order (NNLO and NNNLO) analytic terms to be $\mathcal{O}(1)$ in natural units (as explained following Eq. (16)). (Through NLO, where we have the complete chiral expression, including logarithms, we always leave the LECs Φ_0, L_{s}, L_{v}, and L_a completely unconstrained, while g_π, δ'_A, and δ'_V are constrained by independent analyses as discussed above.) We may similarly

constrain the coefficients of discretization terms to be $\mathcal{O}(1)$ when the terms are written in terms of a reasonable QCD scale (which we take, conservatively, to be 600 MeV). Among the 18 fits we consider, some have higher-order chiral terms and discretization terms completely unconstrained, and others constrain either the chiral terms, or the discretization terms, or both.

In Eq. (21), m_Q denotes the valence charm mass. To take into account the physical effects of the charm sea masses we can introduce a parameter k_1' to Eq. (21):

$$\Phi_0 \to \Phi_0 \left(1 + k_1 \frac{\Lambda_{\rm HQET}}{m_Q} + k_2 \frac{\Lambda_{\rm HQET}^2}{m_Q^2} + k_1' \frac{\Lambda_{\rm HQET}}{m_c'}\right) \left(1 + c_1 \alpha_S (a\Lambda)^2 + c_2 (a\Lambda)^4\right) , \qquad (27)$$

where m_c' is the mass of the charm mass in the sea. One of our 18 fits adds the parameter k_1'. Further, discretization errors coming from the charm sea masses can be included by adding $c_3' \alpha_S (am_c')^2 + c_4' (am_c')^4$ to the analytic terms in Eq. (8), and one of the fits makes that addition. It is interesting to note that it is possible to obtain another acceptable fit in which c_2 in Eq. (21) is restricted by priors to be much smaller than its value in the central fit, but the c_3' and c_4' terms are added. This shows that our lattice data cannot distinguish in detail between various sources of higher-order discretization effects. However, the results in the continuum limit are rather insensitive to these differences.

Since all 18 fits considered have acceptable p values and give correction terms reasonably consistent with expectations from chiral perturbation theory and power counting, whether or not such terms are constrained, we have no strong reason to choose one fit or groups of fits as preferred in comparison to the rest. We therefore choose our "central fit" simply by requiring that it be a fit to all ensembles and that it give results for Φ_{D+} and Φ_{D_s} that are as close as possible to the center of the histograms for these quantities from all the fits and from all systematic variations in the inputs (*i.e.*, from the "continuum extrapolation" column in Table VI). This central fit has 27 free parameters, with g_π fixed to 1-sigma below its nominal value, and with the k_1', c_3', and c_4' terms discussed in the previous paragraph dropped, but all discretization terms aside from c_3' and c_4' kept. In the central fit, c_2 in Eq. (21) is equal to 1.3 with $\Lambda = 600$ MeV; while the HQET parameters are $k_1 = -1.0$ and $k_2 = 0.5$, with $\Lambda_{\rm HQET} = 600$ MeV.

Figure 16 shows our central fit to partially quenched data at all four lattice spacings. Extrapolating the parameters to the continuum, adjusting the strange sea-quark mass and charm valence- and sea-quark masses to their physical values, and setting the light sea-

quark mass equal to the light valence mass (up to the small difference between m_d and $m_l = (m_u + m_d)/2$) gives the orange band. Putting in the physical light-quark mass then gives the black burst, which is the result for Φ_{D^+}. Note that the effect of isospin violation in the valence quarks is included in our result. The effect of isospin violation in the sea has not been included, but we may easily estimate its size by putting in our values for m_u and m_d (instead of the average sea mass m_l) in Eq. (8) and in the NNLO and NNNLO analytic terms. This results in a change of only 0.01% in f_{D^+}, and a still smaller change in f_{D_s}.

The width of the band shows the statistical error coming from the fit, which is only part of the total statistical error, since it does not include the statistical errors in the inputs of the quark masses and the lattice scale. To determine the total statistical error of each output quantity, we divide the full data set into 100 jackknife resamples. The complete calculation, including the determination of the inputs, is performed on each resample, and the error is computed as usual from the variations over the resamples. (For convenience, we kept the covariance matrix fixed to that from the full data set, rather than recomputing it for each resample.) Each jackknife resample drops approximately ten consecutive stored configurations (50 to 60 trajectories) from each ensemble with $\approx$1000 configurations. This procedure controls for autocorrelations, since all our measures of the autocorrelations of these quantities indicate that they are negligible after four or eight consecutive configurations. For the physical-mass 0.06 fm ensemble with 583 configurations, we are forced to drop only about six consecutive stored configurations at a time. Our expectation is that the effect of any remaining autocorrelations, while perhaps not completely negligible, is small compared to other sources of error. The total statistical errors computed from the jackknife procedure are only about 10% larger than the statistical error from the chiral/continuum fit, indicating that the inputs are statistically quite well determined. The same procedure is performed to find the total statistical error of a and am_s at each lattice spacing.

Figure 17 illustrates how data for Φ_{D^+} and Φ_{D_s} depend on lattice spacing after adjustment to physical values of the quark masses (blue circles). There is a 2–3% variation between these points and the continuum value (green square at $a^2 = 0$). Note that there is clear curvature in the plot, evidence of significant a^4 terms in addition to the formally leading $\alpha_S a^2$ terms. Both the small absolute size of the errors, and the competition between formally leading and subleading terms, are typical of highly improved actions such as the HISQ action. The red stars show the contribution from the chiral logarithms (with known taste splittings) to the a^2

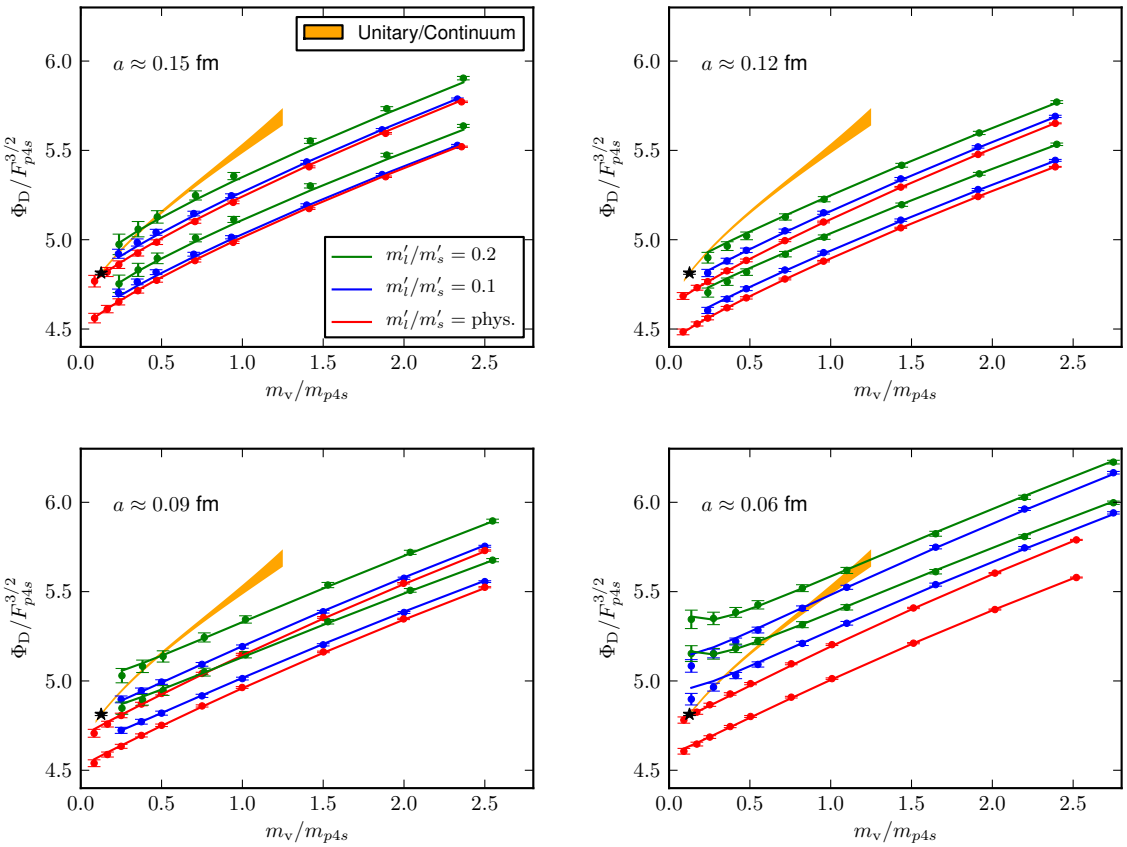

FIG. 16: Simultaneous chiral fit to Φ_D as a function of m_v, the valence-quark mass (in units of m_{p4s}), at all four lattice spacings: $a \approx 0.15$ fm and 0.12 fm (top row), and 0.09 fm and 0.06 fm (bottom row). This fit has $\chi^2/\text{dof} = 347/339$, giving $p = 0.36$. In the fit lines for each ensemble, the light valence-quark mass varies, with all sea-quark masses held fixed. The orange band, labeled as "unitary/continuum," is identical in each panel. It gives the result after extrapolating to the continuum, setting the light valence-quark and sea-quark masses equal (up to the small difference between m_d and $m_l = (m_u + m_d)/2$), and adjusting the strange and charm masses to their physical values. The width of the band shows the statistical error coming from the fit. The black bursts indicate the value of Φ_{D^+} at the physical light-quark mass point.

dependence of the chiral fit function. The green squares show the corresponding contribution from the analytic fit parameters. The two effects are of comparable magnitudes but the relative sign changes with lattice spacing; both are needed to describe the a^2 dependence of the data.

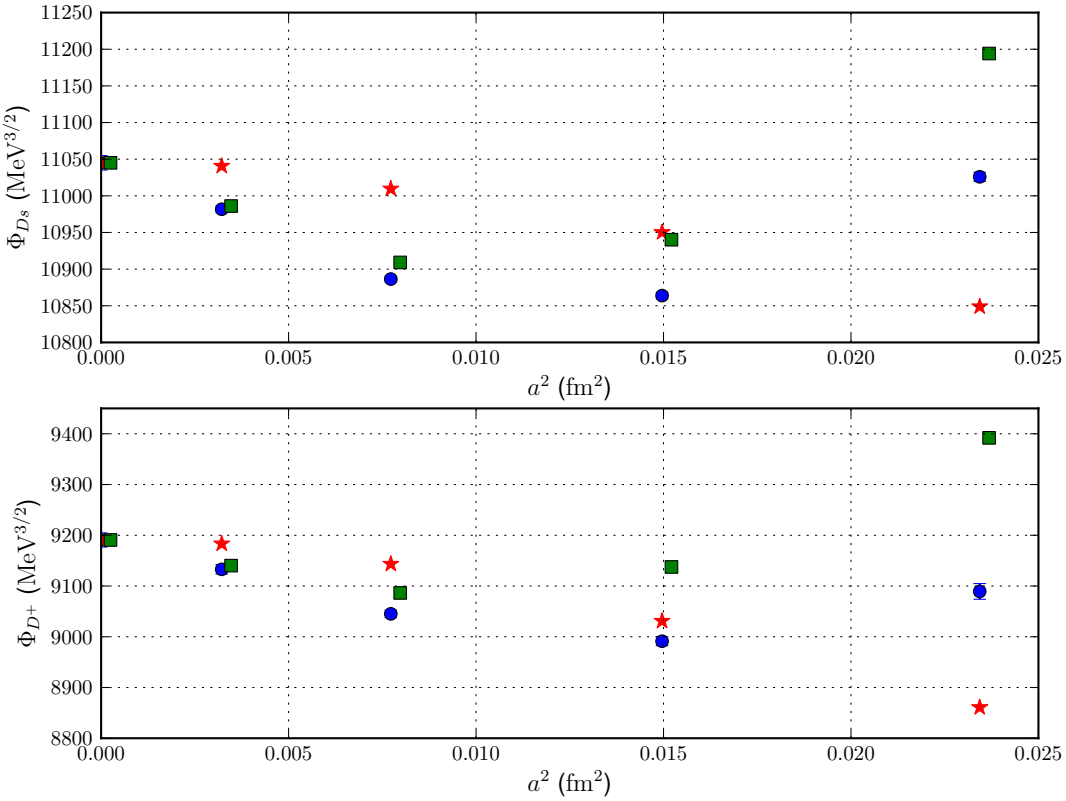

FIG. 17: Lattice spacing dependence of Φ_{D^+} and Φ_{D_s}. The blue circles show the lattice data, after adjustment for mistunings of valence- and sea-quark masses. The red stars show the modification of each continuum value by the a^2 dependence of the chiral logarithms, while the green squares show the corresponding modification by the a^2 dependence induced by the fit parameters. Red stars and green squares overlap at $a^2 = 0$ (only the green square is visible). Neglecting small cross terms, the deviation of the blue circles from the continuum value are given by the algebraic sum of the deviations of the red stars and the green squares.

4. Continuum extrapolation and systematic uncertainties

To determine the systematic error associated with the continuum extrapolation (and chiral interpolation) of the charm decay constants in the chiral perturbation theory analysis, we rerun the analysis with alternative continuum/chiral fits, and with alternative inputs that come from different continuum extrapolations of the physical-mass analysis, listed in the "continuum extrapolation" column in Table VI.

As mentioned above, we have a total of 18 acceptable versions of the continuum/chiral fits. We also have the six versions of the continuum extrapolations used in the physical-mass

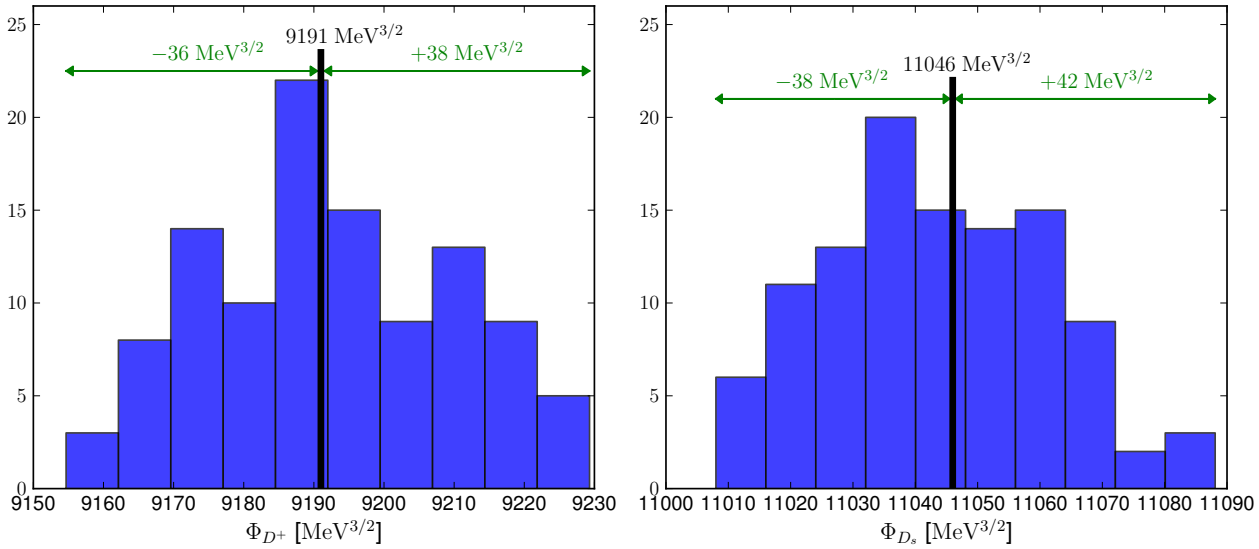

FIG. 18: Histograms of Φ_{D^+} and Φ_{D_s} values obtained from various versions of the continuum/chiral extrapolation and various inputs of quark masses and scale values from the physical-mass analysis. Our central fit gives $\Phi_{D^+} = 9191$ MeV$^{3/2}$ and $\Phi_{D_s} = 11046$ MeV$^{3/2}$; those values are marked with vertical black lines. At the top of each histogram, we show the range taken as the systematic error of the self-contained chiral analysis of the current section.

analysis that leads to the inputs of quark masses and the lattice scale. This gives a total of 108 versions of the analysis. Histograms of the 108 results for Φ_{D^+} and Φ_{D_s} are shown in Fig. 18. Conservatively, we take the maximum difference seen in these results with our central values as the "self-contained" estimate of the continuum extrapolation errors within this chiral analysis. The central fit is chosen to give results that are close to the centers of the histograms, which results in more symmetrical error bars than in the preliminary analysis reported in Ref. [25]. Note that the "acceptable" fits entering the histograms all have $p > 0.1$. If the cutoff is instead taken to be $p > 0.05$, the additional fits allowed would not change the error estimates. However a cutoff of 0.01 or lower would give some additional outliers that would increase the width of the histograms.

In practice, the NLO finite volume corrections are included in our fit function, Eq. (8), when it is applied to the data, and the volume is sent to infinity when the continuum results are extracted. We may conservatively estimate the residual finite volume error in the heavy-light data either by turning off all finite volume corrections and repeating the fit, or by using the current fit to find the size of the NLO finite volume correction on our

most-important, 0.06 fm physical-mass ensemble. Yet another way to make the estimate is by direct comparison of our results on the $32^3 \times 64$, $\beta = 6.0$, $m'_l/m'_s = 0.1$ ensemble (which is similar in physical size to our other $m'_l/m'_s = 0.1$ ensembles) and the $40^3 \times 64$, $\beta = 6.0$, $m'_l/m'_s = 0.1$ ensemble. All three methods indicate that there are negligible direct finite volume effects in the heavy-light lattice data. Nevertheless, there are non-negligible finite volume effects in our final answers, which appear due to the scale setting in the light-quark sector through, ultimately, f_{π^+}. (The value of F_{p4s} in physical units that we use comes by comparison with f_{π^+}.) We then propagate the errors in the inputs through our analysis. Electromagnetic errors in the light quark masses are similarly propagated through our analysis.

Results for Φ_{D^+}, Φ_{D_s} and their ratio at various values of the mass ratio of light to strange sea quarks are shown in Table IX; only the top subsection of the table gives physical results. To quantify the effect of isospin violations, we also report Φ_D and $\Phi_{D^+} - \Phi_D$, where Φ_D is the value of Φ in the isospin limit, when the light valence mass is equal to $m_l = (m_u + m_d)/2$ instead of m_d. Note that the valence masses do not vary in the three different subsections of the table, so changes in results show only the effects of the light sea mass.

In Table X, we report additional results for the case when the light valence mass is kept equal to the light sea mass and $m'_l/m_s = 0.1$ or 0.2. These unphysical results may be useful for normalizing other calculations, such as those of B-system decay constants, as described in Sec. V.

At each β value, we have reported, in Table VIII, the values for the lattice spacing a and the strange mass in lattice units am_s, which come from our scale-setting procedure using M_{p4s}/F_{p4s} and aF_{p4s}. For the estimates of the extrapolation errors in these quantities, we have used the six versions of the continuum extrapolation for the inputs, which are the quark-mass ratios, M_{p4s}/F_{p4s}, and F_{p4s} in physical units. Finite volume and electromagnetic errors come simply from propagating the errors in f_{π^+} and the light quark masses through the analysis.

TABLE IX: Results for Φ from the chiral analysis, for three choices of the light sea mass m'_l. Φ_D is the value of Φ when the light valence mass $m_{\rm v} = m_l \equiv (m_u + m_d)/2$. Valence masses here are always taken to be the physical values m_d, m_s or m_l, independent of the value of m'_l, and the strange sea mass is always physical ($m'_s = m_s$). The negative central value of $\Phi_{D^+} - \Phi_D$ for $m'_l/m_s = 0.2$ is an effect of partial quenching, but note that the systematic errors are large in this case.

$m'_l = m_l$	$\Phi_{D^+} = 9191 \pm 16_{\rm stat}\,{}^{+38}_{-36}|_{a^2\,\rm extrap} \pm 13_{\rm FV} \pm 1_{\rm EM}$ MeV$^{3/2}$
	$\Phi_{D_s} = 11046 \pm 12_{\rm stat}\,{}^{+42}_{-38}|_{a^2\,\rm extrap} \pm 12_{\rm FV} \pm 4_{\rm EM}$ MeV$^{3/2}$
	$\Phi_{D_s}/\Phi_{D^+} = 1.2018 \pm 0.0010_{\rm stat}\,{}^{+0.0024}_{-0.0032}|_{a^2\,\rm extrap} \pm 0.0004_{\rm FV} \pm 0.0005_{\rm EM}$
	$\Phi_D = 9168 \pm 16_{\rm stat}\,{}^{+39}_{-40}|_{a^2\,\rm extrap} \pm 13_{\rm FV} \pm 1_{\rm EM}$ MeV$^{3/2}$
	$\Phi_{D^+} - \Phi_D = 23.6 \pm 0.3_{\rm stat}\,{}^{+4.7}_{-1.6}|_{a^2\,\rm extrap} \pm 0.1_{\rm FV} \pm 1.0_{\rm EM}$ MeV$^{3/2}$
$m'_l/m_s = 0.1$	$\Phi_{D^+} = 9412 \pm 16_{\rm stat}\,{}^{+46}_{-86}|_{a^2\,\rm extrap} \pm 13_{\rm FV} \pm 1_{\rm EM}$ MeV$^{3/2}$
	$\Phi_{D_s} = 11128 \pm 13_{\rm stat}\,{}^{+36}_{-42}|_{a^2\,\rm extrap} \pm 12_{\rm FV} \pm 4_{\rm EM}$ MeV$^{3/2}$
	$\Phi_{D_s}/\Phi_{D^+} = 1.1824 \pm 0.0010_{\rm stat}\,{}^{+0.0078}_{-0.0036}|_{a^2\,\rm extrap} \pm 0.0004_{\rm FV} \pm 0.0003_{\rm EM}$
	$\Phi_D = 9402 \pm 16_{\rm stat}\,{}^{+48}_{-95}|_{a^2\,\rm extrap} \pm 13_{\rm FV} \pm 1_{\rm EM}$ MeV$^{3/2}$
	$\Phi_{D^+} - \Phi_D = 10.4 \pm 0.3_{\rm stat}\,{}^{+9.4}_{-2.4}|_{a^2\,\rm extrap} \pm 0.1_{\rm FV} \pm 0.5_{\rm EM}$ MeV$^{3/2}$
$m'_l/m_s = 0.2$	$\Phi_{D^+} = 9709 \pm 19_{\rm stat}\,{}^{+53}_{-140}|_{a^2\,\rm extrap} \pm 13_{\rm FV} \pm 2_{\rm EM}$ MeV$^{3/2}$
	$\Phi_{D_s} = 11250 \pm 15_{\rm stat}\,{}^{+44}_{-47}|_{a^2\,\rm extrap} \pm 12_{\rm FV} \pm 4_{\rm EM}$ MeV$^{3/2}$
	$\Phi_{D_s}/\Phi_{D^+} = 1.1588 \pm 0.0011_{\rm stat}\,{}^{+0.0140}_{-0.0038}|_{a^2\,\rm extrap} \pm 0.0003_{\rm FV} \pm 0.0002_{\rm EM}$
	$\Phi_D = 9714 \pm 19_{\rm stat}\,{}^{+56}_{-154}|_{a^2\,\rm extrap} \pm 13_{\rm FV} \pm 2_{\rm EM}$ MeV$^{3/2}$
	$\Phi_{D^+} - \Phi_D = -5.3 \pm 0.3_{\rm stat}\,{}^{+15.0}_{-3.3}|_{a^2\,\rm extrap} \pm 0.1_{\rm FV} \pm 0.0_{\rm EM}$ MeV$^{3/2}$

The self-contained chiral analysis of the current section gives:

$$f_{D^+} = 212.6 \pm 0.4_{\rm stat}\,{}^{+0.9}_{-0.8}|_{a^2\,\rm extrap} \pm 0.3_{\rm FV} \pm 0.0_{\rm EM} \pm 0.3_{f_\pi\,\rm PDG}\ \text{MeV} \quad (28)$$

$$f_{D_s} = 249.0 \pm 0.3_{\rm stat}\,{}^{+1.0}_{-0.9}|_{a^2\,\rm extrap} \pm 0.2_{\rm FV} \pm 0.1_{\rm EM} \pm 0.4_{f_\pi\,\rm PDG}\ \text{MeV} \quad (29)$$

$$f_{D_s}/f_{D^+} = 1.1712(10)_{\rm stat}({}^{+24}_{-31})_{a^2\,\rm extrap}(3)_{\rm FV}(5)_{\rm EM} \quad (30)$$

$$f_{D^+} - f_D = 0.47(1)_{\rm stat}({}^{+11}_{-\ 4})_{a^2\,\rm extrap}(0)_{\rm FV}(2)_{\rm EM}\ \text{MeV}\ , \quad (31)$$

where f_D is the decay constant in the isospin limit, $m_u = m_d = m_l$. In finding $f_{D^+} - f_D$ from $\Phi_{D^+} - \Phi_D$ in Table IX, we use the experimental value for M_{D^+} and our result, $M_{D^+} - M_{D^0} = 2.6$ MeV, obtained from the pure-QCD analysis in Sec. IV A. Note that the experimental

TABLE X: Results for Φ for two choices of light sea masses. Here the valence mass for Φ_D is taken equal to the light sea mass: $m_{\rm v} = m'_l$. The quantities denoted by "phys" are those tabulated in Table IX for the case $m'_l = m_l$.

$m'_l/m_s = 0.1$	$\Phi_D = 9477 \pm 15_{\rm stat}\,{}^{+39}_{-66}|_{a^2\,\rm extrap} \pm 13_{\rm FV} \pm 2_{\rm EM}$ MeV$^{3/2}$
	$\Phi_{D_s} = 11128 \pm 13_{\rm stat}\,{}^{+36}_{-42}|_{a^2\,\rm extrap} \pm 12_{\rm FV} \pm 4_{\rm EM}$ MeV$^{3/2}$
	$\Phi_D/\Phi_D^{\text{"phys"}} = 1.0338 \pm 0.0005_{\rm stat}\,{}^{+0.0009}_{-0.0031}|_{a^2\,\rm extrap} \pm 0.0000_{\rm FV} \pm 0.0001_{\rm EM}$
	$\Phi_D/\Phi_{D^+}^{\text{"phys"}} = 1.0311 \pm 0.0004_{\rm stat}\,{}^{+0.0010}_{-0.0036}|_{a^2\,\rm extrap} \pm 0.0000_{\rm FV} \pm 0.0002_{\rm EM}$
	$\Phi_{D_s}/\Phi_{D_s}^{\text{"phys"}} = 1.0075 \pm 0.0003_{\rm stat}\,{}^{+0.0005}_{-0.0006}|_{a^2\,\rm extrap} \pm 0.0000_{\rm FV} \pm 0.0000_{\rm EM}$
$m'_l/m_s = 0.2$	$\Phi_D = 9870 \pm 17_{\rm stat}\,{}^{+39}_{-71}|_{a^2\,\rm extrap} \pm 13_{\rm FV} \pm 2_{\rm EM}$ MeV$^{3/2}$
	$\Phi_{D_s} = 11250 \pm 15_{\rm stat}\,{}^{+44}_{-47}|_{a^2\,\rm extrap} \pm 12_{\rm FV} \pm 4_{\rm EM}$ MeV$^{3/2}$
	$\Phi_D/\Phi_D^{\text{"phys"}} = 1.0766 \pm 0.0011_{\rm stat}\,{}^{+0.0017}_{-0.0038}|_{a^2\,\rm extrap} \pm 0.0001_{\rm FV} \pm 0.0002_{\rm EM}$
	$\Phi_D/\Phi_{D^+}^{\text{"phys"}} = 1.0738 \pm 0.0011_{\rm stat}\,{}^{+0.0017}_{-0.0043}|_{a^2\,\rm extrap} \pm 0.0001_{\rm FV} \pm 0.0002_{\rm EM}$
	$\Phi_{D_s}/\Phi_{D_s}^{\text{"phys"}} = 1.0185 \pm 0.0007_{\rm stat}\,{}^{+0.0014}_{-0.0010}|_{a^2\,\rm extrap} \pm 0.0000_{\rm FV} \pm 0.0000_{\rm EM}$

mass difference $M_{D^+} - M_{D^0} = 4.8$ MeV includes EM effects.

V. RESULTS AND CONCLUSIONS

Our main results are for the charm decay constants and their ratio. We take the more precise determinations from the self-contained chiral perturbation theory analysis using the full set of sea-quark ensembles, Eqs. (28)–(30), for our best estimate of the central values and statistical errors. We then use the results of the simpler physical-mass analysis to help estimate the systematic uncertainties. For the continuum extrapolation error, we consider the differences in the central values of f_{D^+}, f_{D_s}, and f_{D_s}/f_{D^+}, obtained with various continuum-extrapolation Ansätze in the physical-mass analysis, and take those differences as the uncertainty whenever they are larger than the error from the chiral analysis. Figure 19 shows the histograms from Fig. 18 overlaid with the results from the various continuum extrapolations considered in Sec. IV A (vertical red lines), as well as our final estimates for the systematic errors of the continuum extrapolation. The analysis on the physical-mass ensembles also gives alternative, and comparably-sized, estimates for the finite-volume and EM errors to those in Eqs. (28)–(30) (see Table VI), and we take the larger value as the

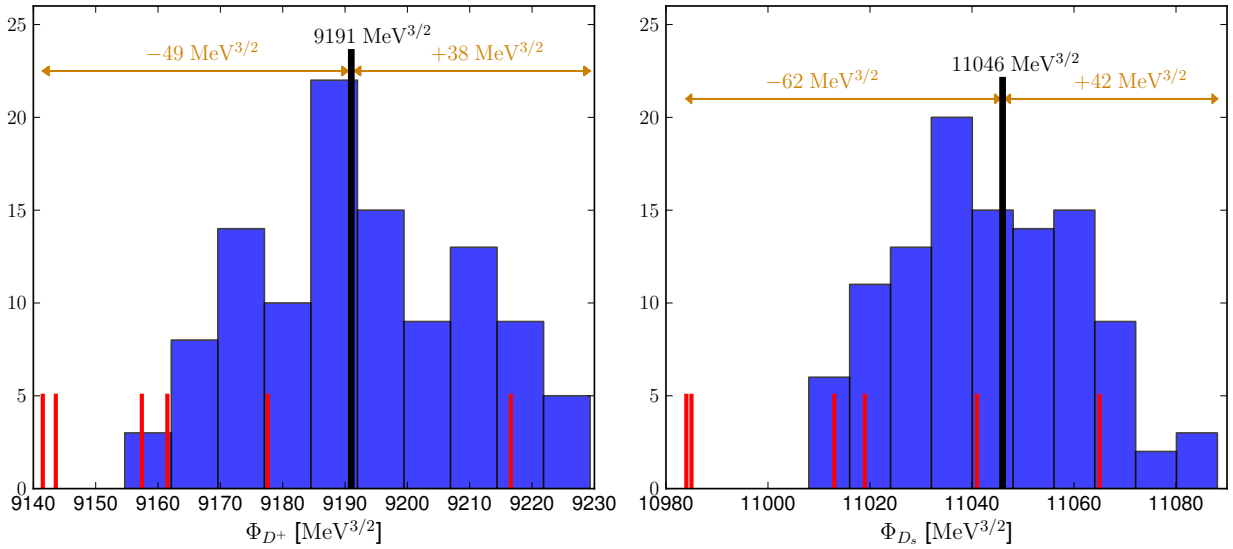

FIG. 19: Same as Fig. 18, but the histograms of Φ_{D^+} and Φ_{D_s} from the chiral analysis have been overlaid with results from various continuum extrapolations in the physical-mass analysis, shown as vertical red lines. We take the full ranges shown at the top of each plot as the final estimates of the systematic errors coming from the continuum extrapolation.

uncertainty in each case. This procedure yields our final results for f_{D^+}, f_{D_s} and f_{D_s}/f_{D^+}:

$$f_{D^+} = 212.6 \pm 0.4_{\text{stat}} \, {}^{+0.9}_{-1.1}|_{a^2\,\text{extrap}} \pm 0.3_{\text{FV}} \pm 0.1_{\text{EM}} \pm 0.3_{f_\pi\,\text{PDG}} \text{ MeV} \tag{32}$$

$$f_{D_s} = 249.0 \pm 0.3_{\text{stat}} \, {}^{+1.0}_{-1.4}|_{a^2\,\text{extrap}} \pm 0.2_{\text{FV}} \pm 0.1_{\text{EM}} \pm 0.4_{f_\pi\,\text{PDG}} \text{ MeV} \tag{33}$$

$$f_{D_s}/f_{D^+} = 1.1712(10)_{\text{stat}}(^{+28}_{-31})_{a^2\,\text{extrap}}(3)_{\text{FV}}(6)_{\text{EM}} \,. \tag{34}$$

For the effects of isospin violation we find

$$f_{D^+} - f_D = 0.47(1)_{\text{stat}}(^{+25}_{-\ 4})_{a^2\,\text{extrap}}(0)_{\text{FV}}(2)_{\text{EM}} \text{ MeV}, \tag{35}$$

where the continuum-extrapolation error has been increased relative to that in Eq. (31) to take into account the difference from the result of the physical-mass analysis.

We also update our determination of the decay-constant ratio f_{K^+}/f_{π^+} in Ref. [3] from the physical-mass analysis using additional configurations on the 0.06 fm physical quark mass ensemble, and include results for quark-mass ratios coming from the tuning procedure

and continuum extrapolation described in Sec. IV A:

$$f_{K^+}/f_{\pi^+} = 1.1956(10)_{\rm stat}\,{}^{+23}_{-14}|_{a^2\,\rm extrap}(10)_{\rm FV}(5)_{\rm EM} \quad (36)$$

$$m_s/m_l = 27.352(51)_{\rm stat}\,{}^{+80}_{-20}|_{a^2\,\rm extrap}(39)_{\rm FV}(55)_{\rm EM} \quad (37)$$

$$m_c/m_s = 11.747(19)_{\rm stat}\,{}^{+52}_{-32}|_{a^2\,\rm extrap}(6)_{\rm FV}(28)_{\rm EM}\,. \quad (38)$$

Although our analysis also determines m_u/m_d, we do not quote a final result, because the errors in this ratio are dominated by electromagnetic effects. If we take the results from our preliminary study of EM effects on pion and kaon masses reported in Ref. [36] at face value, we obtain a central value for $m_u/m_d = 0.4482(48)_{\rm stat}\,{}^{+21}_{-115}|_{a^2\,\rm extrap}(1)_{\rm FV}$, where we include the uncertainties from all sources other than EM. Once the full analysis of m_u/m_d from our QCD+QED simulations is complete, we expect the EM error to lie between 0.0150 and 0.0230. Even the more conservative estimate for the EM error on m_u/m_d, however, would not impact the uncertainties on our final results in Eqs. (32) through (38) significantly; the electromagnetic error is subdominant for most of these quantities, and one of several comparably sized errors in the case of m_s/m_l. With the charm-quark mass tuned to match the D_s mass, our analysis gives a mass for the η_c of $2982.33(0.35)(^{+2.34}_{-2.07})$ MeV. While this mass is in good agreement with the experimental value, it should be remembered that our calculation does not include the effects of disconnected contractions or decay channels to the η_c mass. Finally, we note that we are computing the values of the decay constants as they are conventionally defined, in a pure-QCD world. Comparison to experiment thus requires a matching of the decay rates between QCD and QCD+QED. The errors in such a matching are not included in our error budgets for the decay constants, but are accounted for in our determinations of CKM matrix elements in Sec. VI.

Figures 20, 21, 22 and 23 compare our results for m_s/m_l, m_c/m_s, f_{K^+}/f_{π^+} and the charm decay constants with other unquenched calculations. Our results agree with most determinations at the 1–2σ level. In particular, our value for f_{D_s} agrees with the second-most-precise determination from HPQCD obtained using HISQ valence quarks on the (2+1)-flavor MILC Asqtad ensembles [69]. We disagree slightly with HPQCD's determination of the ratio f_{D_s}/f_{D^+} [72], but only by 1.2σ. Our result for f_{D_s} is more precise than previous determinations primarily for two reasons. First, the statistical errors in our data points for the decay amplitudes are two or more times smaller than those obtained by, for example, HPQCD [69]. Second, our use of ensembles with the physical light-quark mass eliminates

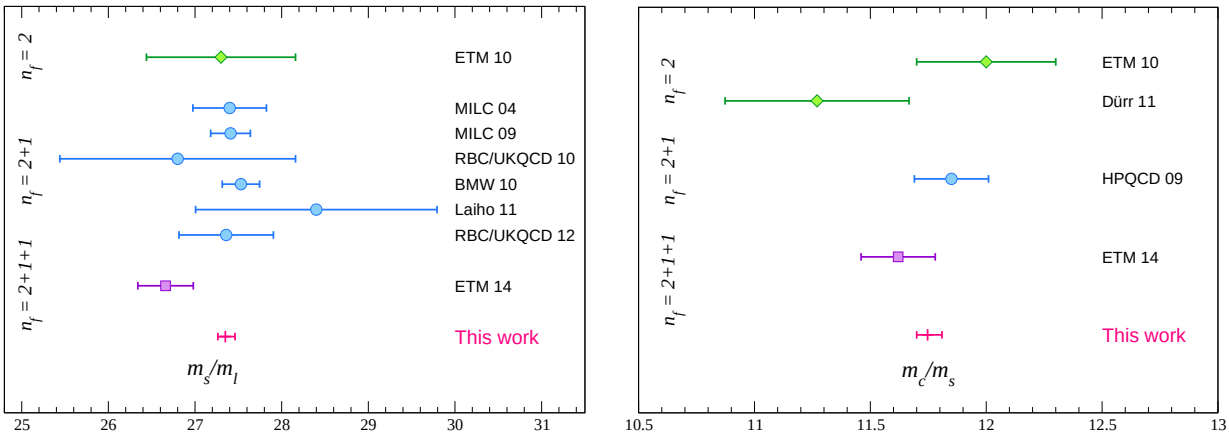

FIG. 20: Unquenched lattice results for m_s/m_l [26, 48–53] and m_c/m_s [48, 54–56]. Results are grouped by the number of flavors from top to bottom: $n_f = 2$ (green diamonds), $n_f = 2+1$ (blue circles), and $n_f = 2+1+1$ (purple squares). Within each grouping, the results are in chronological order. Our new results are denoted by magenta crosses and displayed at the bottom of each plot.

the significant (although not dominant) uncertainty from the chiral extrapolation. For f_{D^+} and f_{D_s}/f_{D^+}, we also have significantly smaller continuum-extrapolation errors due to the use of the HISQ sea-quark action and lattice spacings down to $a \approx 0.06$ fm.

The dominant source of uncertainty in our results is from the continuum extrapolation, and will be reduced once we include a still finer ensemble in our analysis with $a \approx 0.045$ fm and $m_l/m_s = 0.2$, generation of which is in progress. In fact, we already have some preliminary data on this ensemble, albeit with small statistics, and have tried including this data in the current chiral fits. The fits have acceptable p values and give results that are less than one statistical sigma away from those in Eqs. (32) through (36). Once we have ensembles with lattice spacings as fine as $a \approx 0.03$ fm, we expect to be able to use the same methods employed here to compute bottom decay constants. In the meantime, however, our results for D-meson decay constants using HISQ charm quarks can be combined with calculations of the ratios Φ_{B_s}/Φ_{D_s} using Fermilab heavy quarks to improve the determinations of decay constants in the B system, where the use of the HISQ action is more difficult. The ratios of continuum-extrapolated decay constants at various unphysical values of the light-quark mass may also be useful for this approach. The analysis of B- and D-meson decay constants with Fermilab heavy quarks on the 2+1 flavor asqtad ensembles is presently being finalized [78].

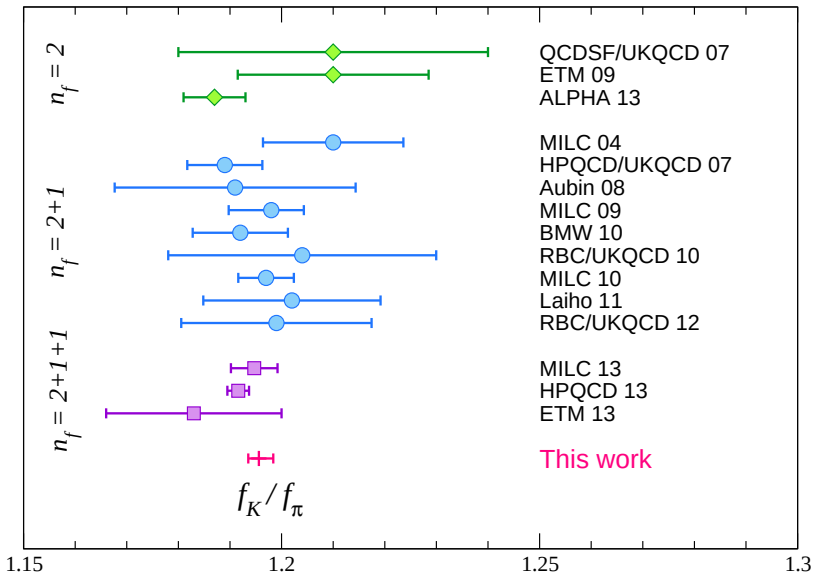

FIG. 21: Unquenched lattice results for f_K/f_π [26, 49–53, 57–65]. The previous results are reviewed in [66]. Results are grouped by the number of flavors from top to bottom: $n_f = 2$ (green diamonds), $n_f = 2+1$ (blue circles), and $n_f = 2+1+1$ (purple squares). Within each grouping, the results are in chronological order. Our new result is denoted by a magenta cross and displayed at the bottom. In this plot we do not distinguish between results done in the isospin symmetric limit (degenerate up and down quarks) and results including isospin violation. The difference is small [66] and does not affect the qualitative picture. (Our result does include the up-down quark mass difference, and so is for f_{K^+}/f_{π^+}.)

VI. IMPACT ON CKM PHENOMENOLOGY

We now use our decay constant results to obtain values for CKM matrix elements within the Standard Model, and to test the unitarity of the first and second rows of the CKM matrix.

The decay-constant ratio f_{K^+}/f_{π^+} can be combined with experimental measurements of the corresponding leptonic decay widths to obtain a precise value for the ratio $|V_{us}|/|V_{ud}|$ [1]. Combining our updated result for f_{K^+}/f_{π^+} from Eq. (36) with recent experimental results for the leptonic branching fractions [31] and an estimate of the hadronic structure-dependent EM correction [79], we obtain

$$|V_{us}|/|V_{ud}| = 0.23081(52)_{\rm LQCD}(29)_{{\rm BR}(K_{\ell 2})}(21)_{\rm EM}\,. \tag{39}$$

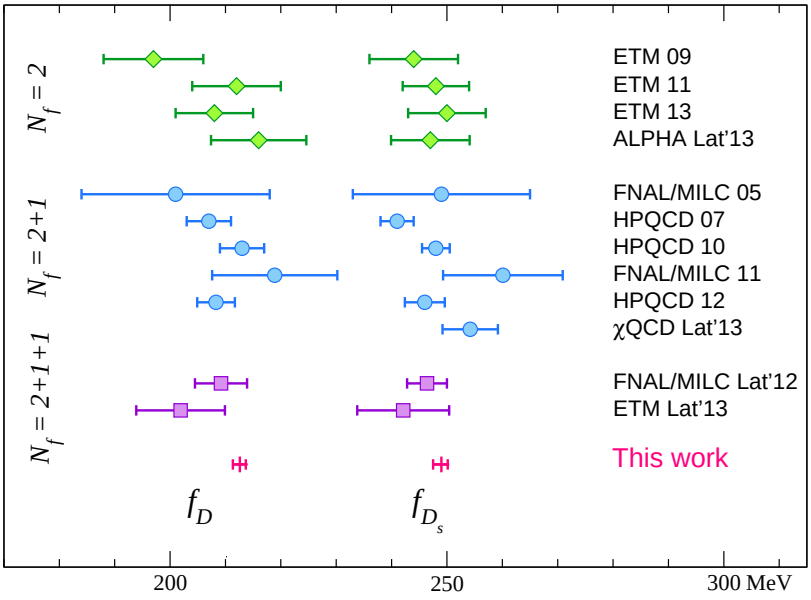

FIG. 22: Unquenched lattice results for f_D and f_{D_s} [27, 65, 67–75]. We do not include Ref. [76] because of the small volume used, and Ref. [77] because of the lack of a continuum extrapolation. Results are grouped by the number of flavors from top to bottom: $n_f = 2$ (green diamonds), $n_f = 2 + 1$ (blue circles), and $n_f = 2 + 1 + 1$ (purple squares). Within each grouping, the results are in chronological order. Our new results are denoted by magenta pluses and displayed at the bottom. Again, we do not distinguish results in the isospin symmetric limit from those with non-degenerate up and down quarks, where we have estimated the difference in Eq. 35.

Taking $|V_{ud}|$ from nuclear β decay [80], we also obtain

$$|V_{us}| = 0.22487(51)_{\rm LQCD}(29)_{{\rm BR}(K_{\ell 2})}(20)_{\rm EM}(5)_{V_{ud}} \,. \tag{40}$$

This result for $|V_{us}|$ is more precise than our recent determination from a calculation of the kaon semileptonic form factor on the physical-mass HISQ ensembles [81], and larger by 1.8σ. Figure 24 shows the unitarity test of the first row of the CKM matrix using our result for f_{K^+}/f_{π^+}. We find good agreement with CKM unitarity, and obtain a value for the sum of squares of elements of the first row of the CKM matrix consistent with the Standard-Model prediction zero at the level of 10^{-3}:

$$1 - |V_{ud}|^2 - |V_{us}|^2 - |V_{ub}|^2 = 0.00026(51) \,. \tag{41}$$

Thus our result places stringent constraints on new-physics scenarios that would lead to deviations from first-row CKM unitarity. Finally, we note that, now that the uncertainty

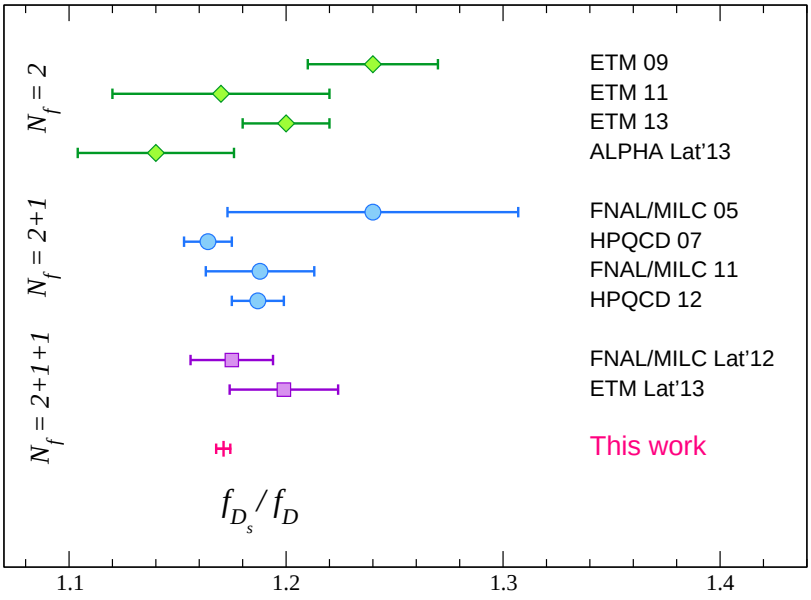

FIG. 23: Unquenched lattice results for f_{D_s}/f_D [27, 65, 67–74]. Results are grouped by the number of flavors from top to bottom: $n_f = 2$ (green diamonds), $n_f = 2+1$ (blue circles), and $n_f = 2+1+1$ (purple squares). Within each grouping, the results are in chronological order. Our new result is denoted by magenta crosses and displayed at the bottom.

in $|V_{us}|^2$ is approximately the same as that in $|V_{ud}|^2$, it is especially important to scrutinize the current uncertainty estimate for $|V_{ud}|$.

The D^+- and D_s-meson decay constants can be combined with experimental measurements of the corresponding leptonic decay widths to obtain $|V_{cd}|$ and $|V_{cs}|$. The values $f_{D^+}|V_{cd}| = 46.06(1.11)$ MeV and $f_{D_s}|V_{cs}| = 250.66(4.48)$ MeV in the PDG [82] are obtained from averaging the experimentally-measured decay rates into electron and muon final states including an estimate of structure-dependent Bremsstrahlung effects that lowers the $D^+ \to \mu^+\nu_\mu$ rate by $\sim 1\%$ [83, 84]. The PDG determinations of $f_{D^+}|V_{cd}|$ and $f_{D_s}|V_{cs}|$ do not, however, take into account other electroweak corrections (*c.f.* Refs. [1] and [85] and references therein). Such contributions are estimated for pion and kaon leptonic decay constants to be $\sim$ 1–2%, and the uncertainties in these corrections, in particular from the contributions that depend on the hadronic structure, lead to $\sim 0.1\%$ uncertainties in $|V_{us}|/|V_{ud}|$ and $|V_{us}|$ obtained from leptonic decays. Now that the uncertainties in the charm decay constants are at the half-a-percent level, it is timely to consider including electroweak corrections when extracting $|V_{cd}|$ and $|V_{cs}|$ from leptonic D decays, and we attempt to pro-

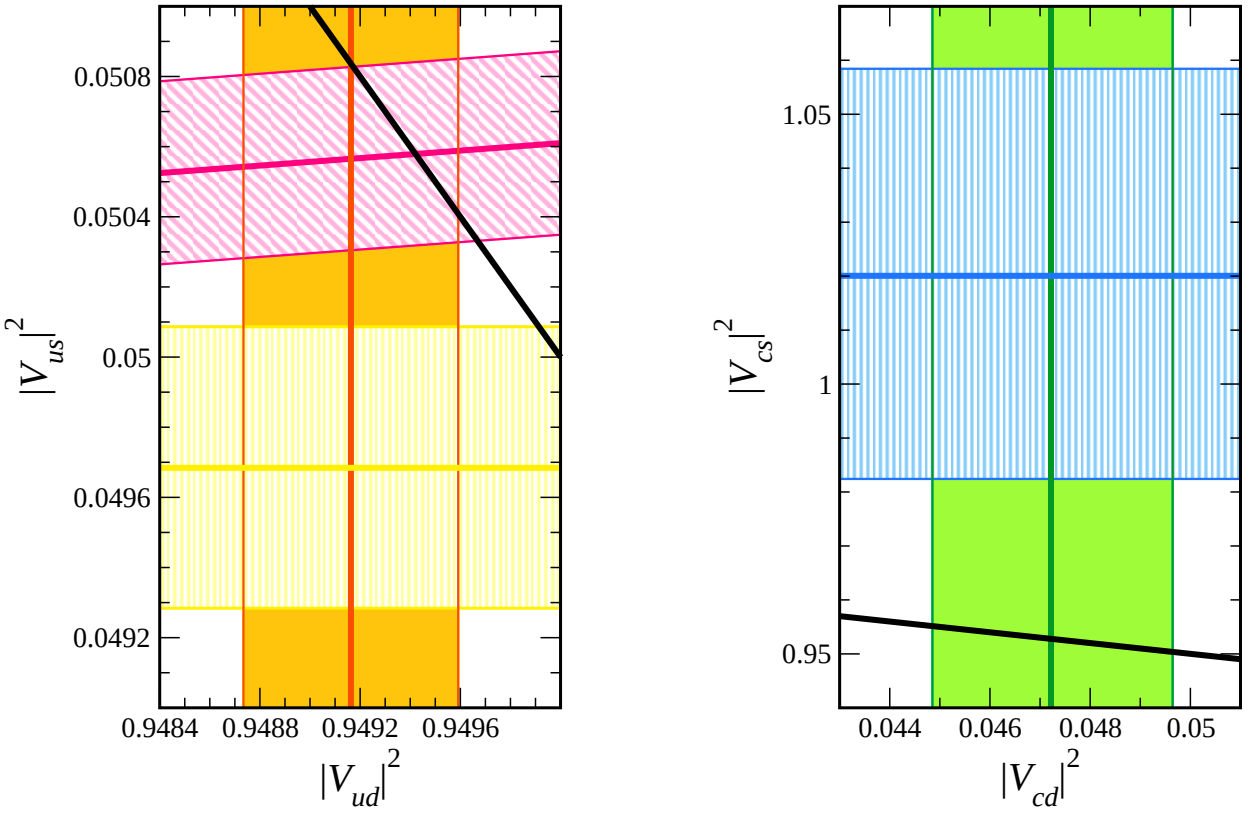

FIG. 24: Unitarity tests of the Cabibbo-Kobayashi-Maskawa matrix. Left: squared magnitudes of elements of the first row of the CKM matrix. The magenta diagonal band shows $(|V_{us}|/|V_{ud}|)^2$ obtained using f_{K^+}/f_{π^+} from this work, the vertical orange band shows $|V_{ud}|^2$ from nuclear β decay [80], and the horizontal yellow band shows $|V_{us}|^2$ obtained using our recent calculation of the kaon semileptonic form factor at $q^2 = 0$ [81]. The diagonal black line is the unitary prediction, and lies well within the region of overlap of the magenta and orange bands. Right: squared magnitudes of elements of the second row of the CKM matrix. The green vertical and blue horizontal bands show $|V_{cd}|^2$ and $|V_{cs}|^2$ obtained using f_{D^+} and f_{D_s} from this work. The black diagonal line does not intersect with the region of overlap of the two colored bands, indicating a slight tension with CKM unitarity.

vide a rough estimate of their possible size here. We consider all of the contributions that have been estimated for pion and kaon leptonic decays. Not all of the necessary calculations have been performed for the charm system, however, so, where necessary, we use results for the pion and kaon system as a guide and take a generous uncertainty.

The universal long-distance EM contribution to leptonic decays of point-like charged

particles was calculated by Kinoshita [86]. Evaluating this contribution for leptonic D decays into muons (because the experimental averages are dominated by measurements in the muon channel), the long-distance correction lowers both the D^+ and D_s decay rates by about 2.5%. The universal short-distance contribution to leptonic decays of charged pseudoscalar mesons, which accounts for electroweak corrections not included in the definition of G_F, was computed by Sirlin [87]. Choosing M_D for the factorization scale that enters $\ln(M_Z/\mu)$, the "Sirlin factor" increases the D^+ and D_s leptonic decay rates by about 1.8%. Thus the net effect of these two known corrections is a slight increase in the D^+ and D_s rates by less than a percent. Finally, we consider EM effects that depend on the mesons' hadronic structure. The expressions for the structure-dependent contributions to charged pion and kaon decay rates have been computed at $\mathcal{O}(e^2p^2)$ and $\mathcal{O}(e^2p^4)$ in chiral perturbation theory [88, 89]. The dominant $\mathcal{O}(e^2p^2)$ contribution takes the form $c_1^{(P)}\alpha/\pi$, and the coefficients have been estimated numerically in the large-N_c approximation to be $c_1^{(\pi)} = -2.4(5)$ and $c_1^{(K)} = -1.9(5)$ [90]. These calculations do not apply to the charm system, however, because the $D_{(s)}$-meson masses are much heavier than the pion and kaon masses, and well outside the range of validity of the light-meson chiral expansion. We therefore consider the possibility that the analogous coefficients for the D system are 2–5 times larger than for the pion and kaon system. With this assumption, we find a range of the possible size for the hadronic correction to the D^+- and D_s-meson leptonic decay rates from 1.1–2.8%. Corrections of this size would not be negligible compared to the known short-distance and long-distance contributions; thus it is important to obtain a more reliable estimate of the contributions to charged D decays due to hadronic structure in the future.

For the determinations of $|V_{cd}|$ and $|V_{cs}|$ given here, we first adjust the experimental decay rates quoted in the PDG by the known long-distance and short-distance electroweak corrections. We then add an estimate of the uncertainty due to the unknown hadronic structure-dependent EM corrections, taking the lower estimate of 0.6%. With these assumptions, and using our results for f_{D^+} and f_{D_s} from Eqs. (32) and (33), we obtain

$$|V_{cd}| = 0.217(1)_{\rm LQCD}(5)_{\rm expt}(1)_{\rm EM}\,, \tag{42}$$

$$|V_{cs}| = 1.010(5)_{\rm LQCD}(18)_{\rm expt}(6)_{\rm EM}\,, \tag{43}$$

where "EM" denotes the error due to unknown structure-dependent EM corrections. In both cases, the uncertainty is dominated by the experimental error in the branching frac-

tions. Thus the significant improvement in f_{D^+} and f_{D_s} does not, at present, lead to direct improvement in $|V_{cd}|$ and $|V_{cs}|$. Experimental measurements of the D^+ decay rates have improved recently [82], however, such that the error on $|V_{cd}|$ from leptonic D^+ decays is now approximately half that of $|V_{cd}|$ obtained from either neutrinos [31] or semileptonic $D \to \pi\ell\nu$ decay [91].

Our result for $|V_{cd}|$ agrees with the determination from neutrinos. Our $|V_{cd}|$ is 1.0σ lower than the determination from semileptonic D decay in Ref. [91], while our $|V_{cs}|$ is 1.1σ higher than that of Ref. [92]. Figure 24 shows the unitarity test of the second row of the CKM matrix using our results for f_{D^+} and f_{D_s}. We obtain a value for the sum of squares of elements of the second row of the CKM matrix of

$$1 - |V_{cd}|^2 - |V_{cs}|^2 - |V_{cb}|^2 = -0.07(4)\,, \tag{44}$$

showing some tension with CKM unitarity. This test will continue to become more stringent as experimental measurements of the D^+ and D_s decay rates become more precise. At present, even if our rough estimate of the uncertainty due to structure-dependent EM corrections in Eqs. (42) and (43) is too small by a factor of two, the errors on $|V_{cd}|$ and $|V_{cs}|$ would not change significantly. It will be important, however, to obtain a more reliable estimate of the contributions to charged D decays due to hadronic structure in the future.

Acknowledgements

Computations for this work were carried out with resources provided by the USQCD Collaboration, the Argonne Leadership Computing Facility and the National Energy Research Scientific Computing Center, which are funded by the Office of Science of the United States Department of Energy; and with resources provided by the National Center for Atmospheric Research, the National Center for Supercomputing Applications, the National Institute for Computational Science, and the Texas Advanced Computing Center, which are funded through the National Science Foundation's Teragrid/XSEDE Program; and with resources provided by the Blue Waters Computing Project, which is funded by NSF grants OCI-0725070 and ACI-1238993 and the state of Illinois. This work is also part of the "Lattice QCD on Blue Waters" PRAC allocation supported by the National Science Foundation grant OCI-0832315. This work was supported in part by the U.S. Department of Energy under

grants No. DE-FG02-91ER40628 (C.B., J. Komijani), No. DE-FC02-12ER41879 (C.D., J.F., L.L.), No. DE-FG02-91ER40661 (S.G., R.Z.), No. DE-SC0010120 (S.G.), No. DE-FC02-06ER41443 (R.Z.), No. DE-FG02-13ER42001 (D.D., A.X.K.), No. DE-FG02-04ER-41298 (D.T.); No. DE-FG02-13ER-41976 (D.T.), No. DE-FC02-06ER-41439 (J. Kim), by the National Science Foundation under Grants No. PHY-1067881 (C.D., J.F., L.L.), No. PHY-1212389 (R.Z.), and No. PHY-1316748 (R.S.); by the URA Visiting Scholars' program (A.X.K.); by the MICINN (Spain) under grant FPA2010-16696 and Ramón y Cajal program (E.G.); by the Junta de Andalucía (Spain) under Grants No. FQM-101, No. FQM-330, and No. FQM-6552 (E.G.); and by European Commission (EC) under Grant No. PCIG10-GA-2011-303781 (E.G.). A.S.K. thanks the DFG cluster of excellence "Origin and Structure of the Universe" at the Technische Universität München for hospitality while this work was being completed. This manuscript has been co-authored by an employee of Brookhaven Science Associates, LLC, under Contract No. DE-AC02-98CH10886 with the U.S. Department of Energy. Fermilab is operated by Fermi Research Alliance, LLC, under Contract No. DE-AC02-07CH11359 with the United States Department of Energy.

Appendix A: Expansion of Φ_0 in terms of $1/m_Q$

Equation (8) contains the effects of hyperfine splittings (*e.g.*, $M_D^* - M_D$) and flavor splittings (*e.g.*, $M_{D_s} - M_D$), but no other $1/m_Q$ effects. Boyd and Grinstein [38] find some other contributions at the same order as hyperfine and flavor splittings. However, one can show that most of these terms only produce $1/m_Q$ corrections to the LECs relevant to the pseudoscalar-meson decay constants. (Some of the terms violate heavy-quark spin symmetry, and therefore give different contributions to the pseudoscalar and vector-meson decay constants at this order, but we are not concerned with vector-meson decay constants here.) Following Eq. (20) of Ref. [38], at the order of $\mathcal{O}(1/m_Q, m_q^0)$ where m_q is a light quark mass, the $1/m_Q$ terms can be included by replacing Φ_0 by $\Phi_0(1 + \text{const.}/m_Q)$. This dependence can be simply absorbed in Φ_0 for a fixed value of m_Q. However, in our analysis the charm mass varies by about 10%, which leads to a correction comparable to that produced by terms of $\mathcal{O}(m_q) \sim \mathcal{O}(m_\pi^2)$. Therefore, replacing Φ_0 by $\Phi_0(1 + const./m_Q)$ in Eq. (8) should be considered a NLO correction. At this order the rate for $D^* \to D\pi$ is governed by $g_\pi(1 + \text{const.}/m_Q))$ instead of g_π, which is already taken into account by incorporating the

range $g_\pi = 0.53(8)$ in the fits. We do not allow any further dependence of g_π on m_Q in our analysis, because this dependence is formally NNLO.

On each ensemble, we have data with two different values of the valence charm mass: m_c' and $0.9m_c'$, where m_c' is the charm sea mass of the ensemble. In Fig. 25, the ratio of Φ_D at m_c' to Φ_D at $0.9m_c'$ is shown in terms of $m_{\rm v}$ for our four lattice spacings. The fact that $\Phi_D(m_c')/\Phi_D(0.9m_c')$ does not vary much as a function of the light valence-quark mass is evidence that the $1/m_Q$ effects can be absorbed in the overall factor in front of the full one-loop result as discussed above. On the other hand, Φ_D computed at m_c' and at $0.9m_c'$ are highly correlated so that their ratio is known precisely. Since our fits take the correlations into account, the p values will be low unless the chiral form is able to reproduce the ratio to high accuracy. Therefore, the expansion of the overall factor, Φ_0, in terms of $1/m_Q$ needs to be taken beyond the first order; for acceptable fits we need to introduce a $1/m_Q^2$ term as well as the $1/m_Q$ term, as indicated in Eq. (21). Furthermore, good fits require the LEC k_1 in Eq. (21) to have generic dependence on a; such dependence for k_2 is also strongly preferred by the fits.

Note finally that Fig. 25 shows a roughly 4% difference between Φ_D at m_c' and at $0.9m_c'$. As claimed in the discussion above Eq. (21), this is comparable to the chiral NLO effects of a nonzero pion mass, which may be estimated from the fits shown in Fig. 16. Indeed, those fits imply that the difference between the physical value of Φ_{D^+} and its value in the (two-flavor) chiral limit is roughly 3%.

---

[1] W. J. Marciano, Phys. Rev. Lett. **93**, 231803 (2004) [hep-ph/0402299].

[2] C. Aubin *et al.* [MILC Collaboration], Phys. Rev. D **70**, 114501 (2004), [hep-lat/0407028].

[3] A. Bazavov *et al.* [MILC Collaboration], Phys. Rev. Lett. **110**, 172003 (2013) [arXiv:1301.5855 [hep-ph]].

[4] E. Follana *et al.* [HPQCD Collaboration], Phys. Rev. D **75**, (2007) 054502 [hep-lat/0610092].

[5] A. Bazavov *et al.* [MILC Collaboration], PoS LATTICE2008, 033 (2008) [arXiv:0903.0874]; A. Bazavov *et al.*, PoS LAT2009 123 (2009), [arXiv:0911.0869]; PoS(Lattice 2010), 320 (2010), [arXiv:1012.1265].

[6] A. Bazavov *et al.*, Phys. Rev. D **82**, 074501 (2010), [arXiv:1004.0342].

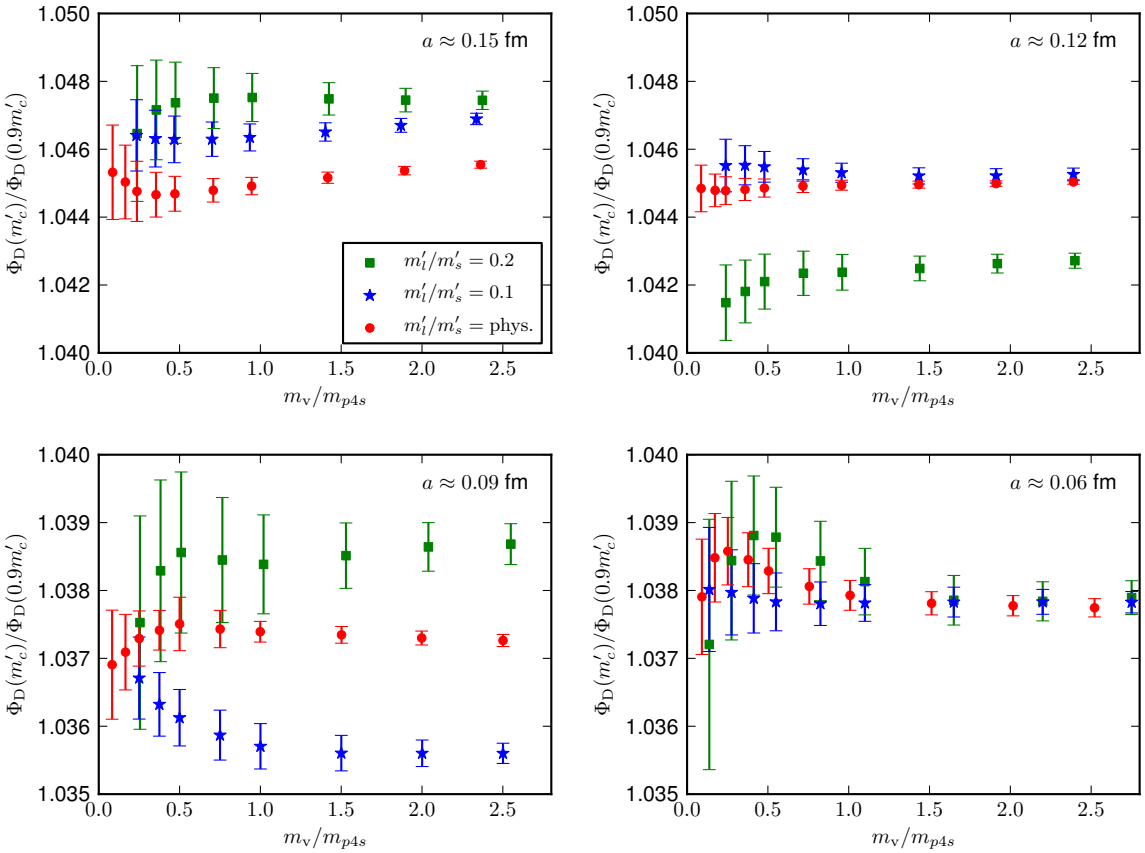

FIG. 25: The ratio $\Phi_D(m_c')/\Phi_D(0.9m_c')$ (where m_c' is the charm sea mass of the ensembles) as a function of m_v, the light valence-quark mass. The upper left panel shows data at $a \approx 0.15$ fm. The upper right panel shows the data at $a \approx 0.12$ fm from the ensembles with m_s tuned close to its physical value. In the second row, we show $a \approx 0.09$ fm (left) and $a \approx 0.06$ fm (right) data.

[7] A. Bazavov *et al.* [MILC Collaboration], Phys. Rev. **D87**, 054505 (2013), [arXiv:1212.4768].

[8] E. Marinari, G. Parisi and C. Rebbi, Nucl. Phys. B **190**, 734 (1981).

[9] S. Prelovsek. Phys. Rev. D**73**, 014506 (2006).

[10] C. Bernard, Phys. Rev. D**73**, 114503 (2006).

[11] C. Bernard, M. Golterman, and Y. Shamir. Phys. Rev. D**73**, 114511 (2006).

[12] C. Bernard, C. DeTar, Z. Fu, and S. Prelovsek. Phys. Rev. D**76**, 094504 (2007).

[13] Y. Shamir. Phys. Rev. D**71**, 034509 (2005).

[14] Y. Shamir. Phys. Rev. D**75**, 054503 (2007).

[15] E. Follana, A. Hart, and C.T.H. Davies. Phys. Rev.Lett. **93**, 241601 (2004).

[16] S. Dürr, C. Hoelbling, and U. Wenger. Phys. Rev. D**70**, 094502 (2004).

[17] S. Dürr and C. Hoelbling. Phys. Rev. D**71**, 054501 (2005).

[18] K. Y. Wong and R.M. Woloshyn. Phys. Rev. D**71**, 094508 (2005).

[19] S. Dürr and C. Hoelbling. Phys. Rev. D**74**, 014513 (2006).

[20] G. Donald, C.T.H. Davies, E. Follana, and A.S. Kronfeld. Phys. Rev. D**84**, 054504 (2011).

[21] W. -J. Lee and S. R. Sharpe, Phys. Rev. D **60**, 114503 (1999) [hep-lat/9905023].

[22] S. R. Sharpe, Phys. Rev. D **56**, 7052 (1997) [Erratum-ibid. D **62**, 099901 (2000)] [hep-lat/9707018].

[23] C. Aubin and C. Bernard, Phys. Rev. D **68**, 034014 (2003) [hep-lat/0304014]; Phys. Rev. D **68**, 074011 (2003) [hep-lat/0306026].

[24] J. Komijani and C. Bernard, PoS(LATTICE 2012) 199 [arXiv:1211.0785]; C. Bernard and J. Komijani, Phys. Rev. D88, 094017 (2013), [arXiv:1309.4533].

[25] A. Bazavov *et al.* [Fermilab Lattice and MILC Collaborations], PoS(LATTICE 2013)405 [arXiv:1312.0149].

[26] A. Bazavov *et al.*, Rev. Mod. Phys. **82**, 1349 (2010), [arXiv:0903.3598].

[27] J.A. Bailey *et al.* [Fermilab Lattice and MILC Collaborations], PoS(Lattice2011)320 [arXiv:1112.3978]; A. Bazavov *et al.* [Fermilab Lattice and MILC Collaborations], Phys. Rev. D **85** 114506 (2012) [arXiv:1112.3051].

[28] S. Aoki *et al.*, Phys.Rev. D62 (2000) 094501.

[29] G.W. Kilcup and S.W. Sharpe, Nucl. Phys. **B283** (1987) 493.

[30] E. Follana *et al.* [HPQCD and UKQCD Collaborations], Phys. Rev. D **75**, 054502 (2007) [arXiv:hep-lat/0610092].

[31] J. Beringer *et al.* [Particle Data Group], Phys. Rev. D **86**, 010001 (2012).

[32] G.P. Lepage, In: From Actions to Answers: Proceedings of the 1989 Theoretical Advanced Study Institute in Elementary Particle Physics, eds. T. DeGrand and D. Toussaint (World Scientific, Singapore, 1990) p. 197.

[33] C. Davies *et al.*, Nucl. Phys. Proc. Suppl. **119**, 595 (2003) [hep-lat/0209122].

[34] S. Basak *et al.* [MILC Collaboration], PoS LATTICE **2012**, 137 (2012) [arXiv:1210.8157 [hep-lat]].

[35] S. Basak *et al.* [MILC Collaboration], PoS CD **12**, 030 (2013) [arXiv:1301.7137 [hep-lat]].

[36] MILC Collaboration talk by C. Bernard at *Lattice 2014*, Columbia University, June 23 to June 28, 2014, https://indico.bnl.gov/materialDisplay.py?contribId=

129&sessionId=2&materialId=slides&confId=736.

[37] A. Bazavov *et al.* [Fermilab Lattice and MILC Collaborations], Phys. Rev. D **85**, 114506 (2012) [arXiv:1112.3051].

[38] C. G. Boyd and B. Grinstein, Nucl. Phys. **B442**, 205 (1995), [arXiv:hep-ph/9402340].

[39] I. W. Stewart, Nucl. Phys. B **529**, 62 (1998) [hep-ph/9803227]; D. Becirevic, S. Prelovsek and J. Zupan, Phys. Rev. D **68**, 074003 (2003) [hep-lat/0305001].

[40] A. Bazavov *et al.* [MILC Collaboration], PoS LATTICE **2011**, 107 (2011) [arXiv:1111.4314 [hep-lat]], and work in progress.

[41] C. Aubin and C. Bernard, Phys. Rev. D76, 014002 (2007), [arXiv:hep-lat/0704.0795].

[42] D. Arndt and C. J. D. Lin, Phys. Rev. D70, 014503 (2004) [arXiv:hep-lat/0403012].

[43] T. Appelquist and J. Carazzone, Phys. Rev. D **11**, 2856 (1975).

[44] D. Becirevic and F. Sanfilippo, Phys. Lett. **B721**, 94 (2013) [arXiv:1210.5410]; K. U. Can, G. Erkol, M. Oka, A. Ozpineci, and T. T. Takahashi, Phys. Lett. **B719**, 103 (2013) [arXiv:1210.0869].

[45] W. Detmold, C. J. D. Lin, and S. Meinel, Phys. Rev. D**85**, 114508 (2012) [arXiv:1203.3378].

[46] W. Bernreuther and W. Wetzel, Nucl. Phys. B **197**, 228 (1982) [Erratum-ibid. B **513**, 758 (1998)].

[47] A. Manohar and M. Wise, *Heavy Quark Physics*, Cambridge University Press (2000).

[48] B. Blossier *et al.* [ETM Collaboration], Phys. Rev. D **82**, 114513 (2010) [arXiv:1010.3659 [hep-lat]].

[49] C. Aubin *et al.* [MILC Collaboration] Phys. Rev. **D** 70, 114501 (2004) [arXiv:hep-lat/0407028].

[50] Y. Aoki *et al.* [RBC/UKQCD Collaboration], Phys. Rev. D**83** (2011) 074508 [arXiv:1011.0892].

[51] S. Dürr *et al.* [BMW Collaboration], Phys. Rev. D **81**, 054507 (2010) [arXiv:1001.4692].

[52] J. Laiho and R.S. Van de Water, PoS **LAT2011** (2011) 293, [arXiv:1112.4861].

[53] R. Arthur *et al.*, Phys. Rev. D **87** (2013) 094514 [arXiv:1208.4412].

[54] N. Carrasco, A. Deuzeman, P. Dimopoulos, R. Frezzotti, V. Gimenez, G. Herdoiza, P. Lami and V. Lubicz *et al.*, arXiv:1403.4504 [hep-lat].

[55] S. Dürr and G. Koutsou, Phys. Rev. Lett. **108**, 122003 (2012) [arXiv:1108.1650 [hep-lat]].

[56] C. T. H. Davies, C. McNeile, K. Y. Wong, E. Follana, R. Horgan, K. Hornbostel, G. P. Lepage and J. Shigemitsu *et al.*, Phys. Rev. Lett. **104**, 132003 (2010) [arXiv:0910.3102 [hep-ph]].

[57] G. Schierholz *et al.*, PoS **LAT2007**, 133.

[58] B. Blossier *et al.*, JHEP **0907**, (2009) 043, [arXiv:0904.0954].

[59] S. Lottini [ALPHA Collaboration], PoS **LATTICE2013** (2013) 315, [arXiv:1311.3081].

[60] E. Follana, C. T. H. Davies, G. P. Lepage and J. Shigemitsu [HPQCD/UKQCD Collaboration], Phys. Rev. Lett. **100** (2008) 062002 [arXiv:0706.1726].

[61] C. Aubin, J. Laiho and R.S. Van de Water, PoS LAT2008 (2008) 105, [arXiv:0810.4328].

[62] A. Bazavov *et al.* [MILC Collaboration], PoS LATTICE2010, 074 (2010) [arXiv:1012.0868].

[63] A. Bazavov *et al.* [MILC Collaboration], Phys. Rev. Lett. **110**, 172003 (2013), [arXiv:1301.5855].

[64] R.J. Dowdall, C.T.H. Davies, G.P. Lepage and C. McNeile [HPQCD Collaboration], Phys. Rev. D **88** (2013) 074504, [arXiv:1303.1670];

[65] L. Riggio *et al.*, PoS(LATTICE 2013) 314, [arXiv:1311.3080].

[66] S. Aoki, Y. Aoki, C. Bernard, T. Blum, G. Colangelo, M. Della Morte, S. Dürr and A. X. El Khadra *et al.*, [arXiv:hep-lat/1310.8555]

[67] C. Aubin *et al.* [Fermilab lattice and MILC Collaborations], Phys. Rev. Lett. **95**, 122002(2005), [arXiv:hep-lat/0506030].

[68] E. Follana *et al.* [HPQCD Collaboration], Phys. Rev. Lett. **100**, 062002 (2008), [arXiv:0706.1726].

[69] C. Davies *et al.* [HPQCD Collaboration], Phys. Rev. D **82**, 114504 (2010), [arXiv:1008.4018].

[70] B. Blossier *et al.* [ETM Collaboration], JHEP **0907** 043 (2009), [arXiv:0904.0954].

[71] P. Dimopoulos *et al.* [ETM Collaboration], JHEP **01**, 046 (2012), [arXiv:1107.1441].

[72] H. Na *et al.* [HPQCD Collaboration], Phys. Rev. D **85** 125029 (2012) [arXiv:1206.4936].

[73] A. Bazavov *et al.* [Fermilab Lattice and MILC Collaborations], PoS(Lattice 2012)159 [arXiv:1210.8431].

[74] J. Heitger *et al.*, PoS(LATTICE 2013) 475, [arXiv:1312.7693].

[75] Y.B. Yang *et al.*, PoS(LATTICE 2013) 500, [arXiv:1401.1487].

[76] W.P. Chen *et al.*, [arXiv:1404.3648].

[77] Y. Namekawa *et al.* [PACS-CS Collaboration], Phys. Rev. D **84** (2011) 074505, [arXiv:1104.4600].

[78] A. Bazavov *et al.* [Fermilab Lattice and MILC Collaborations], *in preparation.*

[79] M. Antonelli *et al.*, Eur. Phys. J. C **69**, 399 (2010) [arXiv:1005.2323 [hep-ph]].

[80] J. C. Hardy and I. S. Towner, Phys. Rev. C **79**, 055502 (2009) [arXiv:0812.1202 [nucl-ex]].

[81] A. Bazavov *et al.* [Fermilab Lattice and MILC Collaborations], Phys. Rev. Lett. **112**, 112001 (2014) [arXiv:1312.1228 [hep-ph]].

[82] J. L. Rosner and S. Stone, arXiv:1309.1924 [hep-ex].

[83] G. Burdman, J. T. Goldman and D. Wyler, Phys. Rev. D **51**, 111 (1995) [hep-ph/9405425].

[84] B. A. Dobrescu and A. S. Kronfeld, Phys. Rev. Lett. **100**, 241802 (2008) [arXiv:0803.0512 [hep-ph]].

[85] V. Cirigliano, G. Ecker, H. Neufeld, A. Pich and J. Portoles, Rev. Mod. Phys. **84**, 399 (2012) [arXiv:1107.6001 [hep-ph]].

[86] T. Kinoshita, Phys. Rev. Lett. **2**, 477 (1959).

[87] A. Sirlin, Nucl. Phys. B **196**, 83 (1982).

[88] M. Knecht, H. Neufeld, H. Rupertsberger and P. Talavera, Eur. Phys. J. C **12**, 469 (2000) [hep-ph/9909284].

[89] V. Cirigliano and I. Rosell, JHEP **0710**, 005 (2007) [arXiv:0707.4464 [hep-ph]].

[90] S. Descotes-Genon and B. Moussallam, Eur. Phys. J. C **42**, 403 (2005) [hep-ph/0505077].

[91] H. Na *et al.*, Phys. Rev. D **84**, 114505 (2011) [arXiv:1109.1501 [hep-lat]].

[92] H. Na, C. T. H. Davies, E. Follana, G. P. Lepage and J. Shigemitsu, Phys. Rev. D **82**, 114506 (2010) [arXiv:1008.4562 [hep-lat]].